

# **EFFECT OF SIZE AND SHAPE OF COBALT OXIDE NANOPARTICLES ON THE FENTON CATALYTIC ACTIVITY**



*Your world to a better future*

A dissertation submitted to the Faculty of Applied and Computer Science, Vaal University of Technology in fulfilment of the requirement for the degree of  
Magister Technologiae: Chemistry.

**by**

**Student Name: Miss. Semakaleng Vivian Kganyago**

**Student Number: 211126144**

**Supervisor:**

Dr. Elvera Viljoen (VUT, Department of Chemistry)

**Co-supervisor:**

Prof. Augustine Ofomaja (VUT, Department of Chemistry)

January 2019

## **DECLARATION**

I, Semakaleng Vivian Kganyago, student number 211126144, declare that this dissertation is my own work. It has been submitted in partial fulfilment for the degree of Magister Technologiae Chemistry in the Faculty of Applied and Computer Sciences at the Vaal University of Technology. It has not been submitted for any degree or examination in any other university.

Signature .....

Date.....

## DEDICATIONS

*My beloved mother, Reineth Kganyago,*

*My grand-mother Rosinah Kganyago, and*

*my aunt, Mmatshipi Kganyago*

*You are amazing. May God of heavens bless you all.*

## **PRESENTATIONS**

CATSA 2016: Poster presentation: Effect of size of  $\text{Co}_3\text{O}_4$  nanoparticles on the Fenton-like catalytic activity.

SANI 2016: Oral presentation: Manipulating the size and shape of cobalt oxide nanoparticles, and became a recipient for the best oral presenter (position 1) for MSc oral presentations against other delegates from six other South African universities.

VUT 1<sup>st</sup> Interdisciplinary Postgraduate Conference 2016: Oral presentation: Effect of  $\text{Co}_3\text{O}_4$  nanoparticles size on the degradation of methylene blue.

SACI 2017: Poster presentation: Effect of the cobalt oxide nanoparticles size on the heterogeneous Fenton-like activity.

SANI 2017: Oral presentation: Effect of the cobalt oxide nanoparticles size and shape on Fenton-like activity, and became a recipient for the best oral presenter (position 2) for MSc oral presentations against other delegates from six other South African universities.

VUT 2<sup>nd</sup> Interdisciplinary Postgraduate conference 2017: Oral presentation: The Fenton-like catalytic activity of different sizes of cobalt oxide nanoparticles

## **LIST OF PUBLICATIONS**

Semakaleng Kganyago, Elvera Viljoen, and Augustine Ofomaja. Effect of the cobalt oxide nanoparticles size of the degradation of methylene blue, *to be submitted*.

Semakaleng Kganyago, Elvera Viljoen, and Augustine Ofomaja. Effect of size and shape of cobalt oxide nanoparticles size on the degradation of methylene blue, *to be submitted*.

## **ACKNOWLEDGEMENTS**

After an intensive period of two years, today is the day: writing this note of thanks is the finishing touch on my dissertation. It has been a period of intense learning for me, not only in the scientific arena but also on a personal level. Writing this dissertation has had a big impact on me. I would like to reflect on the people who have supported and helped me so much throughout this period.

First, I am truly grateful to God for the good health and well-being that were necessary to complete this research project. Foremost, I would like to express my sincere gratitude to my supervisor, Dr. E.L Viljoen for the patient, aspiring guidance, encouragement, invaluable criticisms and advice she has provided throughout my time as her student. I have been extremely lucky to have a supervisor who cared so much about my work, and who responded to my questions and queries so promptly. She has inspired me to become an independent researcher and helped me realize the power of critical reasoning. She also demonstrated what a brilliant and hard-working scientist could accomplish. There are insufficient words to convey my deep gratitude and respect to the rest of my dissertation advisory: my co-supervisors, Prof A.E Ofomaja and Prof M.J Moloto for their encouragement, insight, comments and questions. During the times when I wanted to give up, Prof Moloto was always there as a pillar of strength and for that I will forever be grateful. I would particularly like to single out my mentor, Dr. K.P Mubiayi, for his continued support and encouragement. I was continually amazed by his willingness to proofread countless pages of my characterization and to offer me valuable comments towards improving my work.

I am most grateful to the National Research Foundations (NRF), Vaal University of Technology, New Generations Scholars (NGS) bursary, Sasol and National Student Financial Aid Scheme (NSFAS) for funding my studies. This work would not have been possible without their financial support.

Completing this work required more than academic support. I have plenty of people to thank for supporting me throughout this journey. I cannot begin to express my gratitude and appreciation for their friendship. In my daily work, I was blessed with a friendly and cheerful group. The A team: Mahadi Lesaoana, Zondi Nate and Daniel Makanyane. These people have been unwavering in their personal and professional support during the times I spent at the university. For the sleepless nights we were working together before the deadlines, and for all the fun we have had in

the past two years. You provided me with the tools and attitude that I needed to choose the right direction and complete my dissertation. People such as Kelebogile Mmelesi, Ola Saheed, and Thapelo Mofokeng also deserve thanks for helping me keep things in perspective.

Most importantly, none of this could have happened without the unfailing support of my mother. It is hard to put into words exactly how thankful I am for you and everything you have done for me over the years. I do not know where I would have been without your support. My gratitude has no end. Thank you for being my rock, my emotional support and most importantly, thank you for all the sacrifices and the tears you sometimes hide. It is because of you that I have grown so strong, taken chances and lived, because I know that you are always with me every step of the way.

To my grandmother, Rosina Kganyago, my aunts, Mmatshipi and Lettie Kganyago, my nieces Bogolo, Tsosoloso, Reagile and Thatego Kganyago and my cousin, Hlologelo Kganyago, every time I was ready to give up, you did not let me. I am truly blessed to have a family like you and after everything that we have been through together, I cannot help but choose to say I love you all. This dissertation stands as a testament of unconditional love. A very special gratitude also goes to Joe Mosweu who has given me so much of himself every moment. It was indeed a great comfort and relief to know that he was willing to stick with me through thick and thin while I completed my dissertation. Thank you all for everything.

Finally, a special mention must be made to a group of people who have contributed to this work. NCAP group, Dr V.E Pakade, Dr F.M Mtunzi, Dr T Xaba, Dr P Edijike, Dr W Omwoyo, Prof Okosun, Dr Mena, Ms I.P Ledwaba M, Mr T.D Ntuli, Mr K Mniqiwu, Mr O.B Nchoe, Mr S.B Sibokoza, Mr W Bout, Ms D.S More, Mr K.E Mokubung, Ms L.C Maremeni, Ms S.C Nkabinde, Ms M Thabethe, Ms N Mabungela, Ms A.R Makamu and Ms N Mgedle. Your comments and advices in the group presentations are really appreciated. My appreciation and respect for you knows no bounds. To Mr. M Ngayo and Ms. N Pholosi, thank you for your assistance with all the analytical instruments. I would also like to acknowledge the Research and Higher Degree Unit at the Vaal University of Technology.

## ABSTRACT

Water is a limited resource and pollution has become an increasing problem due to industrialization. Aromatic organic pollutants are resistant to biodegradation, and thus chemical methods like the Fenton reaction is required for degradation. The Fenton reaction is catalyzed by cobalt oxide. This study aims to investigate the effect of size and shape of cobalt oxide nanoparticles on the catalytic activity. Methylene blue (MB) was used as a model pollutant.

The size and shape of nanoparticles are known to influence the activity of catalysts. The study used a precipitation method to prepare spherical and cubic-shaped cobalt oxide nanoparticles of different sizes using preparation parameters like cobalt precursor, amount and type of oxidant and time of reaction.

The XRD patterns of all the prepared cobalt oxide nanoparticles showed a pure cubic  $\text{Co}_3\text{O}_4$  phase. The shape of the nanoparticles changed from spherical to cubic when the cobalt precursor was changed from cobalt nitrate to cobalt acetate. The size of the nanoparticles increased when lower amounts of hydrogen peroxide and longer reaction times were used. Nanoparticles between 4.6 to 19.5 nm for spherical particles and between 6.6 and 43.3 nm for cubic particles were prepared. FTIR spectra analysis showed the presence of both nitrate and acetate ions on the surface of cobalt oxide nanoparticles. The TGA results indicated that the adsorption of the acetate ions is stronger than the nitrate ions on the surface of the cobalt oxide nanoparticles.

The rate of degradation of methylene blue, the pseudo first order rate constant and the amount of leaching increased with a decrease in the nanoparticles size. The Turn Over Frequency (TOF), which is the moles of methylene blue converted per mole of surface cobalt atoms, decreased with a decrease in the size for both the spherical and cubic nanoparticles. The TOF for the spherical and cubic nanoparticles were similar indicating that the catalytic activity may not be dependent on the shape of the nanoparticles. FTIR analyses showed that degradation occurred, and that methylene blue was not just decolourised to leuco methylene blue.

# Table of Contents

DECLARATION .....	ii
DEDICATIONS.....	iii
PRESENTATIONS.....	iv
LIST OF PUBLICATIONS .....	iv
ACKNOWLEDGEMENTS.....	v
ABSTRACT.....	vii
LIST OF ABBREVIATIONS.....	xi
LIST OF FIGURES .....	xii
LIST OF TABLES.....	xv
DISSERTATION OUTLINE.....	xvi
CHAPTER 1 .....	1
1.1 INTRODUCTION .....	1
1.1.1 Background.....	1
1.1.2 Water and environmental concerns.....	1
1.2 PROBLEM STATEMENT .....	3
1.3 AIMS AND OBJECTIVES .....	4
1.4 REFERENCES .....	5
CHAPTER 2 .....	7
2.1 METHYLENE BLUE.....	7
2.2 TECHNIQUES FOR WASTEWATER REMOVAL .....	8
2.3 CATALYST DEACTIVATION.....	13
2.3.1 General heterogeneous catalytic deactivation mechanisms .....	13
2.3.2 Catalyst deactivation during the Fenton reaction.....	13
2.4 RELATIVE ACTIVITY OF TRANSITION METAL NANOPARTICLES.....	14
2.4.1 Heterogeneous oxidation catalysts.....	15
2.5 EFFECT OF SIZE AND SHAPE OF NANOPARTICLES ON THE CATALYTIC ACTIVITY... 16	
2.5.1 Influence of size.....	16
2.5.2 Influence of shape .....	17
2.5.3 Turn over frequency (TOF).....	18
2.6 CATALYST PREPARATION METHODS.....	21
2.6.1 Cobalt oxide nanoparticles (unsupported catalyst) preparation methods.....	21
2.7 REFERENCES .....	24

CHAPTER 3 .....	30
3.1 RESEARCH METHODOLOGY .....	30
3.1.1 Introduction .....	30
3.1.2 Materials .....	30
3.1.3 Methodology .....	31
3.1.4 Characterization of cobalt oxide nanoparticles .....	35
3.1.5 Application of Co <sub>3</sub> O <sub>4</sub> nanoparticles as catalysts for the degradation of methylene blue (MB) .....	36
3.2 REFERENCES .....	39
CHAPTER 4 .....	40
4.1 INTRODUCTION .....	40
4.1 RESULTS AND DISCUSSIONS .....	40
4.1.1 Influence of cobalt precursor .....	40
4.1.2 Influence of H <sub>2</sub> O <sub>2</sub> .....	50
4.1.3 Influence of time .....	58
4.1.4 Concluding remarks .....	65
4.2 REFERENCES .....	67
CHAPTER 5 .....	69
5.1 DEGRADATION STUDIES .....	69
5.1.1 Influence of size using spherical cobalt oxide nanoparticles on the degradation of methylene blue (MB) .....	70
5.1.2 Influence of size using cubic Co <sub>3</sub> O <sub>4</sub> nanoparticles on the degradation of methylene blue (MB) .....	78
5.1.3 Cobalt oxide nanoparticles shape influence on the catalytic activity of methylene blue (MB) .....	81
5.2 REFERENCES .....	83
CHAPTER 6 .....	85
6.1 CONCLUSIONS AND RECOMMENDATIONS .....	85
6.1.1 Conclusions .....	85
6.1.2 Recommendations .....	87
APPENDIXES .....	88
7.1 A1 CALCULATIONS OF AVERAGE CRYSTALLITES SIZES FROM XRD USING SCHERRER EQUATION .....	88
7.2 A2 CALCULATIONS OF COBALT OXIDE NANOPARTICLES YIELD .....	89
7.3 A3 CALCULATIONS OF BAND GAB ENERGIES USING TAUC PLOTS .....	90

7.4	A4.1 CALCULATIONS OF METHYLENE BLUE CONVERSION RATES .....	91
7.5	A4.2 CALCULATIONS OF DEGRADATION EFFICIENCY OF METHYLENE BLUE .....	91
7.6	A5.1 CALCULATION OF THE PSEUDO-FIRST-ORDER RATE CONSTANTS .....	92
7.7	A5.2 CALCULATIONS OF THE PSEUDO SECOND ORDER RATE CONSTANTS .....	92
7.8	A6 CALCULATIONS OF TURN OVER FREQUENCY (TOF) PER SURFACE COBALT ATOMS .....	93
7.9	A7 CALCULATIONS OF TOF USING THE RESULTS OF Wan et al. (2016) .....	95
7.10	A8 CALCULATIONS OF TOF USING Espinosa et al. (2018) results .....	97
7.11	A9 CALCULATIONS OF TOF USING THE RESULTS OF Dong et al. (2007) .....	99
7.12	A10 CORRELATION BETWEEN CALCULATED AREA AND BET SURFACE AREA FROM THE RESULTS OF Wan et al. (2016). .....	101
7.13	A 11 CORRELATION BETWEEN CALCULATED SURFACE AREA AND BET SURFACE ARE FROM THE RESULTS OF Esswein et al. (2009) .....	102

## **LIST OF ABBREVIATIONS**

MB	: Methylene blue
RHB	: Rhodamine B
NPs	: Nanoparticles
AOPs	: Advanced oxidation processes
UV-vis	: Ultra Violet visible spectrometer
PL	: Photoluminescence spectrophotometer
FTIR	: Fourier transform infrared spectroscopy
TGA	: Thermo gravimetric analysis
XRD	: X-Ray diffraction
TEM	: Transmission electron microscope
HPLC	: High performance liquid chromatography
TOF	: Turn over frequency
TOC	: Total organic carbon

## LIST OF FIGURES

<b>Figure 2:1</b> Molecular structure of methylene blue (Ayodamope and Kidak, 2015).....	7
<b>Figure 2:2</b> Proposed degradation pathway of methylene blue using Fenton-like process (Hu et al., 2017). .....	12
<b>Figure 2:3</b> TOF results calculated using TEM sizes of Espinosa et al. (2018).....	19
<b>Figure 2:4</b> TOF results calculated using TEM sizes of (A) Dong et al. (2011) and (B) Wan et al. (2016).....	20
<b>Figure 4:1</b> XRD pattern of the prepared $\text{Co}_3\text{O}_4$ nanoparticles. (a) Reference $\text{Co}_3\text{O}_4$ , (N1) $\text{Co}_3\text{O}_4$ nanoparticles made using $\text{Co}(\text{NO}_3)_2 \cdot 6\text{H}_2\text{O}$ and (N2) $\text{Co}_3\text{O}_4$ nanoparticles prepared using $\text{Co}(\text{CH}_3\text{COO})_2 \cdot 4\text{H}_2\text{O}$ . .....	41
<b>Figure 4:2</b> TEM micrographs and the corresponding histograms of $\text{Co}_3\text{O}_4$ nanoparticles prepared from $\text{Co}(\text{NO}_3)_2 \cdot 6\text{H}_2\text{O}$ (N1) and $\text{Co}(\text{CH}_3\text{COO})_2 \cdot 4\text{H}_2\text{O}$ (N2). .....	42
<b>Figure 4:3</b> FTIR spectra of $\text{Co}_3\text{O}_4$ nanoparticles prepared from $\text{Co}(\text{NO}_3)_2 \cdot 6\text{H}_2\text{O}$ (N1) and $\text{Co}(\text{CH}_3\text{COO})_2 \cdot 4\text{H}_2\text{O}$ (N2). .....	45
<b>Figure 4:4</b> TGA (A) and DTA (B) curves of $\text{Co}_3\text{O}_4$ nanoparticles prepared from $\text{Co}(\text{NO}_3)_2 \cdot 6\text{H}_2\text{O}$ (N1) and $\text{Co}(\text{CH}_3\text{COO})_2 \cdot 4\text{H}_2\text{O}$ (N2). .....	46
<b>Figure 4:5</b> UV-vis spectra of $\text{Co}_3\text{O}_4$ nanoparticles prepared from $\text{Co}(\text{NO}_3)_2 \cdot 6\text{H}_2\text{O}$ (N1) and $\text{Co}(\text{CH}_3\text{COO})_2 \cdot 4\text{H}_2\text{O}$ (N2). .....	48
<b>Figure 4:6</b> Estimation of the direct band gaps from Tauc plots for $\text{Co}_3\text{O}_4$ nanoparticles made using cobalt nitrate (N1) and cobalt acetate (N2). .....	49
<b>Figure 4:7</b> PL spectroscopy of $\text{Co}_3\text{O}_4$ nanoparticles prepared from $\text{Co}(\text{NO}_3)_2 \cdot 6\text{H}_2\text{O}$ (N1) and $\text{Co}(\text{CH}_3\text{COO})_2 \cdot 4\text{H}_2\text{O}$ (N2). Excitation wavelength of 400 nm. ....	50
<b>Figure 4:8</b> XRD diffraction patterns of $\text{Co}_3\text{O}_4$ NPs synthesized using different amounts of $\text{H}_2\text{O}_2$ . Nanoparticles made from (A) $\text{Co}(\text{NO}_3)_2 \cdot 6\text{H}_2\text{O}$ (a) reference $\text{Co}_3\text{O}_4$ , (b) 2.9 mmol $\text{H}_2\text{O}_2$ , (c) 1.4 mmol $\text{H}_2\text{O}_2$ , (d) 0.74 mmol $\text{H}_2\text{O}_2$ , (e) 0.37 mmol $\text{H}_2\text{O}_2$ and (f) 0.14 mmol $\text{H}_2\text{O}_2$ . Nanoparticles made from (B) $\text{Co}(\text{CH}_3\text{COO})_2 \cdot 4\text{H}_2\text{O}$ (a) reference $\text{Co}_3\text{O}_4$ , (b) 2.9 mmol $\text{H}_2\text{O}_2$ , (c) 1.4 mmol $\text{H}_2\text{O}_2$ , (d) 0.74 mmol $\text{H}_2\text{O}_2$ , and (e) 0.37 mmol $\text{H}_2\text{O}_2$ . .....	51
<b>Figure 4:9</b> Selected TEM images of $\text{Co}_3\text{O}_4$ NPs synthesized prepared at 85 °C for 16 hrs by varying the amount of $\text{H}_2\text{O}_2$ . Nanoparticles made using $\text{Co}(\text{NO}_3)_2 \cdot 6\text{H}_2\text{O}$ . (a) 2.9 mmol $\text{H}_2\text{O}_2$ , (b) 1.4 mmol $\text{H}_2\text{O}_2$ , (c) 0.74 mmol $\text{H}_2\text{O}_2$ and (d) 0.37 mmol $\text{H}_2\text{O}_2$ . .....	52

<b>Figure 4:10</b> Selected TEM images of Co <sub>3</sub> O <sub>4</sub> NPs synthesized prepared at 85 °C for 16 hrs by varying the amount of H <sub>2</sub> O <sub>2</sub> . Nanoparticles made using Co(CH <sub>3</sub> COO) <sub>2</sub> .4H <sub>2</sub> O. (a) 2.9 mmol H <sub>2</sub> O <sub>2</sub> , (b) 1.4 mmol H <sub>2</sub> O <sub>2</sub> , (c) 0.74 mmol H <sub>2</sub> O <sub>2</sub> and (d) 0.37 mmol H <sub>2</sub> O <sub>2</sub> .....	53
<b>Figure 4:11</b> Yields of Co <sub>3</sub> O <sub>4</sub> nanoparticles dependence on the amounts of H <sub>2</sub> O <sub>2</sub> .....	54
<b>Figure 4:12</b> Co <sub>3</sub> O <sub>4</sub> TEM size dependence on the amounts of H <sub>2</sub> O <sub>2</sub> : (A) Nanoparticles calculated from (A) TEM and (B) XRD data.....	55
<b>Figure 4:13</b> UV-vis absorption spectra of Co <sub>3</sub> O <sub>4</sub> nanoparticles prepared at different amounts of H <sub>2</sub> O <sub>2</sub> : (A) spherical Co <sub>3</sub> O <sub>4</sub> nanoparticles (a) 2.9 mmol, (b) 1.4 mmol, (c) 0.74 mmol and (d) 0.37 mmol and (e) 0.14 mmol. (B) cubic Co <sub>3</sub> O <sub>4</sub> nanoparticles (a) 2.9 mmol, (b) 1.4 mmol, (c) 0.74 mmol and (d) 0.37 mmol. ....	57
<b>Figure 4:14</b> Estimation of direct band gaps from Tauc plots for Co <sub>3</sub> O <sub>4</sub> nanoparticles made using cobalt nitrate. (a) 4.6 nm, (b) 6.8 nm, (c) 7.7 nm, (d) 11.5 nm and (e) 19.5 nm. ....	57
<b>Figure 4:15</b> Band gap energies of prepared Co <sub>3</sub> O <sub>4</sub> nanoparticles estimated from Tauc plots. (A) O <sup>2-</sup> → Co <sup>3+</sup> and (B) O <sup>2-</sup> → Co <sup>2+</sup> charge transfer process. ....	58
<b>Figure 4:16</b> XRD diffraction patterns of Co <sub>3</sub> O <sub>4</sub> NPs synthesized using different reaction times. Nanoparticles made using (A) Co(NO <sub>3</sub> ) <sub>2</sub> .6H <sub>2</sub> O (a) reference Co <sub>3</sub> O <sub>4</sub> , (b) 1 hour , (c) 4 hrs, (d) 8 hours and (e) 16 hours. Nanoparticles made using (B) Co(CH <sub>3</sub> COO) <sub>2</sub> .4H <sub>2</sub> O (a) reference Co <sub>3</sub> O <sub>4</sub> , (b) 4 hrs, (c) 8 hrs, (d) 16 hrs, (e) 48 hrs and (f) 72 hrs. ....	59
<b>Figure 4:17</b> Selected TEM images of Co <sub>3</sub> O <sub>4</sub> NPs synthesized at 85 °C using Co(NO <sub>3</sub> ) <sub>2</sub> .6H <sub>2</sub> O (a) 1 hr, (b) 4 hrs, (c) 8 hrs and (d) 16 hrs. ....	61
<b>Figure 4:18</b> Selected TEM images of Co <sub>3</sub> O <sub>4</sub> NPs synthesized at 85 °C using Co(CH <sub>3</sub> COO) <sub>2</sub> .4H <sub>2</sub> O. (a) 4 hrs, (b) 8 hrs, (c) 16 hrs and (d) 72 hrs. ....	61
<b>Figure 4:19</b> Yields of Co <sub>3</sub> O <sub>4</sub> nanoparticles dependence on different reaction times. ....	63
<b>Figure 4:20</b> Co <sub>3</sub> O <sub>4</sub> nanoparticles size dependence on time: Spherical and Cubic Co <sub>3</sub> O <sub>4</sub> nanoparticles calculated using (A) TEM and (B) XRD.....	63
<b>Figure 4:21</b> UV-vis absorption spectra of Co <sub>3</sub> O <sub>4</sub> nanoparticles prepared at different reaction times: (A) spherical Co <sub>3</sub> O <sub>4</sub> nanoparticles (a) 1 hr, (b) 4 hrs, (c) 8 hrs and (d) 16 hrs. (B) cubic Co <sub>3</sub> O <sub>4</sub> nanoparticles (a) 4 hrs, (b) 8 hrs, (c) 16 hrs, (d) 48 hrs and (e) 72 hrs. ....	64
<b>Figure 4:22</b> Band gap energies of prepared Co <sub>3</sub> O <sub>4</sub> nanoparticles estimated from Tauc plots. (A) O <sup>2-</sup> → Co <sup>3+</sup> and (B) O <sup>2-</sup> → Co <sup>2+</sup> charge transfer process. ....	65

<b>Figure 5:1</b> Comparison of discoloration of methylene blue in various degradation systems namely (a) without and (b) with spherical $\text{Co}_3\text{O}_4$ nanoparticles. ....	71
<b>Figure 5:2</b> Degradation of methylene blue using spherical $\text{Co}_3\text{O}_4$ nanoparticles of (a) 4.6 nm (b) 19.5 nm. ....	72
<b>Figure 5:3</b> (a) Removal efficiency of MB and (b) Percentage degradation of MB at 20 min with the repeated results for different sizes of spherical $\text{Co}_3\text{O}_4$ nanoparticles. ....	72
<b>Figure 5:4</b> FTIR spectra of (a) MB reaction mixture before degradation and (b) MB reaction mixture after degradation with $\text{Co}_3\text{O}_4$ nanoparticles of 4.6 nm. ....	74
<b>Figure 5:5</b> Plot of $\ln [C_t]$ against time for different sizes of spherical cobalt oxide nanoparticles on methylene blue degradation. ....	75
<b>Figure 5:6</b> TOF and repeated results of different sizes of spherical $\text{Co}_3\text{O}_4$ nanoparticles calculated from (a) TEM and (b) XRD sizes. ....	77
<b>Figure 5:7</b> (a) Removal efficiency of MB and (b) Percentage degradation of MB at 20 min of cubic $\text{Co}_3\text{O}_4$ nanoparticles of different sizes ....	78
<b>Figure 5:8</b> Pseudo first order for different sizes of cubic $\text{Co}_3\text{O}_4$ nanoparticles on the degradation of MB .....	79
<b>Figure 5:9</b> TOF for the different sizes of cubic $\text{Co}_3\text{O}_4$ nanoparticles calculated using (a) TEM and (b) XRD sizes.....	80
<b>Figure 5:10</b> Combined TOF for spherical and cubic $\text{Co}_3\text{O}_4$ nanoparticles using TEM sizes.....	82

## LIST OF TABLES

<b>Table 2:1</b> Absorption species of Methylene blue (Ayodamope and Kidak, 2015).....	8
<b>Table 3:1</b> Percentage purities of chemicals used in this study and their suppliers. ....	30
<b>Table 3:2</b> Different parameters varied during the preparation of $\text{Co}_3\text{O}_4$ nanoparticles.....	33
<b>Table 4:1</b> $\text{Co}_3\text{O}_4$ nanoparticles yields and sizes determination with XRD and TEM.....	43
<b>Table 4:2</b> Infrared assignments of $\text{Co}_3\text{O}_4$ nanoparticles prepared from cobalt nitrate and cobalt acetate. ....	44
<b>Table 4:3</b> $\text{Co}_3\text{O}_4$ nanoparticles yields and size determination with XRD and TEM data.....	54
<b>Table 4:4</b> Bulk $\text{Co}_3\text{O}_4$ data, sizes and band gap energies of the $\text{Co}_3\text{O}_4$ nanoparticles obtained from this study (Tauc plots) and reported band gap values from the literature for comparison. ....	56
<b>Table 4:5</b> $\text{Co}_3\text{O}_4$ nanoparticles sizes determination with XRD and TEM data. ....	62
<b>Table 4:6</b> Effect of reaction time on band gap energies of the prepared $\text{Co}_3\text{O}_4$ nanoparticles calculated using (Tauc plots). ....	65
<b>Table 5:1</b> Selected $\text{Co}_3\text{O}_4$ nano-catalysts for each set (spherical and cubic) with different size range.....	70
<b>Table 5:2</b> Size influenced degradation kinetics of MB using different sizes of selected spherical $\text{Co}_3\text{O}_4$ nanoparticles.....	76
<b>Table 5:3</b> Selected $\text{Co}_3\text{O}_4$ catalysts for cobalt ions leached by oxalic acid. ....	78
<b>Table 5:4</b> Size influenced degradation of methylene blue using cubic $\text{Co}_3\text{O}_4$ nanoparticles. ....	80
<b>Table 5:5</b> Selected cubic $\text{Co}_3\text{O}_4$ catalysts of different sizes for cobalt ions leached by oxalic acid. ....	81

## DISSERTATION OUTLINE

This dissertation is divided into six chapters.

**Chapter 1:** This chapter focuses on the general introduction of water pollution by organic pollutants and some problems faced by society. The problem statements, the aim and the objectives of this study are presented in this chapter.

**Chapter 2:** The literature review of the pollutants generated by industries and different methods that have been used for their removal is discussed in this chapter. The influence of nanoparticle size and shape on different reactions will also be discussed.

**Chapter 3:** This chapter outlines the experimental procedures, different conditions used during the preparations of the nanoparticles, characterization techniques and the application of the cobalt oxide nanoparticles as catalysts for the Fenton-like degradation of methylene blue.

**Chapter 4:** This chapter describes the first part of the results and discussions. The focus of this chapter is on the characterization of the prepared cobalt oxide nanoparticles using different techniques.

**Chapter 5:** This chapter focuses on the catalytic activity studies done for the selected cobalt oxide nanoparticles. The TOF, the rates of degradation of MB, the pseudo first and second order rate constants and the amount of cobalt ions leached are also discussed in this chapter.

**Chapter 6:** This chapter summarizes the findings and concludes the research work presented in this dissertation. Recommendations to be followed from this research are also covered.

# **CHAPTER 1**

## **1.1 INTRODUCTION**

### **1.1.1 Background**

Environmental concerns are found everywhere around the world and pollution has become an increasing problem due to industrialization (Chepape et al., 2017). An approximate estimate of 5-15 percent is released into sewage systems, and is considered a serious threat to human health as well as biotic and abiotic environments (Bhatt et al., 2017, Xu et al., 2011). Moreover, dye pollutants are considered highly toxic, at times carcinogenic and are often resistant to biodegradation or remediation by conventional methods (Xu et al., 2011). Thus, human intervention is required to degrade these pollutants by using oxidation process.

### **1.1.2 Water and environmental concerns**

Water is a limited resource, and industrial growth worldwide results in major water challenges that require alternative means of generating clean water for sustainable growth. Avoiding all types of pollutants from contaminating water cycles is one of the growing environmental concerns. Studies have shown that about 40 percent of the world's population lacks access to clean and purified water resources and death arises from this shortage (Malato et al., 2009). Statistics have shown that a combined amount of about 15 percent is lost during dyeing processes and end up in water streams (Ayodamope and Kidak, 2015). These dyes are mostly used in industry for dyeing processes. The release of dye-containing wastes into streams generates toxic effects such as irritation of the skin (Liotta et al., 2009, Zhu et al., 2013), alters the biological stability of ecosystems Deng et al. (2011) and hinders the transmission of sunlight into streams, which slows down photosynthesis (Ayodamope and Kidak, 2015). These pollutants are produced in large quantities, especially in developed countries. Therefore, oxidation processes that are capable of removing these types of pollutants are required to ensure safe disposal of wastewaters (Bhatt et al., 2017, Wan et al., 2016, Xu et al., 2011).

Various techniques including biological degradation, physical adsorption, and chemical oxidation have been used to remove and lessen the impact of these pollutants on the environment (Wan et al., 2016). However, most of these methods are not efficient and they, in turn, produce secondary pollutants including toxic sludge necessitating further purifications (Bhatt et al., 2017). This way,

it is necessary to use other degradation techniques, such as oxidation treatments that are cost-effective and environmentally friendly. In this regard, Advanced Oxidation Processes (AOPs) like the Fenton process were found to be a promising technology which is effective and environmentally friendly for the degradation of organic pollutants as compared to other conventional methods (Ayodamope and Kidak, 2015, Dutta et al., 2001, Espinosa et al., 2018, Fenton, 1894, Wan et al., 2016, Zhu et al., 2013).

The Fenton process was discovered in 1894, by a scientist, Henry John Horstman Fenton, who reported that hydrogen peroxide ( $\text{H}_2\text{O}_2$ ) could be activated by ferrous ions ( $\text{Fe}^{2+}$ ) to oxidize tartaric acid (Fenton, 1894). The Fenton process is a homogeneous catalytic system where iron (II) ions react with hydrogen peroxide to produce hydroxyl radicals and hydroperoxyl radicals, which then oxidize organic pollutants. However, the Fenton process is found to suffer from drawbacks in the separation and regeneration of homogeneous catalysts (Hu et al., 2017). These drawbacks can be overcome by using heterogeneous catalytic oxidation in the Fenton-like systems, which can also provide the possibility of operating over a broader pH range (Hu et al., 2017). The choice criteria for heterogeneous Fenton-like catalysts are mainly based on the availability, cost and composition of the catalysts. In this study, cobalt oxide nanoparticles were used as heterogeneous Fenton-like catalyst owing to its advantages such as, good catalyst for the activation of  $\text{H}_2\text{O}_2$  into hydroxyl radicals (Costa et al., 2006), cobalt oxide nanoparticles have been reported to be one of the promising materials for effective degradation of organic pollutants (Dhas et al., 2015) and they exhibit high catalytic activity at neutral pHs (Warang et al., 2012). The influence of cobalt oxide nanoparticles size and shape was studied using methylene blue as an organic model.

## **1.2 PROBLEM STATEMENT**

The world-wide high level of production and usage of dyes generates colored wastewaters, which has aroused peoples concern about environmental protection. High amount of effluents from the manufacturing and textile industries are discharged daily into rivers and lakes, altering the biological stability of surrounding ecosystems. Every production line has its own wastewater each with its own composition and, therefore, its own most indicated treatment. If those polluted streams are discharged untreated to the natural resources, serious environmental issues may be encountered. These organic dye pollutants are used in industries for many applications such as dyeing and pharmaceutical products. They possesses many toxic effects including irritation of the skin, and are often considered carcinogenic. These pollutants are aromatic and resistant to degradation and thus chemical methods are required to degrade these pollutants.

Transition metal oxides such as iron oxide and cobalt oxide are used as heterogeneous catalysts to chemically degrade organic pollutants. The particle size and shape play a crucial role in the physical and chemical properties of nano-materials and therefore research is necessary to determine which size and shape will lead to the most active catalyst.

### **1.3 AIMS AND OBJECTIVES**

The main aim of this research project was to study the effect of size and shape of cobalt oxide nanoparticles on the Fenton-like catalytic activity for methylene blue degradation. The objectives of this research project are then described as follows:

- To prepare different shapes of cobalt oxide nanoparticles, which involves the use of cobalt nitrate and cobalt acetate as cobalt sources.
- To prepare different sizes of spherical and cubic shaped cobalt oxide nanoparticles using different amounts of hydrogen peroxide and different reaction times.
- To characterize the prepared cobalt oxide nanoparticles using (XRD, TEM, FTIR spectroscopy, TGA, UV-vis and PL spectroscopy).
- To evaluate the impact of size and shape of cobalt oxide nanoparticles on the catalytic activity of MB.
- To study the effect of size and shape on the amount of cobalt ions leached using oxalic acid.

## 1.4 REFERENCES

- AYODAMOPE, E. O. & KIDAK, R. 2015. Oxidative Degradation of Methylene Blue Using Fenton Reagent. *International Journal of Scientific & Engineering Research* 6, 2229-5518.
- BHATT, C. S., NAGARAJ, B. & SURESH, A. K. 2017. Nanoparticles-shape influenced high-efficient degradation of dyes: Comparative evaluation of nano-cubes vs nano-rods vs nano-spheres. *Journal of Molecular Liquids*, 242, 958-965.
- CHEPAPE, K. F., MOFOKENG, T. P., NYAMUKAMBA, P., MUBIAYI, K. P. & MOLOTO, M. J. 2017. Enhancing Photocatalytic Degradation of methyl blue using PVP-capped and uncapped CdSe nanoparticles. *Journal of Nanotechnology*, 2017, 6.
- COSTA, R. C., LELIS, M., OLIVEIRA, L., FABRIS, J., ARDISSON, J. D., RIOS, R., SILVA, C. & LAGO, R. 2006. Novel active heterogeneous Fenton system based on  $\text{Fe}_{3-x}\text{M}_x\text{O}_4$  (Fe, Co, Mn, Ni): the role of  $\text{M}^{2+}$  species on the reactivity towards  $\text{H}_2\text{O}_2$  reactions. *Journal of Hazardous Materials*, 129, 171-178.
- DENG, H., LU, J., LI, G., ZHANG, G. & WANG, X. 2011. Adsorption of methylene blue on adsorbent materials produced from cotton stalk. *Chemical Engineering Journal*, 172, 326-334.
- DHAS, C. R., VENKATESH, R., JOTHIVENKATACHALAM, K., NITHYA, A., BENJAMIN, B. S., RAJ, A. M. E., JEYADHEEPAN, K. & SANJEEVIRAJA, C. 2015. Visible light driven photocatalytic degradation of Rhodamine B and Direct Red using cobalt oxide nanoparticles. *Ceramics International*, 41, 9301-9313.
- DUTTA, K., MUKHOPADHYAY, S., BHATTACHARJEE, S. & CHAUDHURI, B. 2001. Chemical oxidation of methylene blue using a Fenton-like reaction. *Journal of Hazardous Materials*, 84, 57-71.
- ESPINOSA, J. C., CATALÁ, C., NAVALÓN, S., FERRER, B., ÁLVARO, M. & GARCÍA, H. 2018. Iron oxide nanoparticles supported on diamond nanoparticles as efficient and stable catalyst for the visible light assisted Fenton reaction. *Applied Catalysis B: Environmental*, 226, 242-251.
- FENTON, H. J. H. 1894. LXXIII.—Oxidation of tartaric acid in presence of iron. *Journal of the Chemical Society, Transactions*, 65, 899-910.
- HU, X., LI, R., ZHAO, S. & XING, Y. 2017. Microwave-assisted preparation of flower-like cobalt phosphate and its application as a new heterogeneous Fenton-like catalyst. *Applied Surface Science*, 396, 1393-1402.

- LIOTTA, L., GRUTTADAURIA, M., DI CARLO, G., PERRINI, G. & LIBRANDO, V. 2009. Heterogeneous catalytic degradation of phenolic substrates: catalysts activity. *Journal of Hazardous Materials*, 162, 588-606.
- MALATO, S., FERNÁNDEZ-IBÁÑEZ, P., MALDONADO, M. I., BLANCO, J. & GERNJAK, W. 2009. Decontamination and disinfection of water by solar photocatalysis: recent overview and trends. *Catalysis Today*, 147, 1-59.
- WAN, D., LI, W., WANG, G. & WEI, X. 2016. Size-controllable synthesis of Fe<sub>3</sub>O<sub>4</sub> nanoparticles through oxidation-precipitation method as heterogeneous Fenton catalyst. *Journal of Materials Research*, 31, 2608-2616.
- WARANG, T., PATEL, N., SANTINI, A., BAZZANELLA, N., KALE, A. & MIOTELLO, A. 2012. Pulsed laser deposition of Co<sub>3</sub>O<sub>4</sub> nanoparticles assembled coating: role of substrate temperature to tailor disordered to crystalline phase and related photocatalytic activity in degradation of methylene blue. *Applied Catalysis A: General*, 423, 21-27.
- XU, A., LI, X., YE, S., YIN, G. & ZENG, Q. 2011. Catalyzed oxidative degradation of methylene blue by in situ generated cobalt (II)-bicarbonate complexes with hydrogen peroxide. *Applied Catalysis B: Environmental*, 102, 37-43.
- ZHU, M., MENG, D., WANG, C., DI, J. & DIAO, G. 2013. Degradation of methylene blue with H<sub>2</sub>O<sub>2</sub> over a cupric oxide nanosheet catalyst. *Chinese Journal of Catalysis*, 34, 2125-2129.

## CHAPTER 2

### 2.1 METHYLENE BLUE

One of the organic dyes mostly used in textile industries is methylene blue (MB). Methylene blue is a heterocyclic chemical compound that is aromatic and its molecular formula is shown in Figure 2:1 (Ayodamope and Kidak, 2015, Shahwan et al., 2011). Methylene blue is a cationic dye that absorbs light from 580 to 741 nm and it occurs as a solid dark green powder, which gives a blue solution when dissolved in water. Methylene blue is widely found in dyeing wastewaters and scientists have researched its existence in wastewaters discharged from textile and other industries (Wang et al., 2013). The presence of methylene blue in wastewater can have various harmful effects to human beings and animals (Deng et al., 2011, Wang et al., 2013). Nausea and increased heart rate, skin diseases and irritation to the skin are common health issues encountered (Deng et al., 2011, Mondal et al., 2015). Methylene blue is of high stability and often resistant to degradation by conventional methods (Wang et al., 2013). Methylene blue can have various species with different absorption maxima depending on temperature, pH, and concentration (see Table 2:1).

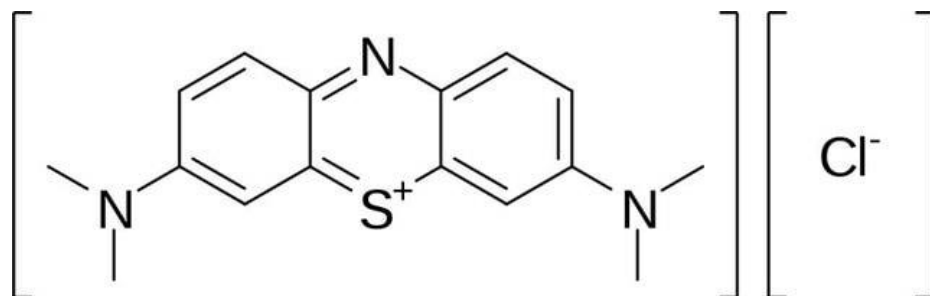


**Figure 2:1** Molecular structure of methylene blue (Ayodamope and Kidak, 2015)

**Table 2:1** Absorption species of Methylene blue (Ayodamope and Kidak, 2015)

Species	Absorption peak	Extinction coefficient ( $\text{dm}^3/\text{mole}\cdot\text{cm}$ )
$\text{MB}^+$ (solution)	664	95000
$\text{MBH}_2^+$ (solution)	741	76000
$(\text{MB}^+)_2$ (solution)	605	132000
$(\text{MB}^+)_3$ (solution)	580	110000

Methylene blue (MB) is a compound that is very important because of its various uses in areas such as biology and chemistry. It is used in industries for dyeing cotton, wood and silk (Deng et al., 2011). It is also used during the manufacturing of paper and for leather treatment (Ayodamope and Kidak, 2015). Methylene blue has disinfectant properties which are useful for medicinal applications (Ayodamope and Kidak, 2015). Its uses also include being an antidote for cyanide poisoning in humans, antiseptic in veterinary medicine and most commonly *in-vitro* diagnostic in biology, cytology, haematology and histology (Shahwan et al., 2011).

## 2.2 TECHNIQUES FOR WASTEWATER REMOVAL

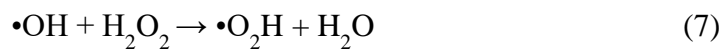
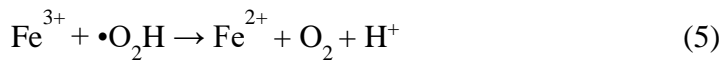
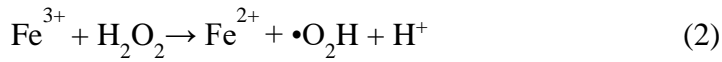
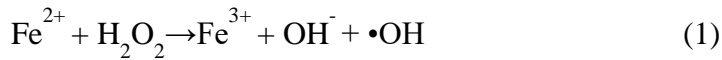
Many methods have been developed for the removal of dye pollutants from industrial effluents or wastewater like biological, physical, and chemical methods (Wang et al., 2016, Zhu et al., 2013, Wan et al., 2016). Biological treatments are cost-effective, proven technology, but their applications have been restricted due to the resistance of many organics to biodegradation and toxicity in microbial processes (Dutta et al., 2001). Physical methods such as liquid-liquid extraction and adsorption (Zhu et al., 2013) are ineffective for pollutants which are not readily absorbable, and they transfer the pollutants to other secondary pollutants rather than destroying them completely (Dutta et al., 2001). Therefore the usage of Fenton reaction and electrochemical degradation techniques were found to be effective and environmentally friendly in treating effluents containing methylene blue and any other dye molecule (Wan et al., 2016, Wang et al., 2013). Typical reaction conditions are room temperature and atmospheric pressure (Zhu et al., 2013).

The use of the homogeneous Fenton process has been widely applied because iron ions are cheap and have low toxicity. Some advantages of the homogenous Fenton process compared to other oxidation techniques are that it needs simple installations and mild operating conditions (Ayodamope and Kidak, 2015). However, despite the simplicity and cost-effectiveness of this method, the toxic iron sludge produced after the reaction has limited its practical applications. The generated toxic sludge can create another environmental health concern (Wang et al., 2013, Warang et al., 2013). Considering the limitations of homogenous Fenton catalysts, there is a focus shift towards the heterogeneous Fenton-like catalyst using solid transition metal oxides like iron oxide and cobalt oxide nanoparticles. Solid catalysts are considered better catalysts over homogeneous catalysts because of easy separation after the reaction and recyclability.

Hydrogen peroxide is an environmentally benign oxidizing agent since it decomposes into oxygen and water (Zhu et al., 2013). Although hydrogen peroxide is relatively costly, the oxidation process using  $H_2O_2$  as an oxidizing agent is advantageous in comparison to processes that use gaseous oxygen (Liotta et al., 2009). The main advantage of  $H_2O_2$  is that it is a common reactant in wastewater when using oxidative treatments and it acts as a free-radical initiator providing hydroxyl and peroxy radicals that promote the degradation of organic pollutants at mild conditions such as pressure and temperature (Liotta et al., 2009).

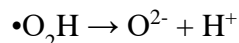
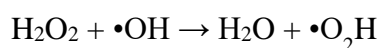
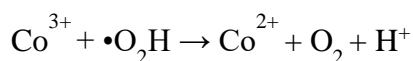
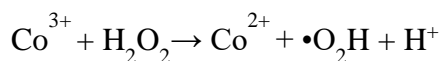
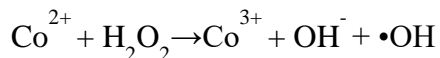
The importance of  $\bullet OH$  radicals have been shown by more than 1700 rate constants for  $\bullet OH$  radical reactions with organic and inorganic compounds in the past few decades (Ayodamope and Kidak, 2015). The Fenton mechanism involved in the generation of hydroxyl radicals is shown below by equations (1) to (10). Equation (1) is recognised as the Fenton reaction and this signifies the oxidation of ferrous to ferric ions to decompose  $H_2O_2$  into hydroxyl radicals. The  $\bullet OH$  radicals are the main reactants in the process capable of degrading a number of organic pollutants by oxidation. The reduction of the produced ferric ions can be slowed down by reacting with more hydrogen peroxide to produce again ferrous ion and more or excess radicals as shown in Equation (2). This reaction is called a Fenton-like reaction, which is much slower than the Fenton reaction and allows ferrous salt ( $Fe^{2+}$ ) to be regenerated in an efficient cyclic mechanism. In a Fenton-like reaction, aside from ferrous ion regeneration, hydro-peroxy radicals ( $\bullet O_2H$ ) are formed. The hydro-peroxy radicals may attack organic pollutants, but hydroxyl radicals are less sensitive to it. However, it

should also be noted that the iron added in small amounts acts as a catalyst while H<sub>2</sub>O<sub>2</sub> is continuously used up to produce and generate hydroxyl radicals. Equations (2) to (5) characterize the rate limiting steps in the Fenton chemistry since hydrogen peroxide is consumed and ferrous iron is recovered from ferric ion through these reactions. Furthermore equations (6) to (9) were said to have occurred during the Fenton process and they are radical–radical reactions or hydrogen peroxide–radical reactions. Breaking down of hydrogen peroxide to molecular oxygen and water occurs in the presence or absence of any organic molecule to be oxidized as shown in Equation (10). This reaction leads to a loss of bulk oxidant and thus an unnecessary increase in treatment cost. Equations (1) to (9) show that the Fenton process follows a complex mechanism. The chain initiation reaction activates the occurrence of the creation of the desired hydroxyl radical, however, hydroxyl radicals can be poached by ferrous ions (Equation (3)), hydrogen peroxide (Equation (7)), hydro-peroxyl radicals (Equation (9)), and or even may be auto scavenged (Equation (6)). The foregoing analysis shows that hydrogen peroxide (H<sub>2</sub>O<sub>2</sub>) may act both as radical generator (Equation (1)) and as scavenger (Equation (7)). Hydroxyl radicals may attack organic radicals generated by organics present in the wastewater. Those radicals react with ferrous and ferric ions, as indicated in the equations below. The Fenton process can occur at room temperature and atmospheric pressure. Furthermore, reagents needed are readily available and they are easy to store and handle, it is safe and they do not cause any damage to the environment.





The formation of OH radicals by the reaction between  $\text{Co}^{2+}$  and  $\text{H}_2\text{O}_2$  have also been reported in literature by Hu et al. (2017) and the following reaction mechanism was proposed:



Dutta et al. (2001) indicated that 98 % of the dye could be removed in one hour in an aqueous solution using a Fenton-like reaction. Shahwan et al. (2011) and Wan et al. (2016) carried out a study to use  $\text{Fe}_3\text{O}_4$  nanoparticles as a catalyst and  $\text{H}_2\text{O}_2$  as an oxidant for the degradation of cationic and anionic dye and the results showed complete degradation of the dyes. Long et al. (2012) reported a complete degradation of methylene blue to  $\text{CO}_2$  and  $\text{H}_2\text{O}$  using cobalt oxide nanoparticles and  $\text{H}_2\text{O}_2$ . Zhu et al. (2013) reported that a high conversion rate of methylene blue could be obtained efficiently by the combination of  $\text{CuO}$  nano-sheets and  $\text{H}_2\text{O}_2$  as an oxidant. Complete photo-Fenton degradation of MB has been reported by Warang et al. (2013) using  $\text{Co}_3\text{O}_4$  nanoparticles coated on thin films as catalysts and  $\text{H}_2\text{O}_2$ . Wang et al. (2013) used ferrocene as a heterogeneous Fenton-like catalyst to degrade methylene blue. The degradation pathway of methylene blue is shown in Figure 2:2 (Hu et al., 2017). Organic acids like oxalic acid is produced during the degradation of methylene blue. The results of George and Anandhan (2015b) indicated that the cobalt oxide nano-fibers were efficient in degrading methylene blue and methyl orange. It was further realized from the literature that the activation of hydrogen peroxide by heterogeneous catalyst plays an important role in the oxidation of organic pollutants. Hence the focus of this study was to investigate the catalytic properties on the degradation of organics.

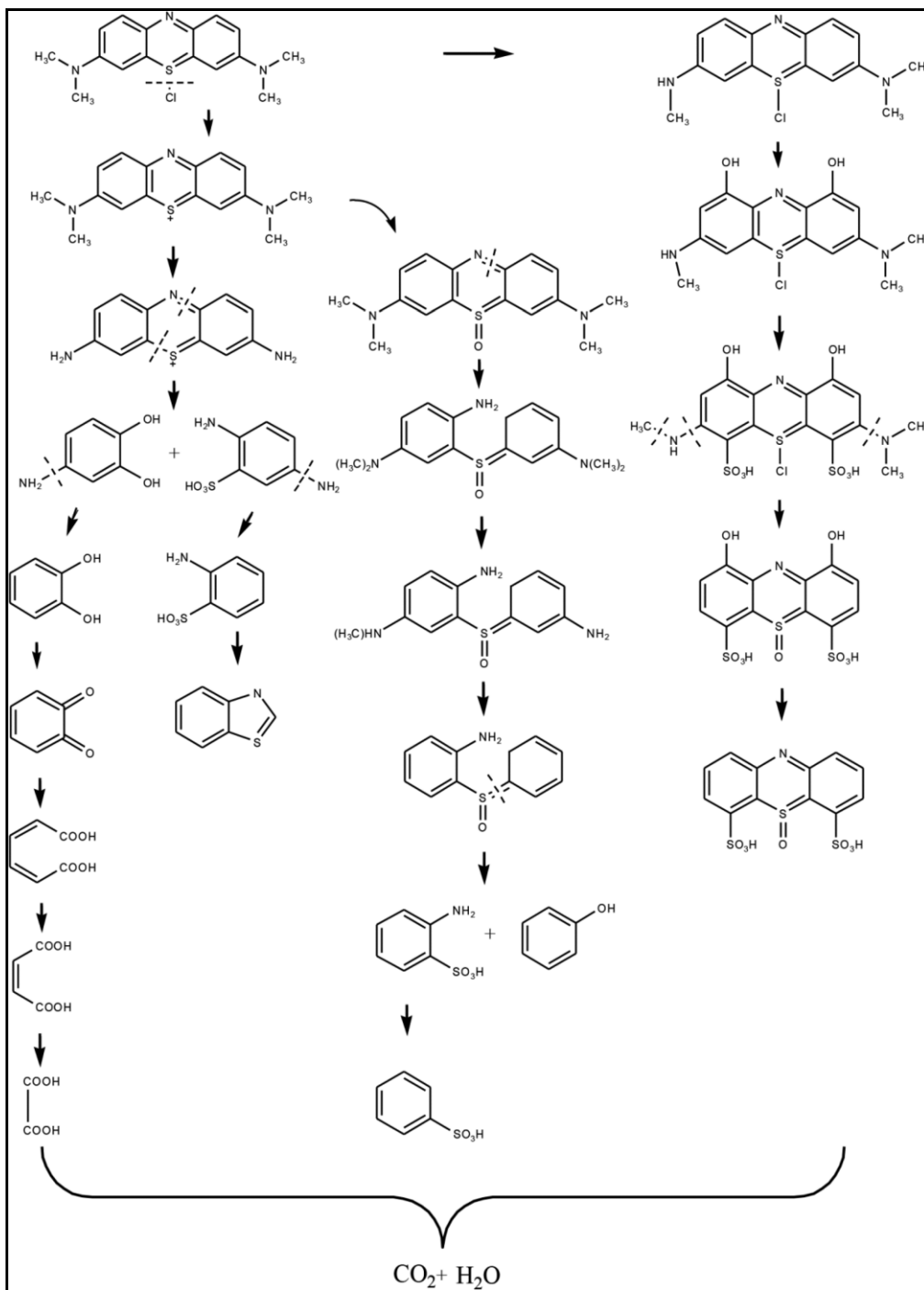


**Figure 2:2** Proposed degradation pathway of methylene blue using Fenton-like process (Hu et al., 2017).

## **2.3 CATALYST DEACTIVATION**

### **2.3.1 General heterogeneous catalytic deactivation mechanisms**

Deactivation of heterogeneous catalysts is a problem that results in the loss of activity of the catalyst with time. When solid catalysts are used to catalyze the Fenton-like process, they present the advantage of being easily recovered. Some catalysts keep their activity and can still be reused several times with the same efficiency. However, a major problem associated with these catalytic systems derives from the deactivation of the catalyst. The deactivation of the catalyst depends greatly on the catalytic systems used and it varies from seconds (in the case of fluid catalytic cracking) to years (Argyle and Bartholomew, 2015). Not only can these catalysts lose their activity but also the high cost of regeneration is encountered. Therefore, it is important to understand factors that lead to the deactivation of the catalyst and develop more catalysts that are resistant to deactivation for some time. Argyle and Bartholomew (2015) classify deactivation of heterogeneous catalysts into three main groups: chemical, thermal, and mechanical deactivation. The main groups can further be divided into more mechanisms which are (a) poisoning, (b) fouling, (c) thermal degradation, (d) vapour compound formation and/or leaching accompanied by transport from the catalyst surface or particle, (e) vapour–solid or solid–solid reactions and (f) attrition/crushing. Thermal deactivation may cause sintering leading to active phase crystallite growth formation of volatile oxides or chlorides of the active phase (Argyle and Bartholomew, 2015).

### **2.3.2 Catalyst deactivation during the Fenton reaction**

Santos et al. (2005) reported that the deactivation of the catalyst on the ozonation of phenol was attributed to the following factors: (a) leaching of metal ion species, (b) formation of carbonaceous deposits that can reduce the specific surface area of the catalyst and (c) poisoning of the catalyst by strong adsorption of intermediate products and complexation of active sites with acid organic compounds, preventing its reactivity with other reactants.

Catalytic leaching is when the metal ions from the support material are released due to the dissolution of minerals and complexation processes (Forzatti and Lietti, 1999). For example, the increase of oxalic acid concentration, which is the intermediate of phenol and MB oxidation,

increases iron leaching (Argyle and Bartholomew, 2015). According to Lu et al. (2015), an acidic aqueous solution may remove the active component from the surface of the catalyst.

Studies have shown that cobalt oxide clusters, which are attached to the support by the weak Van der Waals bonds, are easily leached out into the liquid phase during reaction, whereas the cobalt cations that are incorporated inside the support, which are bonded by the covalent bonds, are stable towards leaching (Crowther and Larachi, 2003). Therefore, an increase in the metal oxide-support interaction will lead to a decrease in leaching. The thermal treatment of 900 °C improved the resistance to leaching of the catalyst by increasing metal oxide-support interaction and reducing leaching. The pre-treatment with acids improved the stability of the Fe<sub>2</sub>O<sub>3</sub> /Al<sub>2</sub>O<sub>3</sub> catalyst, reducing the leaching more for catalyst treated with oxalic acid compared to the one with acetic acid (Di Luca et al., 2014). The research findings of Lu et al. (2015), indicated that the decrease in the rate of phenol oxidation was due to the formation of surface organometallic compounds by carboxylic acid and the iron oxide. The calcination temperature of 200 °C was found to be the optimum temperature responsible for desorbing the carboxylic compounds, regenerating the catalyst.

Leaching during catalysis results in four effects, namely (a) homogenous catalysts by the dissolved metal ions (b) the implementation of an additional step like membrane separation or precipitation to remove the leached metal (c) continuous leaching of catalyst resulting in catalyst deactivation and (d) the pollution of the environment (Forzatti and Lietti, 1999). It is thus important to develop active heterogeneous catalysts with minimized leaching. In this research, the amount of cobalt ions leached will be monitored on different sizes and shapes of cobalt oxide nanoparticles using oxalic acid.

## **2.4 RELATIVE ACTIVITY OF TRANSITION METAL NANOPARTICLES**

Heterogeneous Fenton-like catalysts have been studied widely in recent years and are considered promising catalysts for organic wastewater treatment (Wang et al., 2016). In this study, cobalt oxide nanoparticles were used as a heterogeneous Fenton-like catalyst owing to its advantage of being a good catalyst to activate hydrogen peroxide into hydroxyl radicals (Costa et al., 2006) and it exhibits high catalytic activity at neutral pHs (Warang et al., 2012). The hydrogen peroxide

decomposition studies in the presence of  $\text{Co}_3\text{O}_4$  and  $\text{Fe}_3\text{O}_4$  nanoparticles have been reported by Costa et al. (2006). The results showed that the  $\text{Co}_3\text{O}_4$  nanoparticles were more active with high decomposition rate constant of 0.039 mmol/min as compared to the  $\text{Fe}_3\text{O}_4$  nanoparticles with a decomposition rate constant of 0.008 mmol/min.

Huang et al. (2015) indicated that the greatest total organic carbon (TOC) removal rate was higher for cobalt supported on the activated carbon (AC) than other metals (Fe, Ni, and Mn) supported on activated carbon. Recent reports have demonstrated that cobalt oxide has outperformed similar metal oxides like iron oxide in the catalytic degradation of toluene (Huang et al., 2015). The performances of the  $\text{Co}^{2+}$  system exhibits higher decolourisation efficiency of MB than the  $\text{Fe}^{2+}$  system (George and Anandhan, 2015a). The redox potential of the supported metal ions and the stability of the metal complexes indicates the catalytic activity of the catalysts, hence the following reactivity sequence  $\text{Cu}^{2+} > \text{Co}^{2+} > \text{Mn}^{2+} > \text{Fe}^{3+} > \text{Ni}^{2+}$  has been reported (Salem and El-Maazawi, 2000).

#### **2.4.1 Heterogeneous oxidation catalysts**

Catalytic processing has played an important role in the production of industrial chemicals and derivatives for the past years. The majority of these processes involve heterogeneous catalysts, consisting of transitional metal oxides or metals supported on suitable inorganic oxides (Barkhuizen et al., 2006). Heterogeneous catalysts are considered better catalysts than homogeneous catalysts because of their separation and recyclability after the reaction (Warang et al., 2013, Zhu et al., 2013).

## **2.5 EFFECT OF SIZE AND SHAPE OF NANOPARTICLES ON THE CATALYTIC ACTIVITY**

It is well known that the activity of the catalyst is strongly related to the size and shape of a nanomaterial (Xie and Shen, 2009). A few examples will be discussed to demonstrate the effect of shape and size on the performance of the catalyst.

### **2.5.1 Influence of size**

The influence of nanoparticles size on various catalytic reactions such as hydrocarbon oxidation, Fischer-Tropsch synthesis, methane conversion and Fenton oxidation reactions are of great interest (Dong et al., 2007, Hu et al., 2008, Wan et al., 2016, Warang et al., 2012). The catalytic activity is expected to increase with a decrease in the particles size due to the higher surface area, which results from the smaller nanoparticles; however, the decrease in the size of the nanoparticle may decrease the higher dispersion and more active sites of the catalysts. For example, in the case of the Fischer-Tropsch synthesis, the active phase oxidizes becoming inactive below a certain particle size (Bezemer et al., 2006). Van Steen et al. (2005) has studied the stability of nanocrystal materials and reported that the cobalt crystallines of diameter less than 4.4 nm are likely to be oxidised in Fischer-Tropsch synthesis. Dong et al. (2007), proposed that the nanoparticles size plays a crucial role in the activity of the catalyst. When comparing the  $\text{Co}_3\text{O}_4$  nanoparticles average sizes between 3.5 nm to 70 nm in their Fenton-like reaction. They showed that the catalytic activity for ozonation of phenol was much higher for  $\text{Co}_3\text{O}_4$  nanoparticles than bulk  $\text{Co}_3\text{O}_4$  and the activity further increased with a decrease in the cobalt oxide spherical nanoparticle size from 70 nm to 3.5 nm (Dong et al., 2007). Li et al. (2011) observed high activity for the photocatalytic oxidation of black dye which increased when the  $\text{Co}_3\text{O}_4$  nanorods size decreased from 35 to 15 nm. The electrocatalytic activity for the reduction of  $\text{H}_2\text{O}_2$  increased when the cobalt nanoparticle's size was decreased from about 300 nm to about 30 nm (Song et al., 2011). The  $\text{Co}_3\text{O}_4$  nanoparticles of 18 nm outperformed the 38 nm particles on the photo-degradation of MB (Warang et al., 2013). Wan et al. (2016) prepared different sizes of  $\text{Fe}_3\text{O}_4$  nanoparticles in the range of 30 to 600 nm and evaluated their catalytic activity on the degradation of rhodamine B. Like Dong et al. (2007), the catalytic activity of their results showed an increase with a decrease in the size of the nanoparticles and they concluded that higher catalytic activity of the smallest  $\text{Fe}_3\text{O}_4$  nanoparticles mainly originated from the higher surface area on the smallest nanoparticles that expose more active sites

for the adsorption of the pollutant on the surface of the catalyst. It was further realised from the above literature that different sizes of nanoparticles could be used as potential catalysts for the degradation of organic pollutants. It is well accepted that the particle size of cobalt oxide nanoparticles has a strong effect on their catalytic properties (Dong et al., 2007). An active catalyst consists of small nanoparticles because of an increase in the number of corners and edge atoms for adsorption and activation of the reactants (Xie and Shen, 2009). The particle size of  $\text{Co}_3\text{O}_4$  NPs is generally controlled during their preparations. Therefore it is important to develop a preparation method that gives cobalt oxide nanoparticles size in the range of 3-50 nm at a high yield to study the Fenton-like oxidation activity as a function of size. Larger size nanoparticles are not considered for catalysis due to their low surface area.

### **2.5.2 Influence of shape**

The field of nano-catalysis (in which nanoparticles are used to catalyze different reactions) has been studied lately. The shape of the nanoparticle plays a crucial role in the activity of the catalyst. This is because nanoparticle of different shapes have different facets that could reflect different reactivity's or binding configurations (Bhatt et al., 2017, Hu et al., 2008, Narayanan and El-Sayed, 2004, Xie and Shen, 2009). Several works have already demonstrated the importance of well-defined shape in enhancing catalytic reactivity.

Narayanan and El-Sayed (2004) studied the influence of the shape of Pt nanoparticles (tetrahedral, cubic and spheres) on the reaction kinetics of the electron-transfer reaction between hexacyanoferrate (III) ions and thiosulfate ions in a colloidal solution and found that the cubic Pt nanoparticles showed a higher catalytic activity than the tetrahedral and spherical nanoparticles. Xu et al. (2006) reported that the silver nanocubes exposing more reactive planes show much higher activity than the near-spherical nanoparticles and nanoplates in the oxidation of styrene. Lai et al. (2008) investigated the shape influence of  $\text{Co}_3\text{O}_4$  nanoparticles on the ozonation of phenol and showed that the  $\text{Co}_3\text{O}_4$  nano-rods exhibited a higher catalytic activity than the  $\text{Co}_3\text{O}_4$  nanoparticles. The high index {112} crystal planes of  $\text{Co}_3\text{O}_4$  nano-sheets are more reactive than the {011} planes for methane combustion as reported by Hu et al. (2008). The catalytic activity for methane oxidation using cobalt oxide nano-sheets with {112} surfaces was higher than that for nano-rods with {110} surface planes and nano-cubes with {100} surfaces (Xie and Shen, 2009).

Xie and Shen (2009) have also demonstrated that the  $\text{Co}_3\text{O}_4$  nano-rods are highly active for the low-temperature oxidation of CO when compared to the  $\text{Co}_3\text{O}_4$  nano-spheres and this was attributed to the fact that the nano-rods preferentially expose the {110} plane while the nano-spheres exposed the {111} and {001} planes. Cobalt oxide nanoflowers had a better catalytic activity for the oxidation of gaseous phenol by oxygen than cobalt oxide cubes (Yan et al., 2012).  $\text{Co}_3\text{O}_4$  nano-rods with surfaces {110} were more active than nanoparticles with {100} and {111} surfaces for the catalytic reduction of nitrogen oxides by ammonia (Meng et al., 2013). Cubic-shaped gold nanoparticles showed high performance in comparison to nano-rods and nano-sphered nanoparticles when they were used to catalyze the degradation of organic dyes (Bhatt et al., 2017). It was further realised from the literature that different shapes of nanoparticles can be used as potential catalysts for the degradation of organic pollutants; the current study was then aimed at investigating the catalytic activity of different sizes and shapes of cobalt oxide NPs on the degradation of MB.

### **2.5.3 Turn over frequency (TOF)**

The turn over frequency (TOF) which is defined as the total number of moles of methylene blue (MB) converted into the desired product by one mole of per surface cobalt atom per minute, is independent for structure-insensitive reactions on the particle size of the catalytically active material and greatly dependent for structure-sensitive reactions on the particle size of the catalytically active material (Bezemer et al., 2006). For example, Boudart and McDonald (1984) reported that multiple atom sites or ensembles are required for structure-sensitive reactions to show activity. Different sizes of iron nanoparticles were prepared in the range of 1 to 17 nm, and their effect on Fischer-Tropsch Synthesis (FTS) experiments showed a decrease in TOF rate with decreasing crystallite size for methane formation. The Fischer-Tropsch reaction catalyzed by cobalt requires the B5 and B7 sites which are not accommodated by the smallest nanoparticles as proposed by Van Helden et al. (2016). Van Helden et al. (2016) reported that the site fraction of step sites increases with increasing the nanoparticle size for cubic shaped cobalt particles. This can suggest that one (or more) of these sites are primarily responsible for the reactivity of the metal particle. If the proportion of this site in the composition decreases (corresponding to a decrease in the absolute number of this site on a particle) then the TOF of the particle will also decrease (Van Helden et al., 2016). Bezemer et al. (2006), as well as (Prieto et al., 2009), observed a decrease in

TOF with a decrease in the particle size. Van Santen (2010) hypothesised that the effect of nanoparticle size would only be observed below a size of 15 nm for cobalt nanoparticles on the activation of CO. At the size range of 15 nm, the surfaces of larger metallic cobalt particles are hypothesised to reconstruct to form islands, therefore, displaying a similar TOF at steady state.

For Fenton-like reactions, several works have been published about the influence of nanoparticle size on the activity. Typically, TOF for heterogeneous and homogeneous catalysts are calculated using per surface cobalt atom and per total moles of cobalt respectively. The data of Espinosa et al. (2018) was used to calculate the TOF in two ways, using the total moles of iron and the moles of iron on the surface. Figure 2:3 shows the TOF calculated using two methods. The TOF calculated using per surface iron atom decreases with a decrease in size of the nanoparticles, while that calculated using per total moles of iron increases with a decrease in size of the nanoparticles (see Figure 2:3). In heterogeneous catalysis, the preferred method for calculating TOF is using per surface iron atom since the activity of the catalyst happens on the surface of the iron oxide nanoparticles.

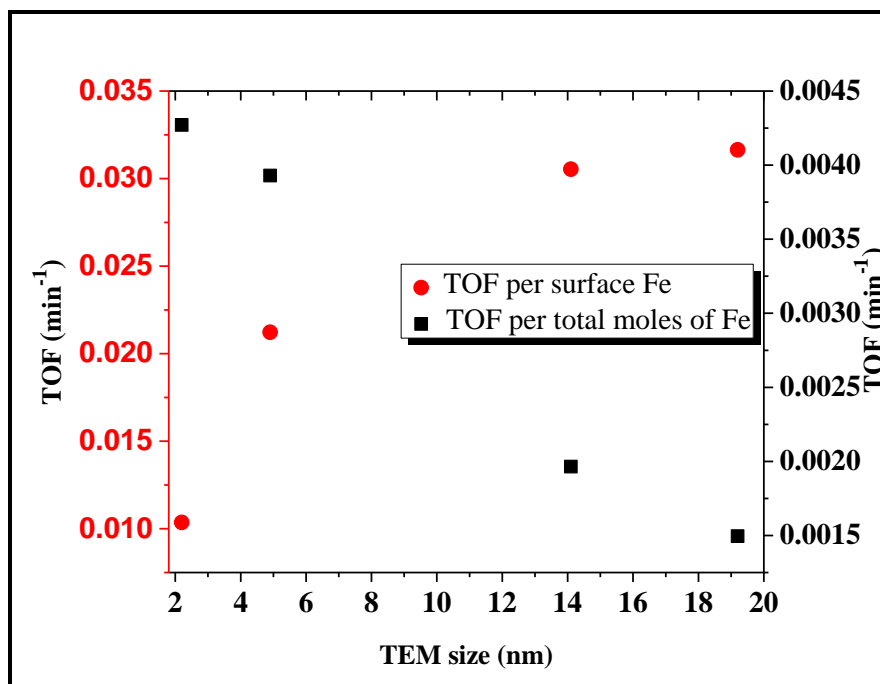


**Figure 2:3** TOF results calculated from the data of Espinosa et al. (2018).

Dong et al. (2007) synthesized different sizes of cobalt oxide nanoparticles in the range of 3.5 to 70 nm and evaluated their activity for ozonation degradation of phenol. The TOF of their results showed a decrease in TOF with a decrease in the nanoparticles size, when recalculated using their data (see Figure 2:4A). The results of Wan et al. (2016) in Figure 2:4B also shows a decrease in TOF with a decrease in iron oxide nanoparticles in the size range of 30 to 600 nm for Fenton-like reaction using rhodamine B as a model molecule. Wan et al. (2016) and Espinosa et al. (2018) used spherical shaped iron oxide nanoparticles with different sizes for the Fenton-like reaction, whereas in this work cubic and spherical cobalt oxide nanoparticles were used. The smallest size Wang et al. (2016) tested was 30 nm. One can argue that smaller size is of more interest since deviations normally occur below about 15 nm (Van Santen et al., 2010), as observed in other reactions like the Fischer Tropsch reaction. Espinosa et al. (2018) has tested very small sizes but it was supported nanoparticles which may complicate the system due to metal oxide support interactions as well as mass transfer limitations during the reaction. Dong et al. (2007) has tested spherical particles down to 3.5 nm for the ozonation reaction and in this work spherical as well as cubic shaped cobalt oxide nanoparticles of different sizes were used as catalysts for the Fenton-like degradation of methylene blue.

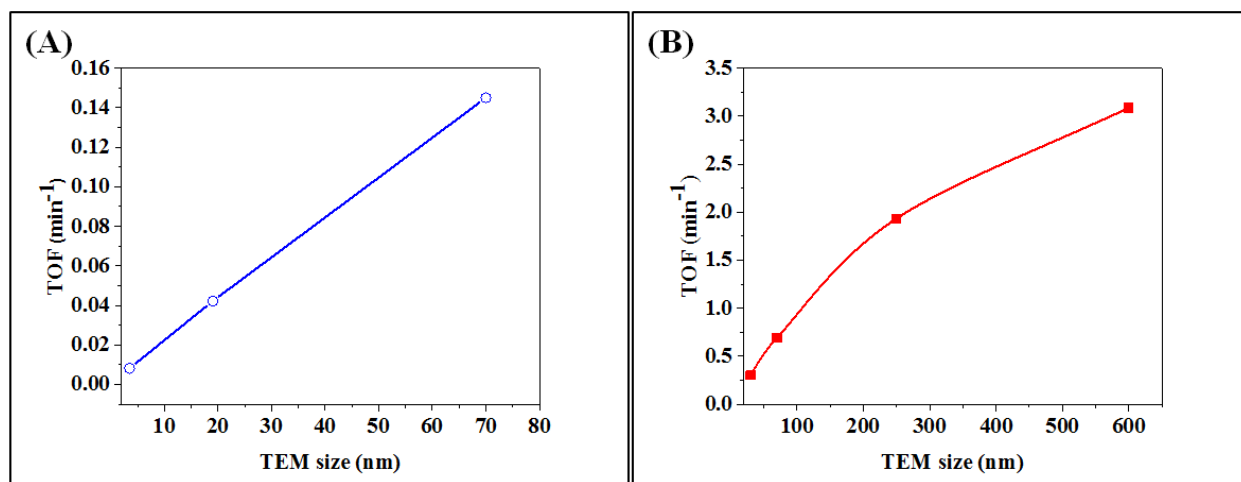


**Figure 2:4** TOF results calculated using the data of (A) Dong et al. (2011) and (B) Wan et al. (2016).

Most published studies, which report a change of TOF with a change in the nanoparticle size report a lower TOF for the smallest particles in comparison to the larger particles. This particular hypothesis was derived based on ensemble theory in catalysts regarding the size-dependent reactivity. The hypothesis says that the activity of the catalyst depends on the availability of specific surface atoms (sites) and that the number of these sites decreases as the size of the particle decreases (Van Helden et al., 2016). The exact origin of the observed size effect is still under investigation. Therefore, the following main effects have been proposed to occur:

- Structural effect: At different metal crystallite sizes different surface sites are exposed leading to different activities and selectivity (Claeys et al., 2000).
- Electronic effect: At smaller crystallite sizes the activation energy for the dissociation of hydrogen is favored over that of carbon monoxide resulting in changes in selectivity (Radstake et al., 2009).
- Oxidation effect: Smaller crystallites are easily re-oxidized under Fischer-Tropsch conditions leading to changes in activity due to a loss in the active material (Swart, 2008).

## **2.6 CATALYST PREPARATION METHODS**

To be able to study the effect of size, a narrow size distribution is required within the nanometer range. The required optimum sizes depend on the condition at which these particles are prepared. Classical synthesis methods like impregnation and hydrothermal, often result in a wide size distribution of the particles and controlling the size distribution to obtain the smallest size is often difficult to achieve. Thus, preparative methods such as precipitation oxidation methods have been developed to produce different shapes and sizes of nanoparticles without the use of complex capping molecules. In this study, unsupported  $\text{Co}_3\text{O}_4$  nanoparticles of different shape and sizes will be used as catalysts.

### **2.6.1 Cobalt oxide nanoparticles (unsupported catalyst) preparation methods**

There are challenges concerning the preparation of nanoparticles because they tend to grow larger during their synthesis. To prevent this, capping agents are used. These capping agents influence the shape and size of the nanocrystals since the challenge is not only to control the size but also the shape of these nanocrystals.

Various methods to synthesize  $\text{Co}_3\text{O}_4$  nanoparticles have been reported including one-pot synthesis (Xu and Zeng, 2004), liquid-phase redox process (He et al., 2005), hydrothermal method (Song et al., 2011, Yang et al., 2007b), chemical co-precipitation method (Sarfraz and Hasanain, 2014) and green synthesis method (Bibi et al., 2017). The precipitation oxidation method is considered simple, most efficient and environmentally friendly to obtain nanoparticles (Wan et al., 2016). When  $\text{Co}_3\text{O}_4$  nanoparticles are to be used as catalysts, complex capping molecules are not desired since the capping molecules can lead to a decrease in the activity of the catalyst due to stronger adsorption on the surface of the catalyst. Thus, this study prepared  $\text{Co}_3\text{O}_4$  nanoparticles of different sizes and shapes without the use of capping molecules.

The shape of cobalt oxide nanoparticles can be affected by capping molecules, changing the anion in the cobalt source and high amount of sodium hydroxide.  $\text{Co}_3\text{O}_4$  nanoparticles with cubic shapes between 3.5-5.7 nm were formed when Tween-85, polyoxyethylene (20) sorbitan trioleate was used as a capping molecule (Xu and Zeng, 2004). They proposed that TWEEN-85, which is an ester, was hydrolyzed forming a carboxylate ion (oleate ion) which adsorbed on the cobalt oxide surface. Cubic shaped cobalt oxide nanoparticles of about 18 nm were also obtained when cobalt acetate was used instead of cobalt nitrate (Yang et al., 2007a). The use of high amounts of sodium nitrate salt is required in order to obtain cobalt oxide nano-cubes from cobalt nitrate. Xia et al. (2014) prepared cobalt oxide nanoparticles using cobalt nitrate and sodium hydroxide. The results of their experiments showed that the shape of the cobalt oxide nanoparticles depended strongly on the amount of the two chemicals used. When the amount of cobalt nitrate was increased and sodium hydroxide kept constant, the shape of cobalt oxide changed from cubes to spheres. The influence of acetate ions on the size and shape of cobalt oxide nanoparticles in the form of acetic acid has been reported in the literature by Viljoen et al. (2017). Their results showed that the nanoparticles made from cobalt acetate were cubic in shape in contrast to the spherical nanoparticles prepared using cobalt nitrate and a mixture of cobalt nitrate and acetic acid. Therefore, it may be deduced from the results of (Viljoen et al., 2017, Xu and Zeng, 2004, Yang et al., 2007a) that cubic cobalt oxide nanoparticles can thus be produced in the presence of carboxylate ions using a precipitation-oxidation method.

The particle size of cobalt oxide nanoparticles can be controlled by varying different parameters such as oxidizing agent ( $\text{H}_2\text{O}_2$ ), time, temperature and ethanol content during their preparations. Various size of cobalt oxide nanoparticles have been obtained by varying different amounts of a stronger oxidizing agent, such as  $\text{H}_2\text{O}_2$ , during their preparation (Amiri et al., 2011, Song et al., 2011, Yang et al., 2007b, Zhang et al., 2007). Theoretically, a molar ratio of  $\text{H}_2\text{O}_2$  to  $\text{Co}^{2+}$  of 0.33:1 is required to form  $\text{Co}_3\text{O}_4$ . However, Yang et al (2007a) indicated that experimentally a molar ratio of  $\text{H}_2\text{O}_2$  to  $\text{Co}^{2+}$  above 2.5:1.0 is required to form only  $\text{Co}_3\text{O}_4$  since  $\text{H}_2\text{O}_2$  is lost due to decomposition. The research findings of Amiri et al (2011) indicated that a molar ratio of  $\text{H}_2\text{O}_2$  to  $\text{Co}^{2+}$  of 20:1 is required (assuming a  $\text{H}_2\text{O}_2$  concentration of 30%) to form only  $\text{Co}_3\text{O}_4$ . Dong et al. (2007) used ammonia and  $\text{Co}(\text{CH}_3\text{COO})_2 \cdot 4\text{H}_2\text{O}$  as starting materials and spherical  $\text{Co}_3\text{O}_4$  nanoparticles with an average size of (3.5, 6, 11, 19 and 70 nm) were obtained through adjusting the ethanol amount in the solvent (the ratio of ethanol to water) or the concentration of raw materials. Spherical  $\text{Co}_3\text{O}_4$  nanoparticles that lie between 13 and 45 nm were formed by annealing in a tube furnace at different temperatures (Sarfranz and Hasanain, 2014). Average particle size of 25.6 nm was found when cobalt oxide nanoparticles were synthesized without using any capping agents.

High molar ratio of  $\text{H}_2\text{O}_2$  and temperature are also needed to prepare pure cobalt oxide nanoparticles and to increase the yield of the nanoparticles. A high reaction temperature of  $150^\circ\text{C}$  or higher is also required to eliminate the cobalt hydroxide like species and to form only  $\text{Co}_3\text{O}_4$  (Jiang et al., 2002, Yang et al., 2007b, Zhang et al., 2007). Therefore, when a low molar ratio of  $\text{H}_2\text{O}_2$  to  $\text{Co}^{2+}$  and low temperature are used, the unreacted cobalt hydroxide-like species need to be dissolved with diluted hydrochloric acid to obtain only the  $\text{Co}_3\text{O}_4$  phase.

## 2.7 REFERENCES

- AMIRI, S. H., VAEZI, M. & KANDJANI, A. E. 2011. A comparison between hydrothermally prepared  $\text{Co}_3\text{O}_4$  via  $\text{H}_2\text{O}_2$  assisted and calcination methods. *Journal of Ceramic Processing Research*, 12, 327-331.
- ARGYLE, M. D. & BARTHOLOMEW, C. H. 2015. Heterogeneous catalyst deactivation and regeneration: a review. *Catalysts*, 5, 145-269.
- AYODAMOPE, E. O. & KIDAK, R. 2015. Oxidative Degradation of Methylene Blue Using Fenton Reagent. *International Journal of Scientific & Engineering Research* 6, 2229-5518.
- BARKHUIZEN, D., MABASO, I., VILJOEN, E., WELKER, C., CLAEYS, M., VAN STEEN, E. & FLETCHER, J. C. 2006. Experimental approaches to the preparation of supported metal nanoparticles. *Pure and Applied Chemistry*, 78, 1759-1769.
- BEZEMER, G. L., BITTER, J. H., KUIPERS, H. P., OOSTERBEEK, H., HOLEWIJN, J. E., XU, X., KAPTEIJN, F., VAN DILLEN, A. J. & DE JONG, K. P. 2006. Cobalt particle size effects in the Fischer–Tropsch reaction studied with carbon nanofiber supported catalysts. *Journal of the American Chemical Society*, 128, 3956-3964.
- BHATT, C. S., NAGARAJ, B. & SURESH, A. K. 2017. Nanoparticles-shape influenced high-efficient degradation of dyes: Comparative evaluation of nano-cubes vs nano-rods vs nano-spheres. *Journal of Molecular Liquids*, 242, 958-965.
- BIBI, I., NAZAR, N., IQBAL, M., KAMAL, S., NAWAZ, H., NOUREN, S., SAFA, Y., JILANI, K., SULTAN, M. & ATA, S. 2017. Green and eco-friendly synthesis of cobalt-oxide nanoparticle: characterization and photo-catalytic activity. *Advanced Powder Technology*, 28, 2035-2043.
- BOUDART, M. & MCDONALD, M. A. 1984. Structure sensitivity of hydrocarbon synthesis from carbon monoxide and hydrogen. *The Journal of Physical Chemistry*, 88, 2185-2195.
- CLAEYS, M., HEARSHAW, M., MOSS, J. & VAN STEEN, E. 2000. Does mono-atomic Ru catalyse the Fischer-Tropsch synthesis? *Studies in Surface Science and Catalysis*. Elsevier.
- COSTA, R. C., LELIS, M., OLIVEIRA, L., FABRIS, J., ARDISSON, J. D., RIOS, R., SILVA, C. & LAGO, R. 2006. Novel active heterogeneous Fenton system based on  $\text{Fe}_3\text{-xM}_x\text{O}_4$  (Fe, Co, Mn, Ni): the role of  $\text{M}^{2+}$  species on the reactivity towards  $\text{H}_2\text{O}_2$  reactions. *Journal of Hazardous Materials*, 129, 171-178.
- CROWTHER, N. & LARACHI, F. Ç. 2003. Iron-containing silicalites for phenol catalytic wet peroxidation. *Applied Catalysis B: Environmental*, 46, 293-305.

DENG, H., LU, J., LI, G., ZHANG, G. & WANG, X. 2011. Adsorption of methylene blue on adsorbent materials produced from cotton stalk. *Chemical Engineering Journal*, 172, 326-334.

DI LUCA, C., MASSA, P., FENOGLIO, R. & CABELLO, F. M. 2014. Improved Fe<sub>2</sub>O<sub>3</sub>/Al<sub>2</sub>O<sub>3</sub> as heterogeneous Fenton catalysts for the oxidation of phenol solutions in a continuous reactor. *Journal of Chemical Technology and Biotechnology*, 89, 1121-1128.

DONG, Y., HE, K., YIN, L. & ZHANG, A. 2007. A facile route to controlled synthesis of Co<sub>3</sub>O<sub>4</sub> nanoparticles and their environmental catalytic properties. *Nanotechnology*, 18, 435602.

DUTTA, K., MUKHOPADHYAY, S., BHATTACHARJEE, S. & CHAUDHURI, B. 2001. Chemical oxidation of methylene blue using a Fenton-like reaction. *Journal of Hazardous Materials*, 84, 57-71.

ESPINOSA, J. C., CATALÁ, C., NAVALÓN, S., FERRER, B., ÁLVARO, M. & GARCÍA, H. 2018. Iron oxide nanoparticles supported on diamond nanoparticles as efficient and stable catalyst for the visible light assisted Fenton reaction. *Applied Catalysis B: Environmental*, 226, 242-251.

FORZATTI, P. & LIETTI, L. 1999. Catalyst deactivation. *Catalysis Today*, 52, 165-181.

GEORGE, G. & ANANDHAN, S. 2015a. Photocatalytic Activity of Sol-Gel Electrospun Co<sub>3</sub>O<sub>4</sub> Nanofibers in Degrading Methylene Blue and Methyl Orange. *Ann Materials Science Engineering*, 2, 1025.

GEORGE, G. & ANANDHAN, S. 2015b. Photocatalytic Activity of Sol-Gel Electrospun Co<sub>3</sub>O<sub>4</sub> Nanofibers in Degrading Methylene Blue and Methyl Orange. *Ann Materials Science Engineering*, 2, 1025.

HE, T., CHEN, D., JIAO, X., WANG, Y. & DUAN, Y. 2005. Solubility-controlled synthesis of high-quality Co<sub>3</sub>O<sub>4</sub> nanocrystals. *Chemistry of Materials*, 17, 4023-4030.

HU, L., PENG, Q. & LI, Y. 2008. Selective synthesis of Co<sub>3</sub>O<sub>4</sub> nanocrystal with different shape and crystal plane effect on catalytic property for methane combustion. *Journal of the American Chemical Society*, 130, 16136-16137.

HU, X., LI, R., ZHAO, S. & XING, Y. 2017. Microwave-assisted preparation of flower-like cobalt phosphate and its application as a new heterogeneous Fenton-like catalyst. *Applied Surface Science*, 396, 1393-1402.

HUANG, F., LUO, M., CUI, L. & WU, G. 2015. Catalytic ozonation of methylene blue in aqueous solution by loading transition metal (Co/Cu/Fe/Mn) on carbon. *Korean Journal of Chemical Engineering*, 32, 268-273.

- JIANG, Y., WU, Y., XIE, B., XIE, Y. & QIAN, Y. 2002. Moderate temperature synthesis of nanocrystalline  $\text{Co}_3\text{O}_4$  via gel hydrothermal oxidation. *Materials Chemistry and Physics*, 74, 234-237.
- LAI, T.-L., LAI, Y.-L., LEE, C.-C., SHU, Y.-Y. & WANG, C.-B. 2008. Microwave-assisted rapid fabrication of  $\text{Co}_3\text{O}_4$  nanorods and application to the degradation of phenol. *Catalysis Today*, 131, 105-110.
- LI, H., FEI, G. T., FANG, M., CUI, P., GUO, X., YAN, P. & DE ZHANG, L. 2011. Synthesis of urchin-like  $\text{Co}_3\text{O}_4$  hierarchical micro/nanostructures and their photocatalytic activity. *Applied Surface Science*, 257, 6527-6530.
- LIOTTA, L., GRUTTADAURIA, M., DI CARLO, G., PERRINI, G. & LIBRANDO, V. 2009. Heterogeneous catalytic degradation of phenolic substrates: catalysts activity. *Journal of Hazardous Materials*, 162, 588-606.
- LONG, X., YANG, Z., WANG, H., CHEN, M., PENG, K., ZENG, Q. & XU, A. 2012. Selective degradation of orange II with the cobalt (II)–bicarbonate–hydrogen peroxide system. *Industrial & Engineering Chemistry Research*, 51, 11998-12003.
- LU, M., YAO, Y., GAO, L., MO, D., LIN, F. & LU, S. 2015. Continuous Treatment of Phenol over an  $\text{Fe}_2\text{O}_3/\gamma\text{-Al}_2\text{O}_3$  Catalyst in a Fixed-Bed Reactor. *Water, Air, & Soil Pollution*, 226, 87.
- MENG, B., ZHAO, Z., WANG, X., LIANG, J. & QIU, J. 2013. Selective catalytic reduction of nitrogen oxides by ammonia over  $\text{Co}_3\text{O}_4$  nanocrystals with different shapes. *Applied Catalysis B: Environmental*, 129, 491-500.
- MONDAL, A., ADHIKARY, B. & MUKHERJEE, D. 2015. Room-temperature synthesis of air stable cobalt nanoparticles and their use as catalyst for methyl orange dye degradation. *Colloids and Surfaces A: Physicochemical and Engineering Aspects*, 482, 248-257.
- NARAYANAN, R. & EL-SAYED, M. A. 2004. Shape-dependent catalytic activity of platinum nanoparticles in colloidal solution. *Nano Letters*, 4, 1343-1348.
- PRIETO, G., MARTÍNEZ, A., CONCEPCIÓN, P. & MORENO-TOST, R. 2009. Cobalt particle size effects in Fischer–Tropsch synthesis: structural and in situ spectroscopic characterisation on reverse micelle-synthesised Co/ITQ-2 model catalysts. *Journal of Catalysis*, 266, 129-144.
- RADSTAKE, P., BEZEMER, G., BITTER, J., FRØSETH, V. & HOLMEN, A. 2009. On the origin of the cobalt particle size effects in Fischer-Tropsch catalysis. *Journal of the American Chemical Society*, 131, 7197-7203.

- SALEM, I. A. & EL-MAAZAWI, M. S. 2000. Kinetics and mechanism of color removal of methylene blue with hydrogen peroxide catalyzed by some supported alumina surfaces. *Chemosphere*, 41, 1173-1180.
- SANTOS, A., YUSTOS, P., CORDERO, T., GOMIS, S., RODRÍGUEZ, S. & GARCÍA-OCHOA, F. 2005. Catalytic wet oxidation of phenol on active carbon: stability, phenol conversion and mineralization. *Catalysis Today*, 102, 213-218.
- SARFRAZ, A. & HASANAIN, S. 2014. Size Dependence of magnetic and optical properties of  $\text{Co}_3\text{O}_4$  nanoparticles. *Acta Physica Polonica, A.*, 125, 75-78
- SHAHWAN, T., SIRRIAH, S. A., NAIRAT, M., BOYACI, E., EROĞLU, A. E., SCOTT, T. B. & HALLAM, K. R. 2011. Green synthesis of iron nanoparticles and their application as a Fenton-like catalyst for the degradation of aqueous cationic and anionic dyes. *Chemical Engineering Journal*, 172, 258-266.
- SONG, X. C., WANG, X., ZHENG, Y. F., MA, R. & YIN, H. Y. 2011. Synthesis and electrocatalytic activities of  $\text{Co}_3\text{O}_4$  nanocubes. *Journal of Nanoparticle Research*, 13, 1319-1324.
- SWART, J. C. W. 2008. A theoretical view on deactivation of cobalt-based Fischer-Tropsch catalysts. University of Cape Town.
- VAN HELDEN, P., CIOBÎCĂ, I. M. & COETZER, R. L. 2016. The size-dependent site composition of FCC cobalt nanocrystals. *Catalysis Today*, 261, 48-59.
- VAN SANTEN, R. Structure sensitivity of methane and CO activation. 9th Novel Gas Conversion Symposium (NGCS), Lyon, France, 2010.
- VAN STEEN, E., CLAEYS, M., DRY, M. E., VAN DE LOOSDRECHT, J., VILJOEN, E. L. & VISAGIE, J. L. 2005. Stability of nanocrystals: thermodynamic analysis of oxidation and re-reduction of cobalt in water/hydrogen mixtures. *The Journal of Physical Chemistry B*, 109, 3575-3577.
- VILJOEN, E., MOLOTO, M. & THABEDE, P. 2017. Impact of acetate ions on the shape of  $\text{Co}_3\text{O}_4$  nanoparticles. *Digest Journal of Nanomaterials and Biostructures*, 12, 571-577.
- WAN, D., LI, W., WANG, G. & WEI, X. 2016. Size-controllable synthesis of  $\text{Fe}_3\text{O}_4$  nanoparticles through oxidation-precipitation method as heterogeneous Fenton catalyst. *Journal of Materials Research*, 31, 2608-2616.
- WANG, N., ZHENG, T., ZHANG, G. & WANG, P. 2016. A review on Fenton-like processes for organic wastewater treatment. *Journal of Environmental Chemical Engineering*, 4, 762-787.

WANG, Q., TIAN, S. & NING, P. 2013. Degradation mechanism of methylene blue in a heterogeneous Fenton-like reaction catalyzed by ferrocene. *Industrial & Engineering Chemistry Research*, 53, 643-649.

WARANG, T., PATEL, N., FERNANDES, R., BAZZANELLA, N. & MIOTELLO, A. 2013. Co<sub>3</sub>O<sub>4</sub> nanoparticles assembled coatings synthesized by different techniques for photo-degradation of methylene blue dye. *Applied Catalysis B: Environmental*, 132, 204-211.

WARANG, T., PATEL, N., SANTINI, A., BAZZANELLA, N., KALE, A. & MIOTELLO, A. 2012. Pulsed laser deposition of Co<sub>3</sub>O<sub>4</sub> nanoparticles assembled coating: role of substrate temperature to tailor disordered to crystalline phase and related photocatalytic activity in degradation of methylene blue. *Applied Catalysis A: General*, 423, 21-27.

XIA, S., YU, M., HU, J., FENG, J., CHEN, J., SHI, M. & WENG, X. 2014. A model of interface-related enhancement based on the contrast between Co<sub>3</sub>O<sub>4</sub> sphere and cube for electrochemical detection of hydrogen peroxide. *Electrochemistry Communications*, 40, 67-70.

XIE, X. & SHEN, W. 2009. Morphology control of cobalt oxide nanocrystals for promoting their catalytic performance. *Nanoscale*, 1, 50-60.

XU, R., WANG, D., ZHANG, J. & LI, Y. 2006. Shape-dependent catalytic activity of silver nanoparticles for the oxidation of styrene. *Chemistry—An Asian Journal*, 1, 888-893.

XU, R. & ZENG, H. C. 2004. Self-generation of tiered surfactant superstructures for one-pot synthesis of Co<sub>3</sub>O<sub>4</sub> nanocubes and their close-and non-close-packed organizations. *Langmuir*, 20, 9780-9790.

YAN, Q., LI, X., ZHAO, Q. & CHEN, G. 2012. Shape-controlled fabrication of the porous Co<sub>3</sub>O<sub>4</sub> nanoflower clusters for efficient catalytic oxidation of gaseous toluene. *Journal of Hazardous Materials*, 209, 385-391.

YANG, Y.-P., HUANG, K.-L., LIU, R.-S., WANG, L.-P., ZENG, W.-W. & ZHANG, P.-M. 2007a. Shape-controlled synthesis of nanocubic Co<sub>3</sub>O<sub>4</sub> by hydrothermal oxidation method. *Transactions of Nonferrous Metals Society of China*, 17, 1082-1086.

YANG, Y.-P., LIU, R.-S., HUANG, K.-L., WANG, L.-P., LIU, S.-Q. & ZENG, W.-W. 2007b. Preparation and electrochemical performance of nanosized Co<sub>3</sub>O<sub>4</sub> via hydrothermal method. *Transactions of Nonferrous Metals Society of China*, 17, 1334-1338.

ZHANG, Y., LIU, Y., FU, S., GUO, F. & QIAN, Y. 2007. Morphology-controlled synthesis of Co<sub>3</sub>O<sub>4</sub> crystals by soft chemical method. *Materials Chemistry and Physics*, 104, 166-171.

ZHU, M., MENG, D., WANG, C., DI, J. & DIAO, G. 2013. Degradation of methylene blue with  $H_2O_2$  over a cupric oxide nanosheet catalyst. *Chinese Journal of Catalysis*, 34, 2125-2129.

## CHAPTER 3

### 3.1 RESEARCH METHODOLOGY

#### 3.1.1 Introduction

This chapter outlines the procedures that were carried out during the process of acquiring data in this study. Stepwise explanations of different synthetic conditions that were carried out for the different studies that were conducted on the catalysts as well as their preparation conditions will be explained thoroughly in this section. The chapter also outlines the analytical techniques that were used to characterize the catalysts.

#### 3.1.2 Materials

The chemicals used in this study were obtained from various manufacturers with different compositions and purities as outlined below:

**Table 3:1** Percentage purities of chemicals used in this study and their suppliers.

Chemicals	Percentage purity (%)	Suppliers
$\text{Co}(\text{NO}_3)_2 \cdot 6\text{H}_2\text{O}$	98.0	Sigma-Aldrich
$\text{Co}(\text{CH}_3\text{COO})_2 \cdot 4\text{H}_2\text{O}$	99.9	Sigma-Aldrich
NaOH	98.0	Sigma-Aldrich
$\text{H}_2\text{O}_2$	30.0	Glassworld
HCl	32.0	Glassworld
$\text{CH}_3\text{OH}$	99.0	Glassworld
$\text{C}_4\text{H}_{10}\text{O}$	99.8	Laboratory Consumables
$\text{C}_6\text{H}_{18}\text{ClN}_3\text{S}$	95.0	Sigma-Aldrich
$\text{C}_2\text{H}_2\text{O}_4$	99.0	Sigma-Aldrich

All chemicals were used without further purification. The preparation method of the cobalt oxide nanoparticles was based on a combination of the methods with slight modification (Feng and Zeng, 2003, Yang et al., 2007). Butanol instead of polyethylene glycol (PEG) was added to the reaction mixture. A temperature of 85 °C was used. Feng and Zeng (2003) used air as an oxidant whereas

in this study, a combination of air and H<sub>2</sub>O<sub>2</sub> was used as an oxidant. The unreacted cobalt hydroxide was dissolved using diluted hydrochloric acid as described in the method of Feng and Zeng (2003).

### **3.1.3 Methodology**

This section details the methods that were applied to study the influences of different parameters have on the particle sizes and shapes of the prepared catalysts as well as the catalytic activity of the catalysts. The addition of H<sub>2</sub>O<sub>2</sub> amounts is outlined in this section. Reproducibility of the results was tested by running the experiments more than once.

#### **3.1.3.1 Preparation method to make spherical and cubic Co<sub>3</sub>O<sub>4</sub> nanoparticles**

The method from Feng and Zeng (2003) with slight modifications was adopted. Two cobalt sources were used (cobalt nitrate and cobalt acetate) to investigate their effect on the shape of the prepared nanoparticles. Cobalt nitrate (Co(NO<sub>3</sub>)<sub>2</sub>·6H<sub>2</sub>O) (5.8178 g) was dissolved in 10 ml of distilled water, and a solution of hydrogen peroxide (2.9 mmol) dissolved in 10 ml of distilled water were mixed at room temperature. Slow bubble formation was observed indicating that the H<sub>2</sub>O<sub>2</sub> decomposed slowly. Sodium hydroxide (1.2743 g) was dissolved in 100 ml of distilled water. Butanol (20 ml) and the mixture of cobalt nitrate/hydrogen peroxide were added to the solution of sodium hydroxide; the mixture turned brown/black. The solution contained in a round-bottom flask was placed in an unheated aluminum metal and heated at 85 °C for 16 hrs while bubbling air and stirring with a magnetic stirrer at 300 rpm. The solution was allowed to cool off to room temperature and centrifuged at 5000 rpm for 5 minutes. The solid product was washed three times with 50 ml 2 M HCl to dissolve the unreacted cobalt hydroxide precursor compounds, twice with 50 ml of distilled water to remove the HCl and finally once with 50 ml of methanol to remove water. The cobalt oxide nanoparticles produced were left to dry in an oven at 120 °C overnight, weighed to calculate the yield of the prepared nanoparticles and kept for characterization. The method to calculate the yield is shown in Appendix A2. The same conditions were used when cobalt acetate was used as the cobalt source.

### **3.1.3.2 Preparation method to make different sizes of spherical and cubic shaped $\text{Co}_3\text{O}_4$ nanoparticles**

The same procedure as the above was used to prepare different sizes of spherical and cubic shaped nanoparticles. The sizes of the nanoparticles were controlled by varying different amounts of hydrogen peroxide ( $\text{H}_2\text{O}_2$ ) and different reaction times during the preparation of  $\text{Co}_3\text{O}_4$  nanoparticles (see Table 3:2 for details). Then the nanoparticles were kept for characterization and later applied as catalysts for the degradation of methylene blue.

**Table 3:2** Different parameters varied during the preparation of Co<sub>3</sub>O<sub>4</sub> nanoparticles.

<b>Catalyst name</b>	<b>Cobalt precursor</b>	<b>Cobalt mass (g)</b>	<b>H<sub>2</sub>O<sub>2</sub> (mmol)</b>	<b>O<sub>2</sub></b>	<b>Reaction temperature (°C)</b>	<b>Time (hrs)</b>
N1	Cobalt nitrate	5.8104	1.4	Yes	85	16
N2	Cobalt acetate	5.8108	1.4	Yes	85	16
N3	Cobalt nitrate	5.8207	6.7	Yes	85	16
N4	Cobalt nitrate	5.8200	5.4	Yes	85	16
N5	Cobalt nitrate	5.8178	5.3	Yes	85	16
N6	Cobalt nitrate	5.8178	2.9	Yes	85	16
N7	Cobalt nitrate	5.8180	1.4	Yes	85	16
N8	Cobalt nitrate	5.8347	0.74	Yes	85	16
N9	Cobalt nitrate	5.8350	0.37	Yes	85	16
N10	Cobalt nitrate	5.8000	0.14	Yes	85	16
N11	Cobalt acetate	5.8008	6.7	Yes	85	16
N12	Cobalt acetate	5.8104	5.4	Yes	85	16

N13	Cobalt acetate	5.8208	2.9	Yes	85	16
N14	Cobalt acetate	5.8106	1.4	Yes	85	16
N15	Cobalt acetate	5.8067	0.74	Yes	85	16
N16	Cobalt acetate	5.8035	0.37	Yes	85	16
N17	Cobalt nitrate	5.0361	5.31	Yes	80	1
N18	Cobalt nitrate	5.0423	5.31	Yes	80	4
N19	Cobalt nitrate	5.0577	5.31	Yes	80	8
N20	Cobalt nitrate	5.0623	5.31	Yes	80	16
N21	Cobalt acetate	5.0017	No	Yes	80	4
N22	Cobalt acetate	5.0013	No	Yes	80	8
N23	Cobalt acetate	5.0102	No	Yes	80	16
N24	Cobalt acetate	5.0032	No	Yes	80	48
N25	Cobalt acetate	5.0105	No	Yes	80	72

### **3.1.4 Characterization of cobalt oxide nanoparticles**

To make sure that the desired cobalt oxide nanoparticles are achieved the following analytical techniques were used:

#### **3.1.4.1 Ultraviolet-visible (UV-vis) spectrometer**

Optical absorption measurements were performed using a double beam spectrometer - Perkin Elmer Lambda 25 UV-vis spectrometer, with a tungsten and deuterium lamp, which collects spectra from 180-1100 nm wavelength using a bandwidth of 1 nm with a fixed slit. A baseline setting was done by using pure water as a reference sample. A very small amount of the solid sample/crystals was dispersed in water. A Tauc plot was used to estimate the value of the direct band gap of  $\text{Co}_3\text{O}_4$  NPs.

#### **3.1.4.2 Photoluminescence spectrophotometer (PL)**

The emission of the nanoparticles was determined using a Jasco spectrofluorimeter FP-8600 equipped with XE lamp, 150 W, with bandwidth excitation slit at 5 nm and the emission ranging from 200-1010 nm. Fluorescent materials absorb UV light which is then emitted at a longer (frequency visible) wavelength. The instrument consists of a UV source; a monochromator for selection of the desired wavelength for irradiation, a sample holder, a second monochromator is used to select the desired wavelength of detection and a phototube amplifier-output assembly. The fluorometer irradiates then records the intensity of the light emitted by the sample on a plate. The wavelength of excitation for all the nanoparticles was at 400 nm. Ultraviolet-visible spectroscopy (UV-vis) and photoluminescence (PL) were used to determine the optical properties of the nanoparticles.

#### **3.1.4.3 Fourier transform infrared (FTIR)**

Infrared spectra were measured using a Perkin Elmer spectrum 400 FT-IR/FT-NIR spectrometer, universal ATR with the diamond detector and a wavelength scan range from  $650\text{ cm}^{-1}$  to  $4000\text{ cm}^{-1}$ .

#### **3.1.4.4 Thermo gravimetric analysis (TGA)**

A Perkin Elmer, STA 6000 simultaneous thermal analyzer TGA was used. The temperature was increased from 30 °C to 900 °C using a ramp rate of 10°/minute with a nitrogen flow rate of 20 ml/minute. A sample mass between 7.0 and 13.0 mg was used for this analysis.

#### **3.1.4.5 X-Ray diffraction (XRD)**

Data on the structure and phase of the Co<sub>3</sub>O<sub>4</sub> nanoparticles were obtained by the measurements using the Shimadzu-XRD 700, X-Ray Diffractometer with Cu K $\alpha$  radiation ( $\lambda$ = 1.15406 Å). A scan speed of 1 °/ minute, current 30 mA, and voltage of 40 kV were used with a scan range of (10-80) two theta degree. The FWHM (full-width half-maximum) was determined by fitting a Gaussian peak using the Fityk program. The FWHM was used to calculate the average crystallite size using the Scherrer equation  $D = K\lambda/\beta\cos\theta$ . A value of 0.94 (Langford and Wilson, 1978, Scherrer, 1912) was used for the Scherrer constant K, 1.154056 Å for  $\lambda$ ,  $\beta$  is the line width FWHM as  $2\theta$ ,  $\theta$  is the Bragg angle, and D is the crystallite size. The strongest diffraction peak, (311), at  $\sim 36^\circ 2\theta$  in the XRD diffraction pattern was used to calculate the average crystallite size. Peak broadening due to the instrument and strain were not taken into account. Thus the size calculated from XRD will give a smaller size than the actual size.

#### **3.1.4.6 Transmission electron microscope (TEM)**

The size and shape of the dried unsupported nanoparticles were determined using a TEM, LEO TEM 912, with an acceleration voltage of 120 kW and a tungsten wire filament. The nanoparticles dispersed in the methanol were pipetted onto carbon coated, copper grids and allowed to dry. The nanoparticles' sizes were measured using the software program ImageJ.

### **3.1.5 Application of Co<sub>3</sub>O<sub>4</sub> nanoparticles as catalysts for the degradation of methylene blue (MB)**

Reactions were carried out in 250 ml beaker covered with foil to avoid photo-degradation, in which 10 ml of methylene blue stock solution (1000 ppm) and 20 ml of distilled water were poured and stirred with a magnetic stirrer at 500 rpm until a temperature of 27 °C was reached. A mass of 0.01 g of catalyst was dissolved in 50 ml of distilled water and sonicated for 30 minutes using an ultrasonic bath. When the desired temperature was reached, a solution of the catalyst was added to

the solution of methylene blue. The mixture was kept in the dark while stirring for 1 hour to ensure the adsorption-desorption equilibrium. The reaction was started with the addition of 20 ml of H<sub>2</sub>O<sub>2</sub>. After selected time intervals, 1 ml of the samples were drawn using a pipette from the beaker and immediately 1 ml of iso-propanol was added to stop the reaction by quenching the remaining radicals. Then the solution was diluted to the mark with cold distilled water in 100 ml volumetric flask after that it was centrifuged to remove the solid catalyst from the liquid phase. Samples were then named and stored in the refrigerator until they were analyzed. The concentration of methylene blue was analyzed by UV-vis spectroscopy at a wavelength of 665 nm. Details of calculations are in Appendix A4.1 and A 4.2. Different sizes and shapes of the prepared Co<sub>3</sub>O<sub>4</sub> nanoparticles were used to investigate their effect on the degradation of MB.

#### **3.1.5.1 Rate of degradation kinetics of methylene blue degradation**

To determine the kinetics compliance of the experimental data, the results were subjected to pseudo first order and pseudo second order kinetics. Appendix A5.1 and A5.2 shows details of the calculations. The general rate law can be given as  $\text{Rate} = k [\text{H}_2\text{O}_2]^x [\text{MB}]^y$ . High amount of hydrogen peroxide (H<sub>2</sub>O<sub>2</sub>) was used and was assumed that the concentration of the hydrogen peroxide did not change significantly during the reactions. Therefore the rate law can be simplified to  $\text{Rate} = k [\text{constant}] [\text{MB}]^y$ , where y can be 1 or 2 depending if the rate of reaction is first order or second order in methylene blue.

#### **3.1.5.2 Leaching studies using oxalic acid**

The cobalt ions leaching test was performed in a 250 ml beaker, at atmospheric pressure. 0.01 g of the catalyst was added to 20 ml of 25 mg/L oxalic acid and was stirred at 200 rpm for an hour. The sample was filtered and analyzed for total cobalt using AA spectroscopy (Rey et al., 2009). Oxalic acid was used as it has been reported as one of the intermediates of phenol and MB oxidation. This experiment was done separately to monitor the cobalt ions leached at the same concentration of oxalic acid.

#### **3.1.5.3 Catalyst reproducibility**

To confirm the reproducibility of the results in the heterogeneous Fenton-like degradation of methylene blue, the catalysts were tested by running the experiments more than once. The same

procedure for the applications of  $\text{Co}_3\text{O}_4$  nanoparticles as catalysts was used to confirm the reproducibility of the results.

#### **3.1.5.4 Atomic absorption spectroscopy (AAS)**

Atomic absorption spectroscopy (AAS). AA-7000 dual atomizer model spectrometer from Shimadzu (Kyoto, Japan) was used to determine the total cobalt ions leached in each sample after degradation. The measurements were measured in a continuous flame atomizer. A cobalt hollow cathode lamp operating at a wavelength of 400 nm and a spectral slit width of 0.2 m was used. Acetylene was used as a purge gas throughout the analysis. The principal concept of flame atomization assimilates the combination of a gaseous sample oxidant with the fuel. In this work, the sample was carried out by acetylene and air (fuel carrier gases) followed by subsequent atomization in the flame. Once the sample has reached the flame, three more successive steps in atomization phase occurred.

#### **3.1.5.5 Turn Over Frequency (TOF)**

XRD and TEM sizes of the prepared cobalt oxide nanoparticles were used and the values of TOF obtained can be seen in (Appendix A6).

### 3.2 REFERENCES

- FENG, J. & ZENG, H. C. 2003. Size-controlled growth of  $\text{Co}_3\text{O}_4$  nanocubes. *Chemistry of Materials*, 15, 2829-2835.
- LANGFORD, J. I. & WILSON, A. 1978. Scherrer after sixty years: a survey and some new results in the determination of crystallite size. *Journal of Applied Crystallography*, 11, 102-113.
- REY, A., FARALDOS, M., CASAS, J., ZAZO, J., BAHAMONDE, A. & RODRÍGUEZ, J. 2009. Catalytic wet peroxide oxidation of phenol over Fe/AC catalysts: influence of iron precursor and activated carbon surface. *Applied Catalysis B: Environmental*, 86, 69-77.
- SCHERRER, P. 1912. Bestimmung der inneren Struktur und der Größe von Kolloidteilchen mittels Röntgenstrahlen. *Kolloidchemie Ein Lehrbuch*. Springer.
- YANG, Y.-P., HUANG, K.-L., LIU, R.-S., WANG, L.-P., ZENG, W.-W. & ZHANG, P.-M. 2007. Shape-controlled synthesis of nanocubic  $\text{Co}_3\text{O}_4$  by hydrothermal oxidation method. *Transactions of Nonferrous Metals Society of China*, 17, 1082-1086.

## **CHAPTER 4**

### **4.1 INTRODUCTION**

This Chapter aims to present and discuss the results of the characterization of cobalt oxide nanoparticles prepared as detailed in Chapter 3. The influence of the cobalt precursor on the shape of the prepared nanoparticles will be discussed. The effect of the amounts of  $H_2O_2$  on the size of the  $Co_3O_4$  nanoparticles as well as the effect of the reaction time on the size of the  $Co_3O_4$  nanoparticles will also be covered.

### **4.1 RESULTS AND DISCUSSIONS**

#### **4.1.1 Influence of cobalt precursor**

Cobalt nitrate (catalyst name N1) and cobalt acetate (catalyst name N2) were two different cobalt precursors used to study the influence of cobalt source or anion on the size and shape of cobalt oxide nanoparticles.

##### **4.1.1.1 XRD analysis**

X-ray diffraction (XRD) was carried out to identify the phase and crystallinity of the prepared cobalt oxide nanoparticles. As shown in Figure 4:1, the intensity peaks and the scattering angle of all the samples showed a cubic phase that is consistent with the standard  $Co_3O_4$  (PDF card No.00-04-1003) diffraction pattern in all the samples. No other diffraction peaks originating from metallic cobalt, cobalt hydroxide or to other cobalt oxides indicating the purification technique with diluted hydrochloric dissolved the cobalt hydroxide-like species as Feng and Zeng (2003) has observed. The average crystallite sizes as calculated by Debye-Sherrer equation is presented in Table 4:1 and was found to be 10.2 nm and 10.0 nm for nanoparticles synthesized using cobalt nitrate and cobalt acetate.

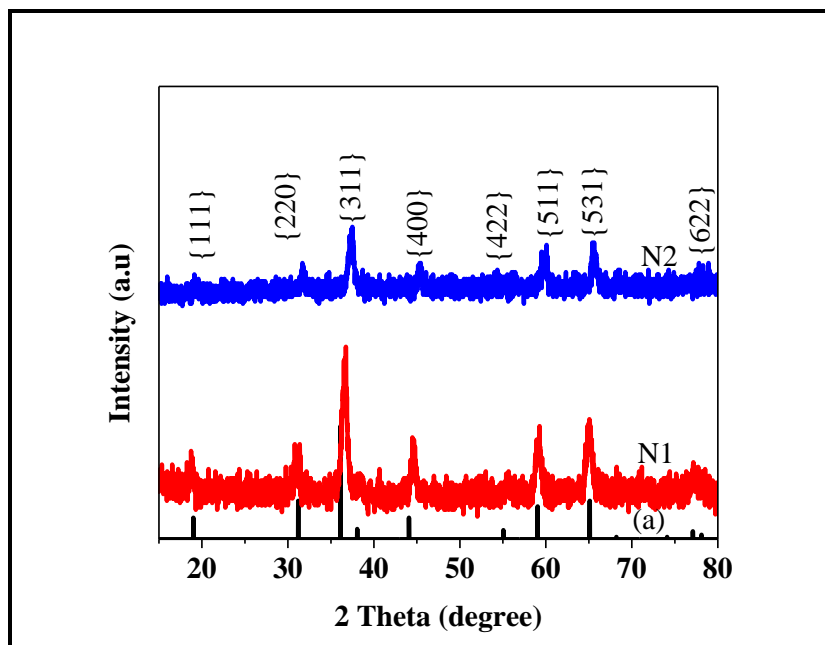


**Figure 4:1** XRD pattern of the prepared  $\text{Co}_3\text{O}_4$  nanoparticles. (a) Reference  $\text{Co}_3\text{O}_4$ , (N1)  $\text{Co}_3\text{O}_4$  nanoparticles made using  $\text{Co}(\text{NO}_3)_2 \cdot 6\text{H}_2\text{O}$  and (N2)  $\text{Co}_3\text{O}_4$  nanoparticles prepared using  $\text{Co}(\text{CH}_3\text{COO})_2 \cdot 4\text{H}_2\text{O}$ .

#### 4.1.1.2 TEM analysis

The Transmission Electron Microscopy (TEM) micrographs and corresponding histograms of cobalt oxide nanoparticles prepared from cobalt nitrate (N1) and cobalt acetate (N2) are shown in Figure 4:2, respectively. The nanoparticles synthesized from cobalt nitrate were spherical while those from cobalt acetate were cubic (see Figure 4:2). This shows that the anion in the cobalt salt has an important effect on the morphology of  $\text{Co}_3\text{O}_4$  NPs. The presence of acetate ions on the nanoparticles prepared from cobalt acetate might be the cause of obtaining the cubic shape instead of spherical shapes. Different shapes of  $\text{Co}_3\text{O}_4$  nanoparticles affected by precipitate compositions have also been reported in the literature by (Zhang et al., 2007).

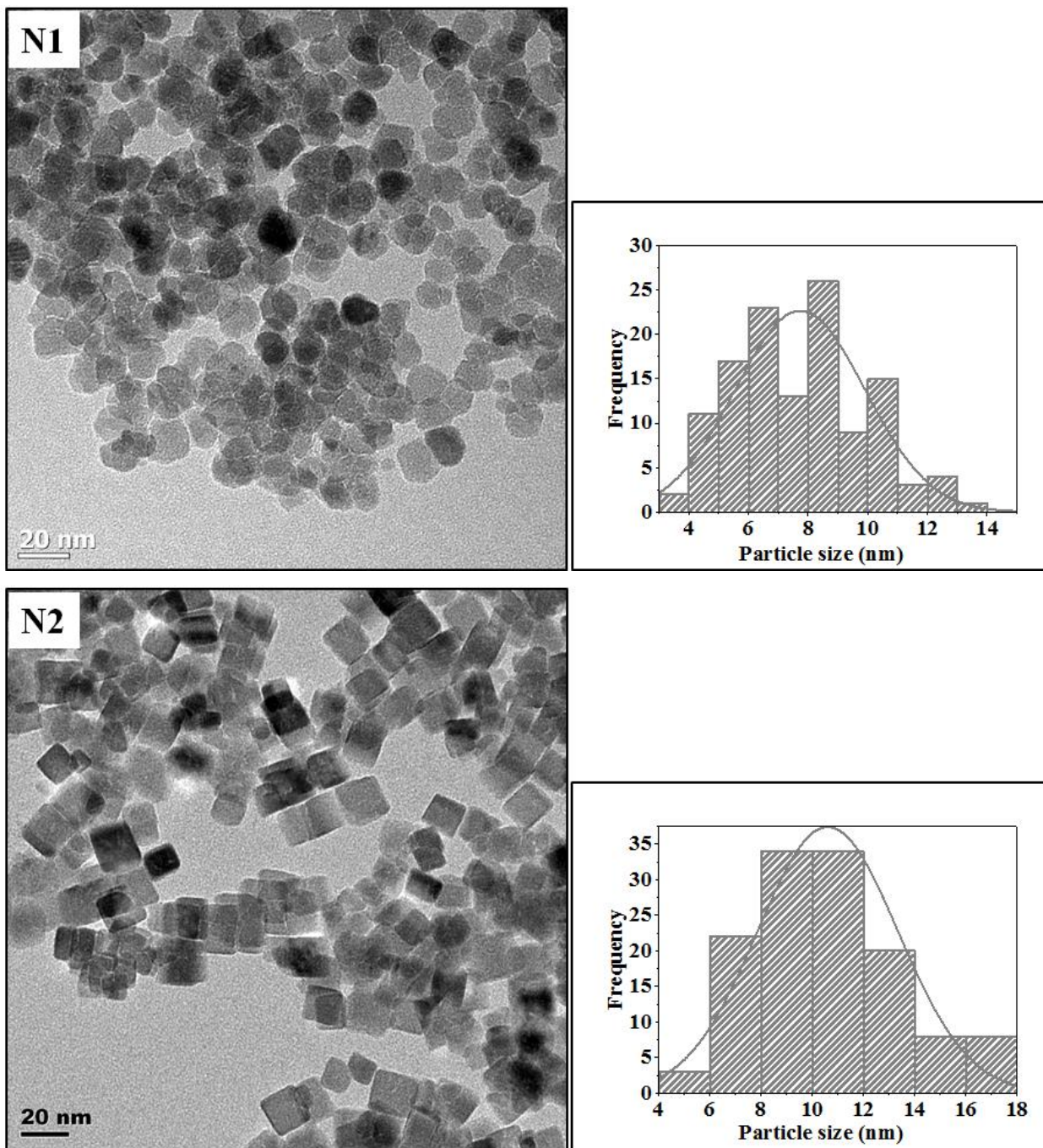


**Figure 4:2** TEM micrographs and the corresponding histograms of  $\text{Co}_3\text{O}_4$  nanoparticles prepared from  $\text{Co}(\text{NO}_3)_2 \cdot 6\text{H}_2\text{O}$  (N1) and  $\text{Co}(\text{CH}_3\text{COO})_2 \cdot 4\text{H}_2\text{O}$  (N2).

The yields and the average particle sizes of the prepared cobalt oxide nanoparticles are presented in Table 4:1. Appendix A2 shows the calculations of the yields of the prepared cobalt oxide nanoparticles. The yield of cobalt oxide nanoparticles was found to be lower for cobalt oxide nanoparticles prepared from cobalt acetate than the nanoparticles from cobalt nitrate. The lower yield for the cobalt oxide nanoparticles prepared using cobalt acetate can be related to a slower rate of reaction due to the acetate molecules as capping molecules which is stronger adsorbed in the surface as compared to nitrate. TEM and XRD indicate that the sizes obtained from different cobalt precursors were similar with the nanoparticles made from cobalt nitrate being slightly smaller and the nanoparticles made from cobalt acetate being slightly larger; data is summarized in Table 4:1. For the nanoparticles prepared from cobalt nitrate, the sizes obtained by XRD were found to be slightly larger than those obtained from TEM, and this slight difference might be due to a few larger nanoparticles that were not in the TEM images.

**Table 4:1** Co<sub>3</sub>O<sub>4</sub> nanoparticles yields and sizes determination with XRD and TEM.

	<b>Nanoparticles made from cobalt nitrate (N1)</b>	<b>Nanoparticles made from cobalt acetate (N2)</b>
TEM size (nm)	7.7	10.6
TEM standard deviation (nm)	2.2	2.8
XRD size (nm)	10.2	10.0
Yield (%)	75.5	35.6

#### 4.1.1.3 FTIR spectroscopy analysis

To investigate the functional groups that were present on the surface of the cobalt oxide nanoparticles, FTIR spectroscopy was used. Figure 4:3 shows the FTIR spectra of Co<sub>3</sub>O<sub>4</sub> nanoparticles prepared from cobalt nitrate (N1) and cobalt acetate (N2). The FTIR bands assignments are summarized in Table 4:2. The broad peaks at 3361 cm<sup>-1</sup> are assigned to the stretching vibration of O-H bond, which indicates the presence of hydroxyl ions due to the metal-OH layer or crystal water (Thota et al., 2009). The small peak at about 1749 cm<sup>-1</sup> may be assigned to C=O stretch. The O-H bending modes of adsorbed water give broad peaks at around 1630 cm<sup>-1</sup>

<sup>1</sup>. The broad peak at 1426 cm<sup>-1</sup> seems to be a combination of more than one peak, and this may be ascribed to COO<sup>-</sup> symmetrical stretching mode and the C-H bending mode (Yang et al., 2007). The peak at 1370 cm<sup>-1</sup> may also be ascribed to C-H bending mode (Kishore and Jeevanandam, 2013). The cobalt oxide nanoparticles prepared using cobalt nitrate (N1) shows a nitrate vibration at around 1350 cm<sup>-1</sup>, respectively. In Figure 4.3 (N2), the characteristic twin peaks at around 1548 and 1426 cm<sup>-1</sup> results from the asymmetric stretching and symmetric stretching mode of COO<sup>-</sup>, respectively. Vibration peaks below 800 cm<sup>-1</sup> arise from COO<sup>-</sup> rocking and bending modes. The Co-O stretches were observed at around 525.59 cm<sup>-1</sup> to 593.9 cm<sup>-1</sup>, respectively in all spectra. Yang et al. (2007) reported values of 1560.45 cm<sup>-1</sup> and 1382.79 cm<sup>-1</sup> for asymmetric and symmetric COO<sup>-</sup> stretches for cobalt acetate and 1384.40 cm<sup>-1</sup> for NO<sub>3</sub><sup>-</sup> for cobalt nitrate. Other studies have shown that capping molecules and ions adsorbed on the surface can change the shape of the nanoparticles by controlling the growth rates along the different crystal directions or making certain crystal Miller indices more stable, with lower surface energy (Xiao and Qi, 2011, Zhang et al., 2007).

**Table 4:2** Infrared assignments of Co<sub>3</sub>O<sub>4</sub> nanoparticles prepared from cobalt nitrate and cobalt acetate.

Band (cm <sup>-1</sup> )	Assignments
3361	-OH stretch
1749	CO stretch
1630	-OH bending
1548	Asymmetric COO <sup>-</sup> stretch
1426	Symmetric COO <sup>-</sup> stretch
1370	-CH bending
1350	NO <sub>3</sub> <sup>-</sup>
525	Co-O

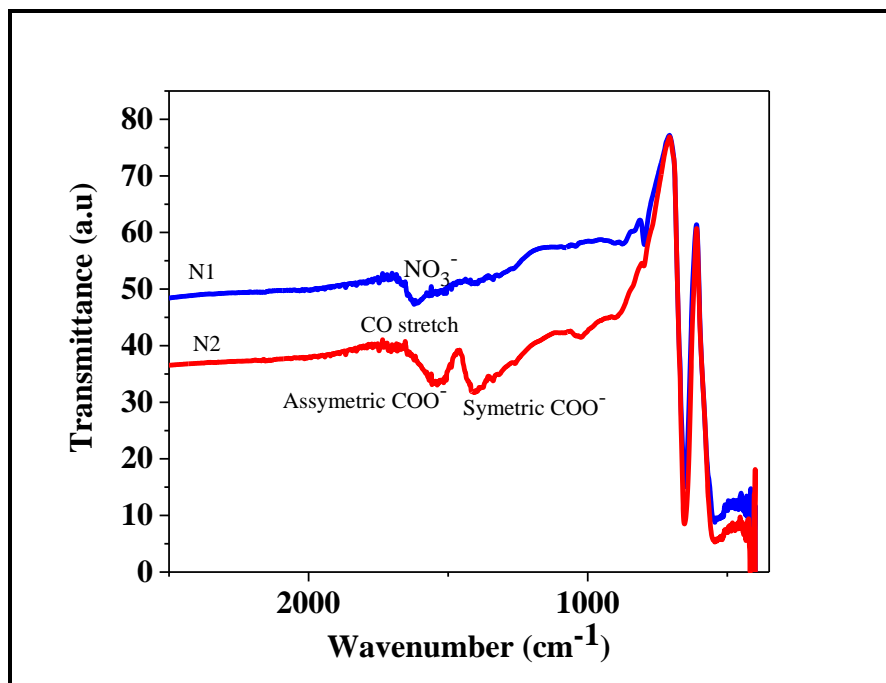


**Figure 4:3** FTIR spectra of  $\text{Co}_3\text{O}_4$  nanoparticles prepared from  $\text{Co}(\text{NO}_3)_2 \cdot 6\text{H}_2\text{O}$  (N1) and  $\text{Co}(\text{CH}_3\text{COO})_2 \cdot 4\text{H}_2\text{O}$  (N2).

#### 4.1.1.4 TGA analysis

TGA was conducted to determine the quantity of anions adsorbed and the strength of adsorption on the cobalt oxide surface. The TGA and DTA curves of the prepared  $\text{Co}_3\text{O}_4$  nanoparticles showed three decomposition processes in both samples (Figure 4:4A and 4:4B). The first weight losses at 100 °C are attributed to desorption of water molecules. The decomposition temperature of cobalt acetate (252 °C) as measured by TGA is higher than that of cobalt nitrate (200 °C). Therefore, the second weight losses around 325 and 152 °C (according to the DTA curve) are attributed to desorption of acetate ions and nitrate ions, respectively, from the surface of the cobalt oxide nanoparticles directly to  $\text{Co}_3\text{O}_4$  (see Figure 4:4A and 4:4B). The higher desorption temperature of the acetate ion in comparison to the nitrate ion indicates the different strength of adsorption of both anions on the surface of cobalt oxide. The last weight loss at about 800 °C is attributed to the decomposition of  $\text{Co}_3\text{O}_4$  to  $\text{CoO}$ . Similar weight losses and decomposed temperature of the prepared  $\text{Co}_3\text{O}_4$  nanoparticles are observed from (Thota et al., 2009) for their synthesized  $\text{Co}_3\text{O}_4$  nanoparticles.

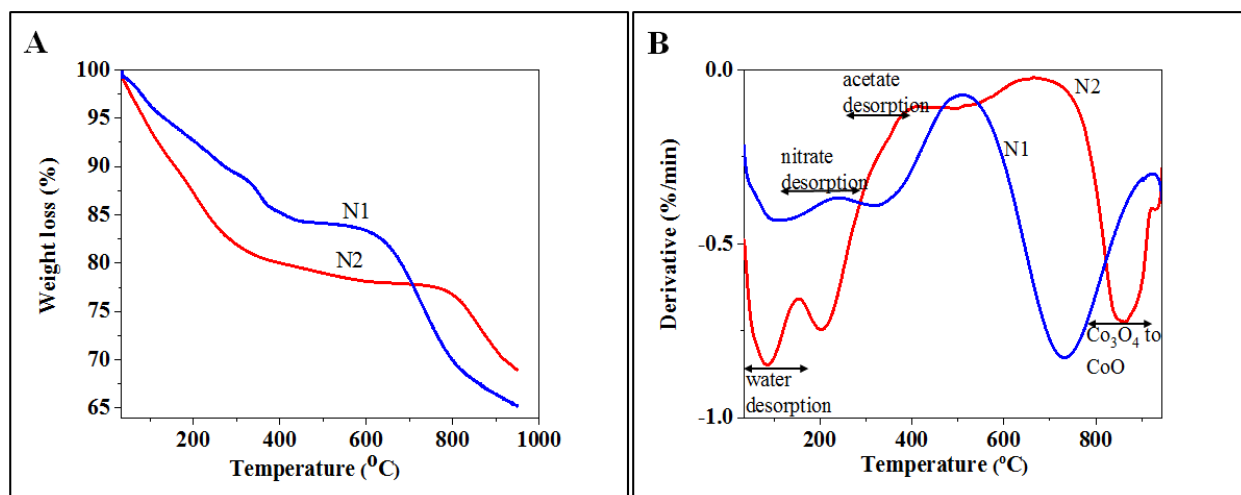


**Figure 4:4** TGA (A) and DTA (B) curves of  $\text{Co}_3\text{O}_4$  nanoparticles prepared from  $\text{Co}(\text{NO}_3)_2 \cdot 6\text{H}_2\text{O}$  (N1) and  $\text{Co}(\text{CH}_3\text{COO})_2 \cdot 4\text{H}_2\text{O}$  (N2).

TGA and FTIR spectroscopy results showed the presence of both nitrate and acetate ions on the surface of the cobalt oxide nanoparticles and that their adsorption characteristics are not the same. The more strongly adsorbed acetate ions on the cobalt oxide nanoparticles made from cobalt acetate may be the cause of obtaining cubic shapes instead of spherical shapes. Capping molecules (such as those containing acetate ions) are believed to change the nanoparticle's shape as they are adsorbed on the surface of the catalyst (Xia et al., 2014). The  $\{100\}$  planes  $\text{Co}_3\text{O}_4$  have a surface energy of  $0.92 \text{ Jm}^{-2}$  which is significantly lower than the surface energy of the  $\{110\}$ ,  $\{112\}$  and  $\{111\}$  planes that have surface energies of  $1.31 \text{ Jm}^{-2}$ ,  $1.47 \text{ Jm}^{-2}$  and  $2.31 \text{ Jm}^{-2}$  respectively (Su et al., 2014). Cubic shaped nanoparticles are mostly made up of  $\{100\}$  surfaces (He et al., 2005). It is therefore, argued that the adsorbed acetate ions on the surface of the cobalt oxide nanoparticles decreased the growth of some of the surfaces and resulted in kinetic control (Xiao and Qi, 2011). Cubic shaped nanoparticles would have also formed under thermodynamic control due to the lower surface energy of the  $\{100\}$  surface. If the size of the cobalt oxide nanoparticles made from cobalt acetate was significantly smaller than those made of cobalt nitrate, one could argue that the shape resulted from thermodynamic control due to slower growth as a result of the adsorbed acetate ions on the surface. However, due to similarities in sizes within the two samples, the average growth rates were similar thus favoring the argument that the shape is affected by kinetic control.

#### 4.1.1.5 UV-vis absorption studies

UV-vis absorption spectroscopy is the commonly used method to determine the optical properties of the nanoparticles; this is because the absorption bands are related to the diameters of the nanoparticles. The recorded UV-vis spectra of the synthesized cobalt oxide nanoparticles are represented in Figure 4:5. The surface plasmon resonance bands of cobalt oxide nanoparticles approximately appeared at a wavelength around 710 nm and 420 nm. Bulk cobalt oxide is composed of continuous valence and conduction bands resulting in a fixed energy band characterized by a single absorption peak. As the cobalt oxide becomes quantized, discrete atomic-like states with energies that are determined by the properties of the nanoparticles arise. Therefore, the first absorption peak at around 710 nm can be assigned to a ligand to metal charge transfer process of  $O^{2-} \rightarrow Co^{3+}$  while the second peak at around 420 nm can be assigned to an  $O^{2-} \rightarrow Co^{2+}$  charge transfer process as observed by Chakrabarty and Chatterjee (2012), Sarfraz and Hasanain (2014), Thota et al. (2009), Warang et al. (2012) for  $Co_3O_4$  nanostructures. These transitions confirm the existence of  $Co_3O_4$  in two oxidation states as Chakrabarty and Chatterjee (2012), Sarfraz and Hasanain (2014), Thota et al. (2009), Warang et al. (2012) have reported. The quantum confinement becomes effective when the size of the material becomes comparable to the Bohr radius of the exciton, and the absorption edge is shifted to a higher frequency (Chakrabarty and Chatterjee, 2012). In this work, the absorption peaks of the prepared  $Co_3O_4$  nanoparticles were blue shifted from their bulk counterparts which are set at 729 nm and 435 nm (Thota et al., 2009). This confirms that the optical band gap energies become larger as the particle size decreases (Chakrabarty and Chatterjee, 2012, Thota et al., 2009). The absorption peak of the nanoparticles made from cobalt nitrate (N1) was at around 408 nm, whereas cobalt acetate (N2) nanoparticles showed a shift of the absorption peak in the spectrum to a higher wavelength of 421 nm respectively. This difference in the absorption peaks signifies that the sizes of the nanoparticles made from cobalt acetate are larger than those made from cobalt nitrate.

To estimate the value of the direct band gap and electron transition energies of the prepared cobalt oxide nanoparticles from the absorption spectra, Tauc plots were used. Figure 4:6 shows the direct band gap estimation and electron transition due to  $O^{2-} \rightarrow Co^{3+}$  and  $O^{2-} \rightarrow Co^{2+}$  charge transfer process for cobalt oxide nanoparticles prepared from cobalt nitrate (N1) and cobalt acetate (N2). The band gap energies of 1.90 and 1.75 eV and electron transition energies of 4.06 and 3.45 eV, respectively

were found for cobalt oxide nanoparticles made using cobalt nitrate and cobalt acetate as shown in Figure 4:6. The band gap and the electron transition energies of the prepared nanoparticles are blue shifted in comparison to that of bulk cobalt oxide which are set at 1.70 and 2.85 eV (Sarfraz and Hasanain, 2014). This shows that a decrease in the sizes of the nanoparticles resulted in an increase in band gap and the electron transition energies. This results are in agreement with the results obtained from TEM and XRD of these nanoparticles as discussed in section 4.2.1.1 and 4.2.1.2.

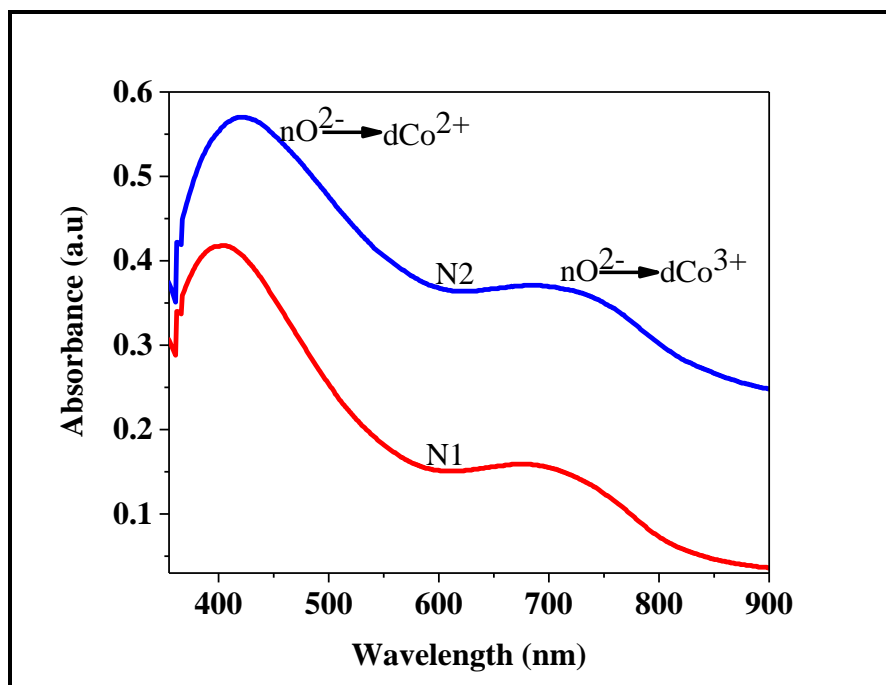


**Figure 4:5** UV-vis spectra of  $\text{Co}_3\text{O}_4$  nanoparticles prepared from  $\text{Co}(\text{NO}_3)_2 \cdot 6\text{H}_2\text{O}$  (N1) and  $\text{Co}(\text{CH}_3\text{COO})_2 \cdot 4\text{H}_2\text{O}$  (N2).

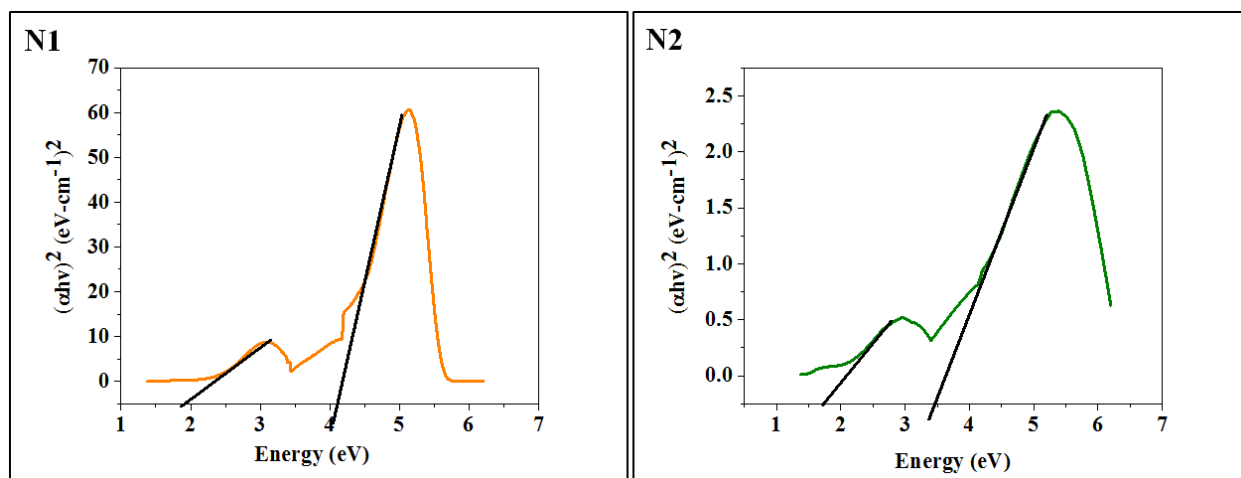


**Figure 4:6** Estimation of the direct band gap and electron transition energies from Tauc plots for  $\text{Co}_3\text{O}_4$  nanoparticles made using cobalt nitrate (N1) and cobalt acetate (N2).

#### 4.1.1.6 Photoluminescence studies

Photoluminescence studies were also carried out to further understand the emission nature of the prepared cobalt oxide nanoparticles and the emission spectra is depicted in Figure 4:7. The excitation wavelength of 400 nm for the lowest energy was used to excite the cobalt oxide nanoparticles as obtained in the UV-vis absorption bands. As can be seen in Figure 4:7, there is only one emission peak for nanoparticles prepared from cobalt nitrate and cobalt acetate. This might be due to that the 400 nm wavelength did not have a high enough energy to excite the higher energy electron transition (peak around 400 nm as seen in the UV-vis spectra) hence only one peak is observed. Cobalt oxide nanoparticles made using cobalt nitrate and cobalt acetate were found to have emission peaks at around 574 and 605 nm, respectively. It is observed that the emission peaks of all the prepared cobalt oxide nanoparticles are narrow, indicating monodispersed particles and the existence of predominantly single morphology. Any defect related emission was hardly seen in the emission spectra. Chakrabarty and Chatterjee (2012) also reported an emission peak of 584 nm that is red shifted from the absorption peak for  $\text{Co}_3\text{O}_4$  nanoparticles.

The emission peaks showed a typical red shift as compared to their corresponding absorption peaks. This is attributed to the excitation of electrons from occupied d bands into states above Fermi level. The absorption and emission peaks of the nanoparticles made from cobalt acetate were slightly at higher wavelengths than those of cobalt nitrate. These results are in agreement

with the calculated sizes from TEM. However, cobalt precursor did not change the size significantly but influenced the shape of the nanoparticles.

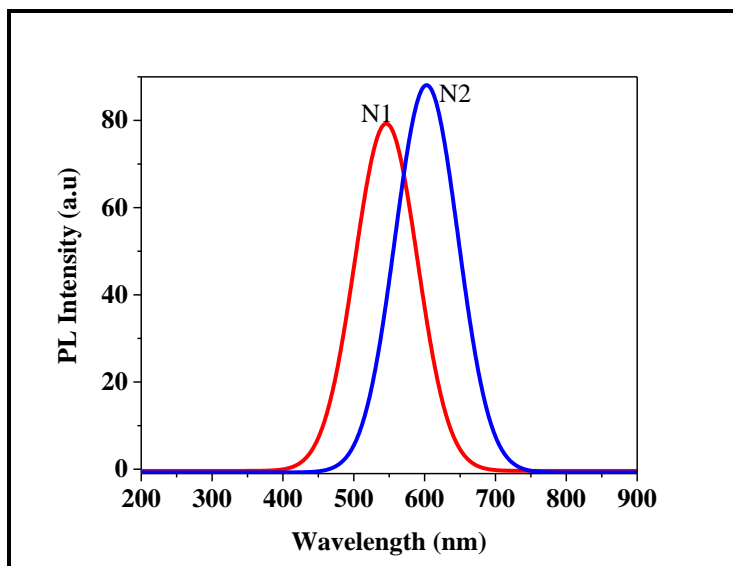


**Figure 4:7** PL spectroscopy of  $\text{Co}_3\text{O}_4$  nanoparticles prepared from  $\text{Co}(\text{NO}_3)_2 \cdot 6\text{H}_2\text{O}$  (N1) and  $\text{Co}(\text{CH}_3\text{COO})_2 \cdot 4\text{H}_2\text{O}$  (N2). Excitation wavelength of 400 nm.

#### 4.1.2 Influence of $\text{H}_2\text{O}_2$

The control size of  $\text{Co}_3\text{O}_4$  nanoparticles through monitoring different amounts of hydrogen peroxide have been studied by many authors in order to improve catalytic performance (Amiri et al., 2011, Jiang et al., 2002, Song et al., 2011, Yang et al., 2007, Zhang et al., 2007). This preparation method is suitable to prepare large enough quantities of catalysts for further testing. Based on the arguments made above, both cobalt nitrate and cobalt acetate were used due to different shapes found in their yielded cobalt oxide nanoparticles. The study was then aimed at preparing different sizes of spherical and cubic shaped cobalt oxide nanoparticles. Different amounts of  $\text{H}_2\text{O}_2$  were varied during the preparation of the nanoparticles, to investigate its effect on the size of the  $\text{Co}_3\text{O}_4$  nanoparticles. The names of the catalyst are N6, N7, N8, N9 and N10 and N13, N14, N15 and N16 for the nanoparticles made using cobalt nitrate and cobalt acetate, respectively.

#### 4.1.2.1 XRD analysis

The XRD pattern of the synthesized cobalt oxide nanoparticles at different amount of  $\text{H}_2\text{O}_2$  using cobalt nitrate (A) and cobalt acetate (B) as cobalt sources is shown in Figure 4:8A and Figure 4:8B. Both patterns show diffraction peaks that are indexed to a pure cubic centered phase of spinel  $\text{Co}_3\text{O}_4$  in all samples. As the amount of  $\text{H}_2\text{O}_2$  was decreasing, the XRD peak intensity was increasing. This shows that there is a change in the sizes of cobalt oxide nanoparticles as the amount of  $\text{H}_2\text{O}_2$  decrease in all samples. The average crystallite sizes were found to be between 5.5-13.2 nm and 4.3-10 nm for nanoparticles made using cobalt nitrate and cobalt acetate as calculated from the Scherrer equation using the most intense peak {311}(see Table 4:3).

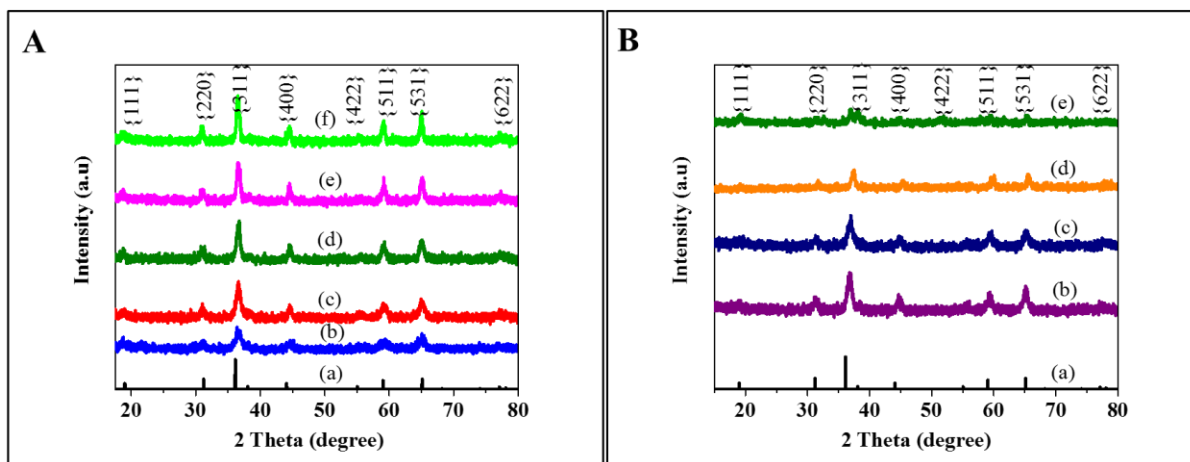


**Figure 4:8** XRD diffraction patterns of  $\text{Co}_3\text{O}_4$  NPs synthesized using different amounts of  $\text{H}_2\text{O}_2$ . Nanoparticles made from (A)  $\text{Co}(\text{NO}_3)_2 \cdot 6\text{H}_2\text{O}$  (a) reference  $\text{Co}_3\text{O}_4$ , (b) 2.9 mmol  $\text{H}_2\text{O}_2$ , (c) 1.4 mmol  $\text{H}_2\text{O}_2$ , (d) 0.74 mmol  $\text{H}_2\text{O}_2$ , (e) 0.37 mmol  $\text{H}_2\text{O}_2$  and (f) 0.14 mmol  $\text{H}_2\text{O}_2$ . Nanoparticles made from (B)  $\text{Co}(\text{CH}_3\text{COO})_2 \cdot 4\text{H}_2\text{O}$  (a) reference  $\text{Co}_3\text{O}_4$ , (b) 2.9 mmol  $\text{H}_2\text{O}_2$ , (c) 1.4 mmol  $\text{H}_2\text{O}_2$ , (d) 0.74 mmol  $\text{H}_2\text{O}_2$ , and (e) 0.37 mmol  $\text{H}_2\text{O}_2$ .

#### 4.1.2.2 TEM analyses

The TEM images of the  $\text{Co}_3\text{O}_4$  nanoparticles prepared by varying the amount of  $\text{H}_2\text{O}_2$  using cobalt nitrate (A) and cobalt acetate (B) as cobalt salts and their corresponding particle size histograms are depicted in Figure 4:9 and Figure 4:10. Table 4:3 shows different sizes and the yields of cobalt oxide nanoparticles obtained by varying the amount of  $\text{H}_2\text{O}_2$  using both cobalt nitrate and cobalt

acetate. As expected the nanoparticles prepared using cobalt nitrate were spherical in shape whereas the nanoparticles made from cobalt acetate were cubic in shape. The histograms of all the  $\text{Co}_3\text{O}_4$  nanoparticles showed a narrow size distribution of particle size and the average diameters were found to be between 4.6 to 19.5 nm and 6.6 to 11.3 nm, respectively, for the nanoparticles prepared using cobalt nitrate and cobalt acetate. A higher amount of  $\text{H}_2\text{O}_2$  resulted in a higher yield (seen in Figure 4:11). The amounts of  $\text{H}_2\text{O}_2$  added influenced the size of  $\text{Co}_3\text{O}_4$  nanoparticles. As the amount of  $\text{H}_2\text{O}_2$  was decreasing from 2.9 to 0.14 mmol, the size of the nanoparticles increased from about (4.6 nm to about 19.5 nm) and (6.6 to 11.3 nm) for nanoparticles prepared using cobalt nitrate and cobalt acetate, respectively. This relation can be seen in Figure 4:12. The higher yield and smaller particle size with increase in the amounts of  $\text{H}_2\text{O}_2$  may be attributed to the high conversion of cobalt hydroxide to cobalt oxide.

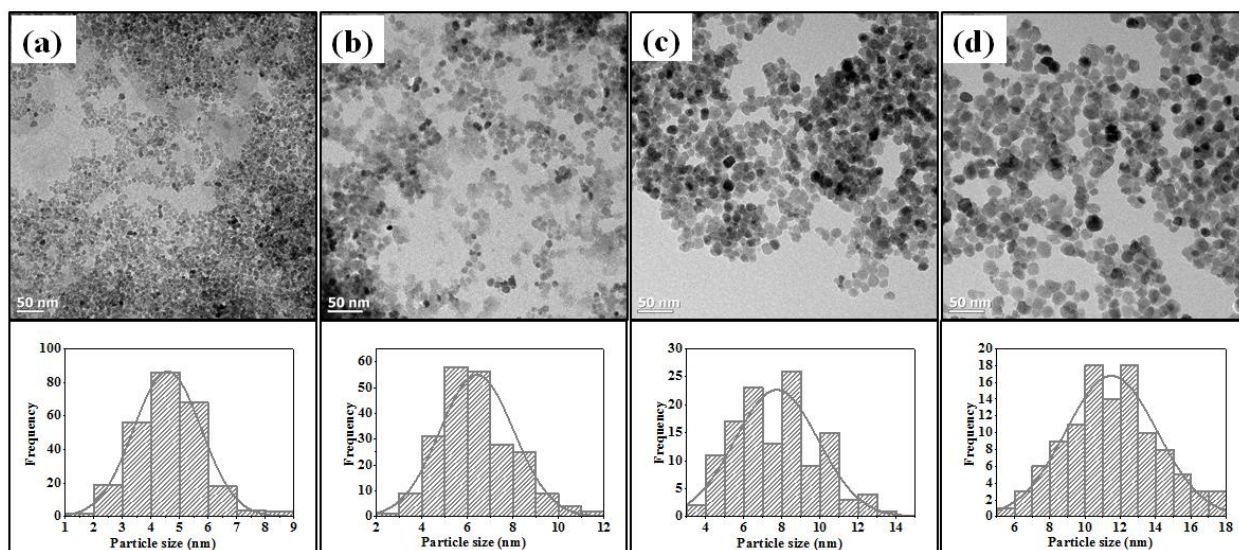


**Figure 4:9** Selected TEM images of  $\text{Co}_3\text{O}_4$  NPs synthesized prepared at 85 °C for 16 hrs by varying the amount of  $\text{H}_2\text{O}_2$ . Nanoparticles made using  $\text{Co}(\text{NO}_3)_2 \cdot 6\text{H}_2\text{O}$ . (a) 2.9 mmol  $\text{H}_2\text{O}_2$ , (b) 1.4 mmol  $\text{H}_2\text{O}_2$ , (c) 0.74 mmol  $\text{H}_2\text{O}_2$  and (d) 0.37 mmol  $\text{H}_2\text{O}_2$ .

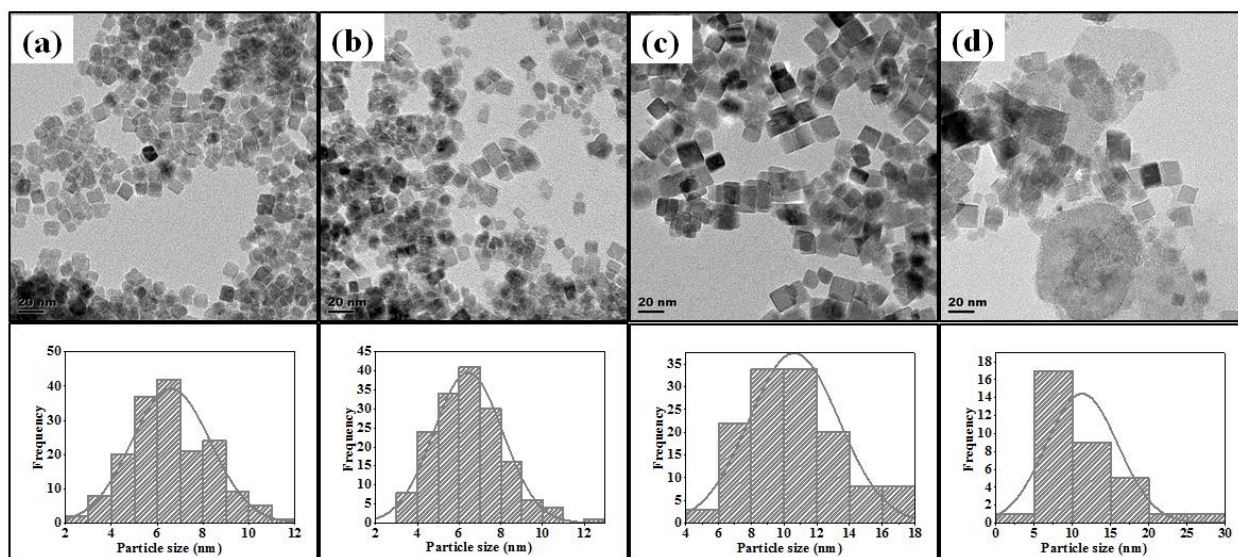


**Figure 4:10** Selected TEM images of  $\text{Co}_3\text{O}_4$  NPs synthesized prepared at  $85^\circ\text{C}$  for 16 hrs by varying the amount of  $\text{H}_2\text{O}_2$ . Nanoparticles made using  $\text{Co}(\text{CH}_3\text{COO})_2 \cdot 4\text{H}_2\text{O}$ . (a) 2.9 mmol  $\text{H}_2\text{O}_2$ , (b) 1.4 mmol  $\text{H}_2\text{O}_2$ , (c) 0.74 mmol  $\text{H}_2\text{O}_2$  and (d) 0.37 mmol  $\text{H}_2\text{O}_2$ .

XRD and TEM showed a decrease in nanoparticle sizes with an increase in the amount of  $\text{H}_2\text{O}_2$ . The difference in sizes from TEM and XRD may be due to peak broadening from the instrument and strain not taken into account or the cracks on the crystals or a few large particles, which may not be observed in the TEM images. An increase in the amount of  $\text{H}_2\text{O}_2$  increased the size of cobalt oxide nanoparticles (Amiri et al., 2011). The results of Song et al. (2011) and this study shows a decrease in the cobalt oxide nanoparticle sizes with an increase in the amount of  $\text{H}_2\text{O}_2$ . This apparent difference may indicate that the size passes through a minimum with an increase in the amount of  $\text{H}_2\text{O}_2$ . A minimum may be explained by that rate of nucleation increasing with an increase in  $\text{H}_2\text{O}_2$  leading to smaller sizes in the low molar ratio of  $\text{H}_2\text{O}_2$  to  $\text{Co}^{2+}$  range, where the rate of nanoparticle growth increased yielding larger sizes at higher amounts of  $\text{H}_2\text{O}_2$ . The formation of smaller particle size may then be attributed to formation of more cobalt oxide nuclei due to faster oxidation by  $\text{H}_2\text{O}_2$ .

**Table 4:3** Co<sub>3</sub>O<sub>4</sub> nanoparticles yields and size determination with XRD and TEM data.

Co <sub>3</sub> O <sub>4</sub> nanoparticles using cobalt nitrate						Co <sub>3</sub> O <sub>4</sub> nanoparticles using cobalt acetate					
Catalyst name	H <sub>2</sub> O <sub>2</sub> (mmol)	XRD size (nm)	TEM size (nm)	TEM std (nm)	Yield (%)	Catalyst name	H <sub>2</sub> O <sub>2</sub> (mmol)	XRD size (nm)	TEM size (nm)	TEM std (nm)	Yield (%)
N3	6.7	2.0	3.0	0.8	98.1	N11	6.7	3.4	3.2	1.0	57.7
N4	5.4	2.1	3.0	0.9	96.6	N12	5.4	3.6	3.4	1.0	53.1
N5	5.3	3.0	3.2	1.1	74.2	N13	2.9	7.3	6.6	1.7	48.4
N6	2.9	5.5	4.6	1.2	73.8	N14	1.4	7.3	6.8	1.9	47.4
N7	1.4	8.9	6.4	1.6	73.3	N15	0.74	10	10.6	2.8	35.6
N8	0.74	10.2	7.7	2.2	75.5	N16	0.37	11.3	11.3	4.7	22.6
N9	0.37	11.3	11.5	2.6	69.1						
N10	0.14	13.2	19.5	5.7	29.3						

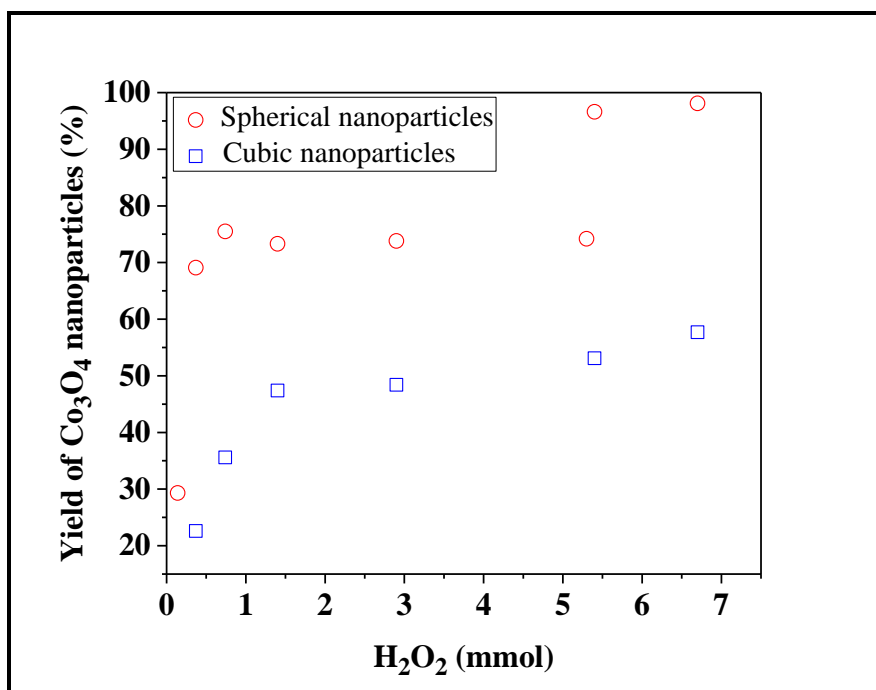


**Figure 4:11** Yields of Co<sub>3</sub>O<sub>4</sub> nanoparticles dependence on the amounts of H<sub>2</sub>O<sub>2</sub>

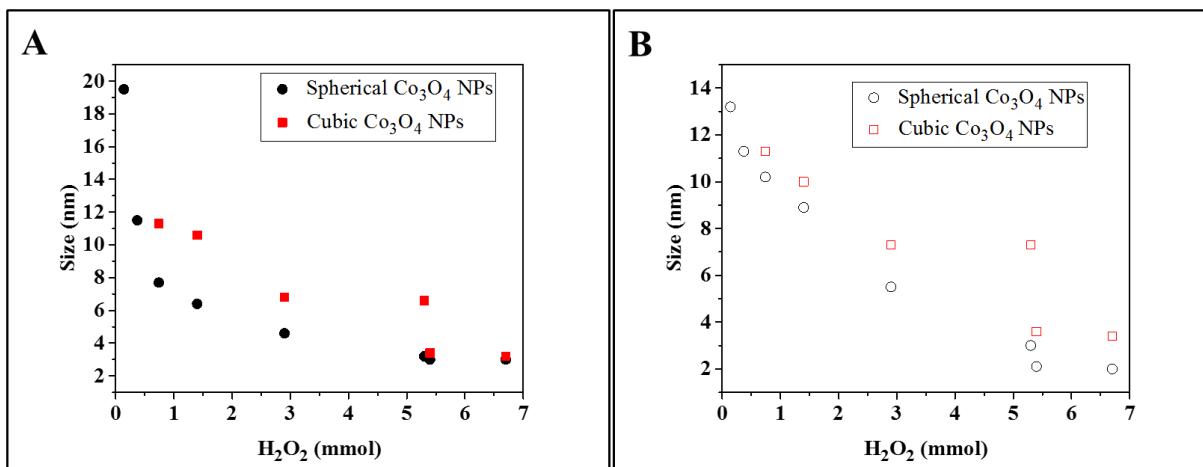


**Figure 4:12** Co<sub>3</sub>O<sub>4</sub> TEM size dependence on the amounts of H<sub>2</sub>O<sub>2</sub>: (A) Nanoparticles calculated from (A) TEM and (B) XRD data

#### 4.1.2.3 UV-vis spectroscopy

To understand the absorption behavior of the prepared cobalt oxide nanoparticles, UV-vis spectroscopy was used. Figure 4:13 shows the absorption spectra of cobalt oxide nanoparticles synthesized by different amounts of H<sub>2</sub>O<sub>2</sub> using cobalt nitrate (A) and cobalt acetate (B). The absorption spectra of all the prepared cobalt oxide nanoparticles showed two transitions around 1.80 and 3.0 eV which are due to O<sup>2-</sup>→Co<sup>3+</sup> and O<sup>2-</sup>→Co<sup>2+</sup> charge transfer process. The presence of these transitions is attributed to the excitations emanating from the presence of cobalt in two (+2 and +3) oxidation states, respectively (Salavati-Niasari et al., 2009, Thota et al., 2009).

Tauc plots were used to estimate the values of the direct band gaps of the prepared cobalt oxide nanoparticles (see Appendix A3 for details of calculations). The values of the estimated band gap energies and the electron transitions for the cobalt oxide nanoparticles prepared from cobalt nitrate are presented in Figure 4:14. Values of the transitions for the nanoparticles made using cobalt acetate were determined similarly. The band gaps for O<sup>2-</sup>→Co<sup>3+</sup> varies from 1.23 to 1.76 eV and the electron transitions for O<sup>2-</sup>→Co<sup>2+</sup> varies from 3.29 to 3.72 eV, respectively as the sizes varies from 4.6 to 19.5 nm as shown in Table 4:4.

As the amount of H<sub>2</sub>O<sub>2</sub> was increasing, the band gaps and the electron transitions increase as shown in Figure 4:15. This suggests that the sizes of the nanoparticle becomes smaller with an increase

in the transitions. However, the cobalt oxide nanoparticle of 19.5 nm shows higher band gap and electron transition than other nanoparticles. This change can be related to a difference in the confinement effects which comes from the differences in the effective masses of the carriers since band gap shift is sensitively dependent on the effective masses of the carriers (Sarfraz and Hasanain, 2014). The obtained results are in agreement with what was obtained by Sarfraz and Hasanain (2014) on the effect of particle size on the magnetic and optical properties of cobalt oxide nanoparticles and Thota et al. (2009) (1.77 and 3.12 eV) for the respective energy transitions for a 20 nm average particle size. The larger values for the  $O^{2-} \rightarrow Co^{2+}$  transitions as compared to the  $O^{2-} \rightarrow Co^{3+}$  transitions is an indication of different confinements at tetrahedral and octahedral symmetries (Sarfraz and Hasanain, 2014).

**Table 4:4** Bulk  $Co_3O_4$  data, sizes and band gap energies of the  $Co_3O_4$  nanoparticles obtained from this study (Tauc plots) and reported band gap values from the literature for comparison.

Bulk $Co_3O_4$ data		Literature			This study		This study	
$E_{g1}$ and $E_{g2}$ (eV)	Author	Size (nm)	$E_{g1}$ and $E_{g2}$ (eV)	Author	Size (nm) spherical	$E_{g1}$ and $E_{g2}$ (eV)	Size (nm) Cubic	$E_{g1}$ and $E_{g2}$ (eV)
1.70 and 2.85	Thota et al. 2009	20	1.77 and 3.12	Thota et al., 2009	4.6	1.55 and 3.72	6.6	1.70 and 3.71
1.48 and 2.19	Salavati et al. 2009	13	1.92 and 3.39	Sarfraz et al. 2014	6.6	1.23 and 3.71	6.8	1.20 and 3.70
		16.8	1.88 and 3.36	Sarfraz et al. 2014	7.7	1.50 and 3.50	10.6	1.39 and 3.40
		26.3	1.83 and 3.26	Sarfraz et al. 2014	11.5	1.50 and 3.48	11.3	1.36 and 2.99
		35.6	1.79 and 3.19	Sarfraz et al. 2014	19.5	1.70 and 3.29		

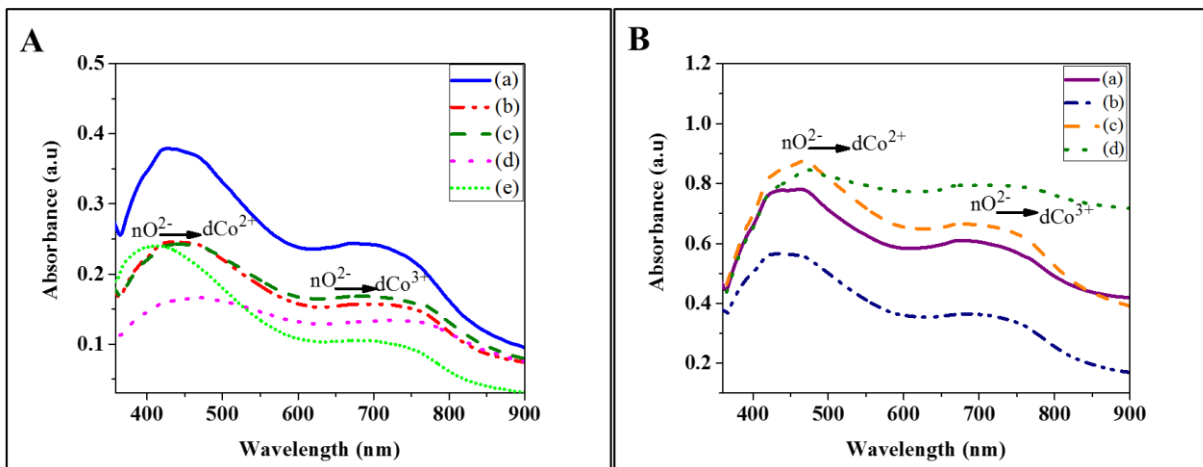


**Figure 4:13** UV-vis absorption spectra of  $\text{Co}_3\text{O}_4$  nanoparticles prepared at different amounts of  $\text{H}_2\text{O}_2$ : (A) spherical  $\text{Co}_3\text{O}_4$  nanoparticles (a) 2.9 mmol, (b) 1.4 mmol, (c) 0.74 mmol and (d) 0.37 mmol and (e) 0.14 mmol. (B) cubic  $\text{Co}_3\text{O}_4$  nanoparticles (a) 2.9 mmol, (b) 1.4 mmol, (c) 0.74 mmol and (d) 0.37 mmol.

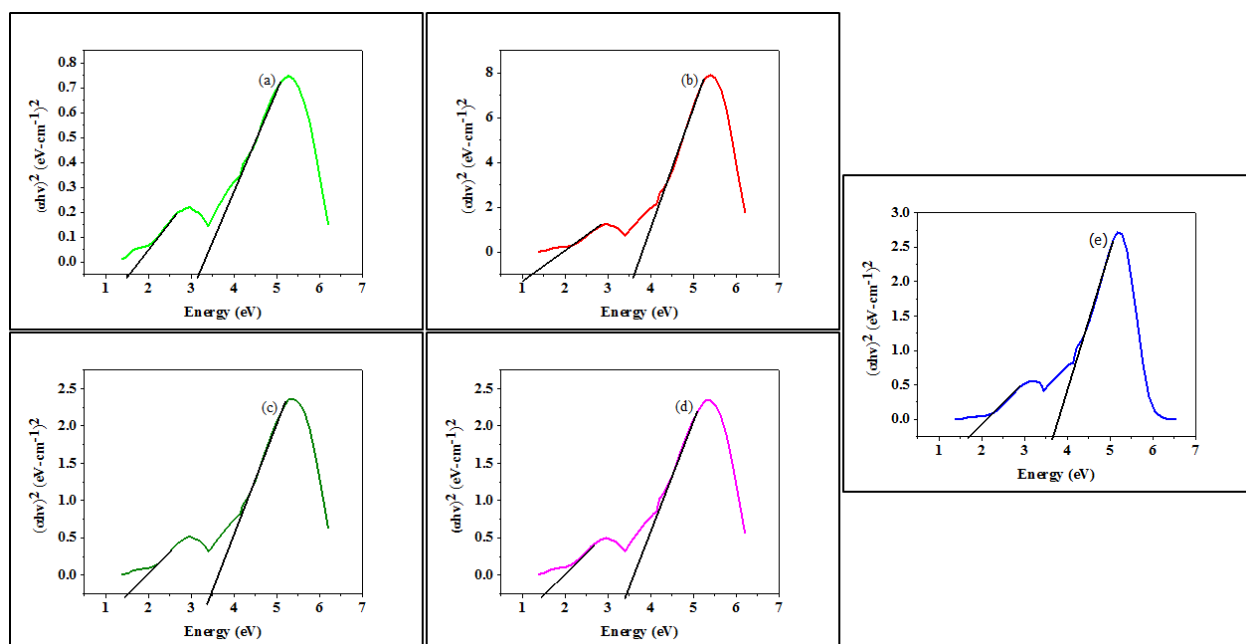


**Figure 4:14** Estimation of direct band gaps and electron transitions from Tauc plots for  $\text{Co}_3\text{O}_4$  nanoparticles made using cobalt nitrate. (a) 4.6 nm, (b) 6.8 nm, (c) 7.7 nm, (d) 11.5 nm and (e) 19.5 nm.

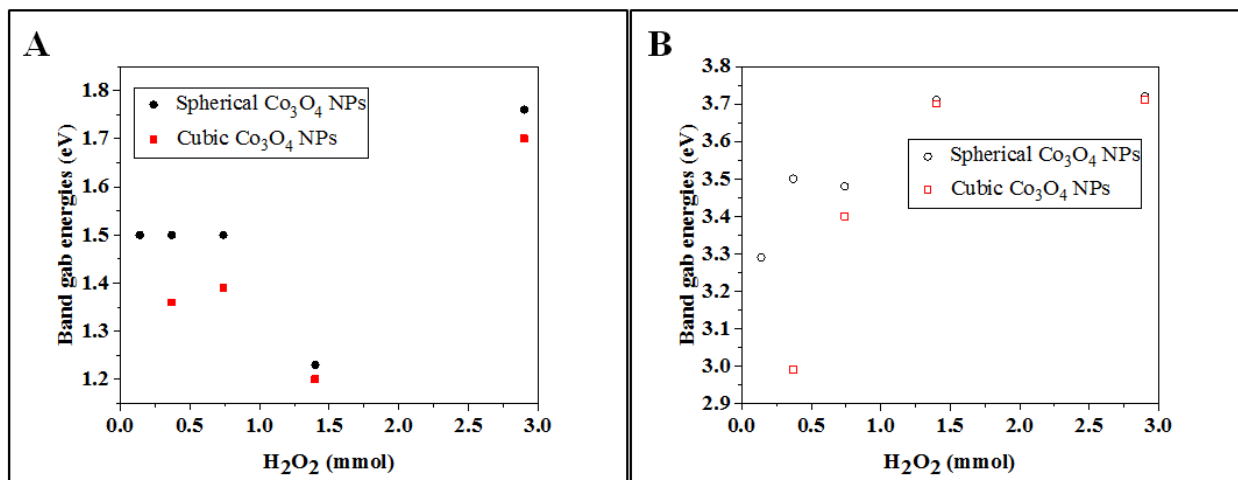


**Figure 4:15** Band gap and electron transition energies of prepared Co<sub>3</sub>O<sub>4</sub> nanoparticles estimated from Tauc plots. (A) O<sup>2-</sup> → Co<sup>3+</sup> and (B) O<sup>2-</sup> → Co<sup>2+</sup> charge transfer process.

The optimum amount of 2.9 mmol H<sub>2</sub>O<sub>2</sub> was found to be a better amount to prepare the Co<sub>3</sub>O<sub>4</sub> nanoparticles using both cobalt nitrate and cobalt acetate. This is because the Co<sub>3</sub>O<sub>4</sub> nanoparticles prepared at this amount yielded better and smaller Co<sub>3</sub>O<sub>4</sub> nano-particles that are mono-dispersed with a low degree of agglomeration. Therefore, the study was further aimed at investigating the influence of reaction time on the cobalt oxide nanoparticles using 2.9 mmol H<sub>2</sub>O<sub>2</sub>.

#### 4.1.3 Influence of time

The size of Co<sub>3</sub>O<sub>4</sub> nanoparticles can be controlled more easily by changing reaction time as reported by Feng and Zeng (2003) and Zhang et al. (2007). Feng and Zeng (2003) reported the increase in size of the Co<sub>3</sub>O<sub>4</sub> nanoparticles from 11.2 nm to 100 nm as the reaction time changed from 3 hrs to 24 hrs. Studies by He et al. (2005) showed that the shape of the nanoparticles can be well faceted when the growth rate is slow and the crystal formation is under thermodynamic control. The slow rate will result in a long reaction time required for adequate growth to take place. A longer reaction time can increase the size of the nanoparticles leading to a broader size distribution (Feng and Zeng, 2003, He et al., 2005, Zhang et al., 2007). Therefore, it is important to optimise the reaction time during the preparation of Co<sub>3</sub>O<sub>4</sub> nanoparticles. The experiment conducted was set in all the standard parameters as given in Table 3.1 in Chapter 3 but with variations of the reaction time for the preparation of the Co<sub>3</sub>O<sub>4</sub> nanoparticles. The cobalt oxide nanoparticles were prepared from cobalt nitrate in the presence of H<sub>2</sub>O<sub>2</sub> of 2.9 mmol and from

cobalt acetate in the absence of H<sub>2</sub>O<sub>2</sub>. The names of the catalysts for nanoparticles prepared from cobalt nitrate and cobalt acetate are N17, N18, N19, N20 and N21, N22, N23, and N25.

#### 4.1.3.1 XRD analysis

The diffraction pattern of Co<sub>3</sub>O<sub>4</sub> nanoparticles synthesized at different reaction times using cobalt nitrate (A) and cobalt acetate (B) are shown in Figure 4:16. Only the Co<sub>3</sub>O<sub>4</sub> phase was observed in the XRD spectra of all samples. As the reaction time was increased in all samples no change was observed in the phase, this showed that the phase of the cobalt oxide nanoparticles is not affected by time. However, the diffraction peak intensity of the cobalt oxide nanoparticles made using cobalt acetate (B) became more intense as the reaction time was prolonged. This is due to change in the crystallite size as the time is increased. For the Co<sub>3</sub>O<sub>4</sub> nanoparticles prepared using cobalt nitrate (A), there was a slight difference in the peak intensity with an increase in time. This indicates a small difference in the crystallite sizes made from this method. The diffraction patterns of the Co<sub>3</sub>O<sub>4</sub> nanoparticles prepared using cobalt nitrate (A) were broadened and less intense as compared to the diffraction patterns of the Co<sub>3</sub>O<sub>4</sub> nanoparticles from cobalt acetate (B). This signifies the smaller size of the nanoparticles. The sizes of the prepared cobalt oxide nanoparticles calculated using XRD data are shown in Table 4:5.

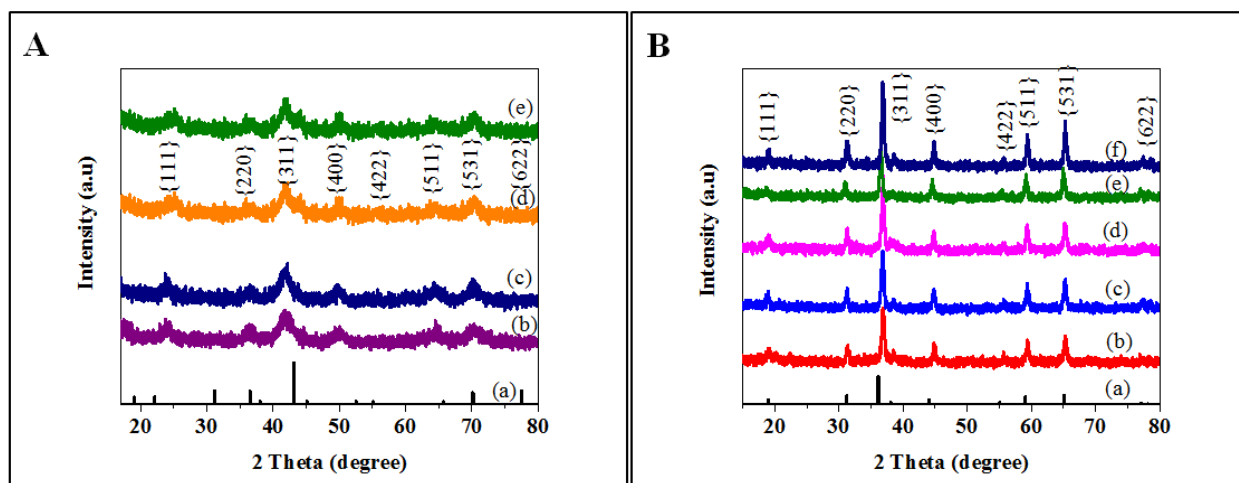


**Figure 4:16** XRD diffraction patterns of Co<sub>3</sub>O<sub>4</sub> NPs synthesized using different reaction times. Nanoparticles made using (A) Co(NO<sub>3</sub>)<sub>2</sub>.6H<sub>2</sub>O (a) reference Co<sub>3</sub>O<sub>4</sub>, (b) 1 hour , (c) 4 hrs, (d) 8 hours and (e) 16 hours. Nanoparticles made using (B) Co(CH<sub>3</sub>COO)<sub>2</sub>.4H<sub>2</sub>O (a) reference Co<sub>3</sub>O<sub>4</sub>, (b) 4 hrs, (c) 8 hrs, (d) 16 hrs, (e) 48 hrs and (f) 72 hrs.

#### 4.1.3.2 TEM analysis

To investigate the influence of time on the morphology and size of  $\text{Co}_3\text{O}_4$  nanoparticles, TEM was used. TEM images of  $\text{Co}_3\text{O}_4$  nanoparticles at different reaction times and their size distribution histograms are shown in Figure 4:17 and Figure 4:18. The sizes and yields of all the nanoparticles prepared at different reaction times are summarized in Table 4:5. As can be seen in Table 4:5, the average diameter was found to be between 2.6 to 5.9 nm, respectively, for cobalt oxide nanoparticles made using cobalt nitrate and 15.0 to 43.3 nm, respectively, for cobalt oxide nanoparticles made from cobalt acetate. Spherical and cubic shaped cobalt oxide nanoparticles were observed when cobalt nitrate and cobalt acetate were used as the cobalt sources (see Figure 4:17 and Figure 4:18). The increase in reaction time from 1 to 72 hrs, resulted in an increase in the size and the yield of the cobalt oxide nanoparticles in all samples as shown in Figure 4:19 and Figure 4:20. The cobalt oxide nanoparticles became well defined in shape with an increase in time and a reaction time of 4 hrs was found to result in cubic shaped nanoparticles. The results of He et al. (2005) showed that the smallest particle size for  $\text{Co}_3\text{O}_4$  nanoparticles with a cube like shape is 2.5 nm. A few 2.5 nm nanocubes were also detected in the HRTEM images of 2 nm nanospheres which confirms that the nanocubes are formed from nanospheres when their size reaches 2.5 nm. In all samples, an increase in the size of cobalt oxide nanoparticles was observed with increase in reaction time. For the nanoparticles, prepared using cobalt nitrate the size varies from 2.6 nm to 5.9 nm as the reaction time increased from 1 to 16 hrs. However, the cobalt oxide nanoparticles prepared from cobalt acetate shows an increase in size from 15.0 nm to 43.3 nm as reaction time is increased from 4 to 72 hrs. The sizes of the nanoparticles prepared from cobalt acetate were found to be larger than those from cobalt nitrate. This is due to the fact that the nanoparticles from cobalt acetate were prepared in the absence of  $\text{H}_2\text{O}_2$ . This result shows that a stronger oxidizing agent,  $\text{H}_2\text{O}_2$  is necessary to reduce the size of the nanoparticles. Feng and Zeng (2003) also found an increase in the size with an increase in the air oxidation time in the absence of  $\text{H}_2\text{O}_2$ . The change in particle size as the reaction time is prolonged agrees well with the published work of (He et al., 2005, Xu and Zeng, 2003, Zhang et al., 2007), where they found that the size increased from 2 nm to 4.7 nm when the reaction time was increased from 1.5 hrs to 2.5 hrs.

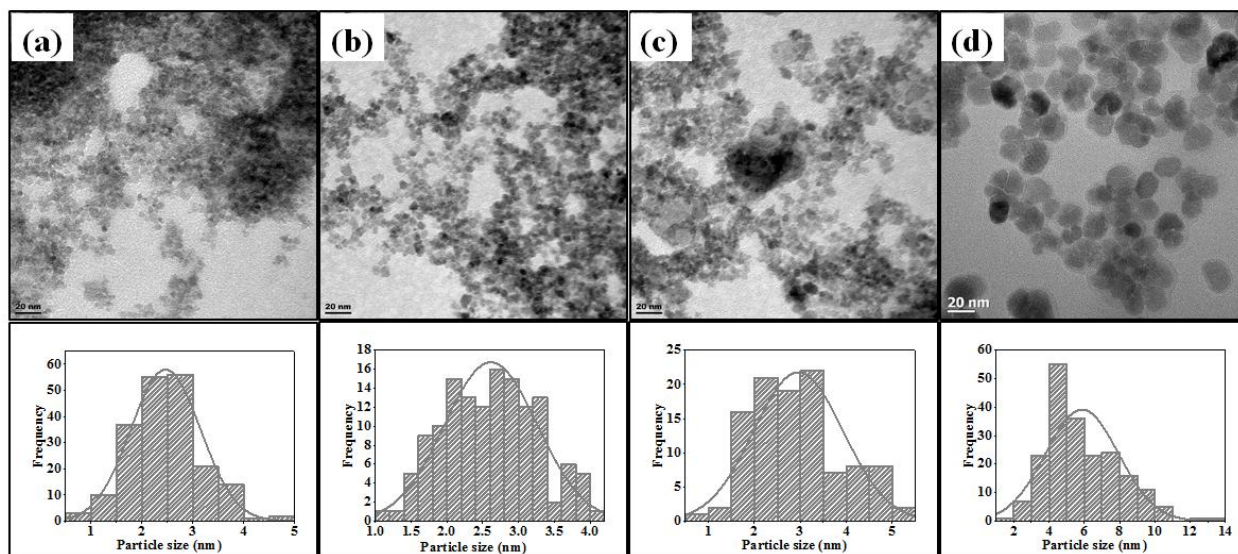


**Figure 4:17** Selected TEM images of  $\text{Co}_3\text{O}_4$  NPs synthesized at  $85^\circ\text{C}$  using  $\text{Co}(\text{NO}_3)_2 \cdot 6\text{H}_2\text{O}$  (a) 1 hr, (b) 4 hrs, (c) 8 hrs and (d) 16 hrs.

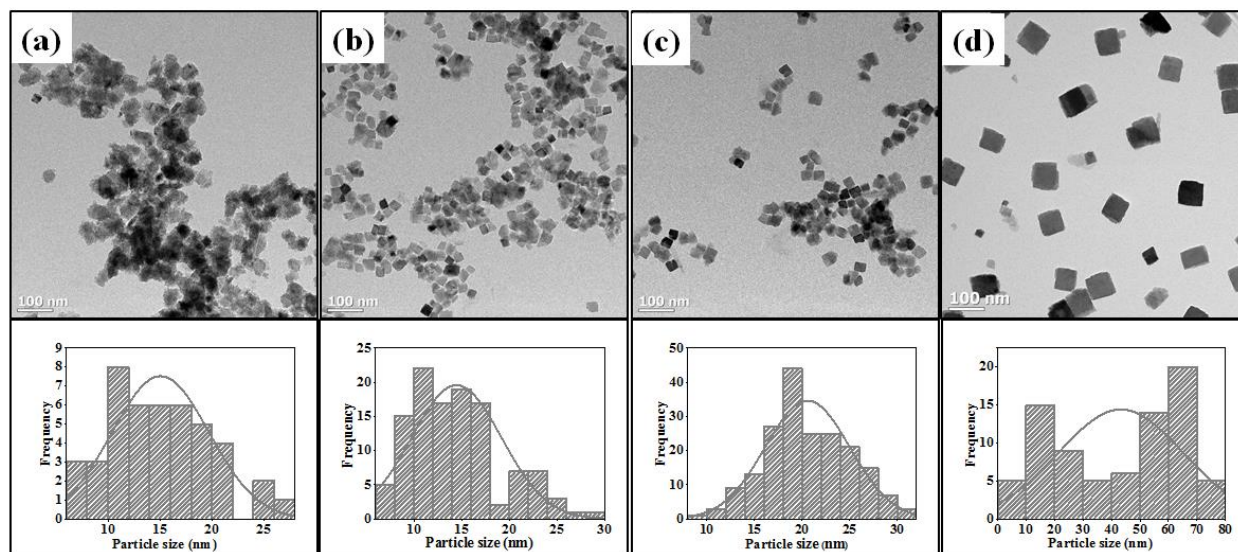


**Figure 4:18** Selected TEM images of  $\text{Co}_3\text{O}_4$  NPs synthesized at  $85^\circ\text{C}$  using  $\text{Co}(\text{CH}_3\text{COO})_2 \cdot 4\text{H}_2\text{O}$ . (a) 4 hrs, (b) 8 hrs, (c) 16 hrs and (d) 72 hrs.

Both XRD and TEM techniques showed an increase in the size and yields of the nanoparticles with increase in the reaction time. Several studies have been done on the influence of reaction time during the preparation of  $\text{Co}_3\text{O}_4$  nanoparticles and they concluded that the increase in particle size

is due to the particle growth. The reaction time of about 3 hrs is required to obtain cubic shaped nanoparticles (Xu and Zeng, 2003). In this study a reaction time of about 4 hrs was found to make cubic shaped nanoparticles. The difference may be due to different preparation methods that were used to prepare the  $\text{Co}_3\text{O}_4$  nanoparticles.

**Table 4:5**  $\text{Co}_3\text{O}_4$  nanoparticles sizes determination with XRD and TEM data.

<b><math>\text{Co}_3\text{O}_4</math> nanoparticles using cobalt nitrate</b>						<b><math>\text{Co}_3\text{O}_4</math> nanoparticles using cobalt acetate</b>					
<b>Catalyst name</b>	<b>Time (hrs)</b>	<b>XRD size (nm)</b>	<b>TEM size (nm)</b>	<b>TEM std (nm)</b>	<b>Yield (%)</b>	<b>Catalyst name</b>	<b>Time (hrs)</b>	<b>XRD size (nm)</b>	<b>TEM size (nm)</b>	<b>TEM std (nm)</b>	<b>Yield (%)</b>
N17	1	2.0	2.6	0.7	66.8						
N18	4	2.3	2.9	0.9	72.6	N21	4	16.2	15.0	4.7	64.4
N19	8	3.0	3.0	1.0	81.6	N22	8	16.8	15.0	4.7	67.4
N20	16	5.9	5.9	2.1	98.1	N23	16	15.6	16.0	4.1	82.9
						N24	48	18.2	20.6	4.4	89.3
						N25	72	14.8	43.3	21.9	—

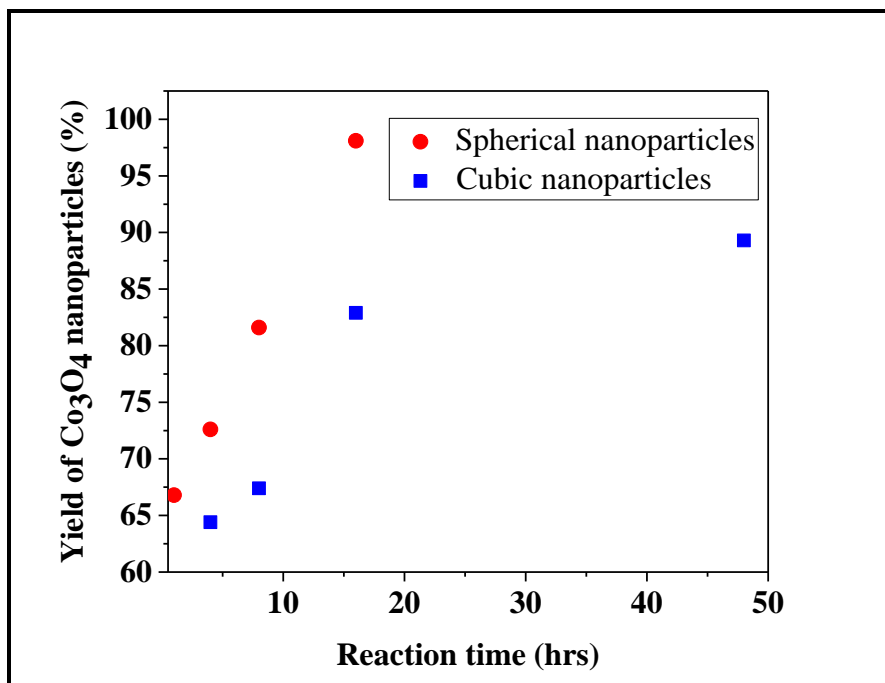


**Figure 4:19** Yields of  $\text{Co}_3\text{O}_4$  nanoparticles dependence on different reaction times.

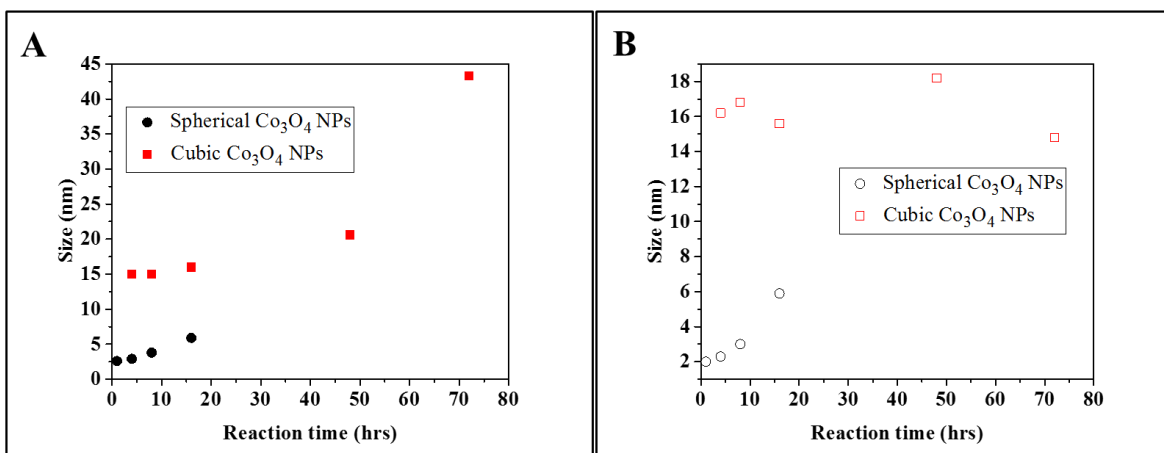


**Figure 4:20**  $\text{Co}_3\text{O}_4$  nanoparticles size dependence on time: spherical and cubic  $\text{Co}_3\text{O}_4$  nanoparticles size calculated using (A) TEM and (B) XRD.

#### 4.1.3.3 UV-vis absorption studies

Figure 4:21, shows the absorption spectra of cobalt oxide nanoparticles made from cobalt nitrate (A) and cobalt acetate (B) at different reaction times. There are two absorption peaks in bulk  $\text{Co}_3\text{O}_4$  at around 729 and 435 nm respectively (Thota et al., 2009). When the crystallite sizes decrease there was a blue shift of the cobalt oxide nanoparticles at around 680 and 400 nm for nanoparticles

made from cobalt nitrate and 700 nm and 430 nm for particles prepared from cobalt acetate (Figure 4:20A and 4:20B). This is associated with the  $\text{Co}_3\text{O}_4$  nanoparticles being smaller than the bulk cobalt oxide.

The transitions of the cobalt oxide nanoparticles were estimated from Tauc plots and are shown in Figure 4:22. Table 4:6 and Figure 4:22 shows a decrease in band gaps and electron transitions with an increase in reaction time of all the prepared nanoparticles. This observation indicates that the sizes of the nanoparticles are becoming larger with an increase in reaction time. The band gaps and the electron transitions of the nanoparticles made from cobalt nitrate vary from 1.70 to 1.75 eV and 2.82 to 2.96 eV, respectively, while those made using cobalt acetate vary from 1.60 to 1.78 eV and 2.56 to 2.78 eV, respectively, for  $\text{O}^{2-} \rightarrow \text{Co}^{3+}$  and  $\text{O}^{2-} \rightarrow \text{Co}^{2+}$  charge transfer processes. The band gaps and electron transition energies of the nanoparticles from cobalt nitrate were larger than the that of the nanoparticles from cobalt acetate. This is another confirmation that the particles made from cobalt acetate are larger than the ones prepared from cobalt nitrate. These results correlate with the results observed from XRD and TEM data.

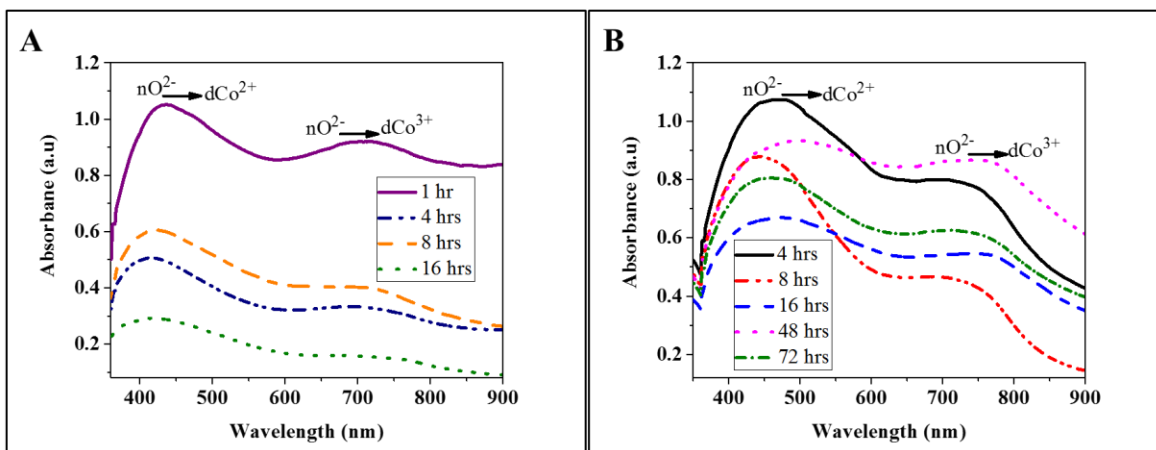


**Figure 4:21** UV-vis absorption spectra of  $\text{Co}_3\text{O}_4$  nanoparticles prepared at different reaction times: (A) spherical  $\text{Co}_3\text{O}_4$  nanoparticles (a) 1 hr, (b) 4 hrs, (c) 8 hrs and (d) 16 hrs. (B) cubic  $\text{Co}_3\text{O}_4$  nanoparticles (a) 4 hrs, (b) 8 hrs, (c) 16 hrs, (d) 48 hrs and (e) 72 hrs.

**Table 4:6** Effect of reaction time on band gap energies of the prepared  $\text{Co}_3\text{O}_4$  nanoparticles calculated using (Tauc plots).

Spherical $\text{Co}_3\text{O}_4$ NPs			Cubic $\text{Co}_3\text{O}_4$ NPs		
Reaction time (hrs)	Size (nm)	$E_{g1}$ and $E_{g2}$ (eV)	Reaction time (hrs)	Size (nm)	$E_{g1}$ and $E_{g2}$ (eV)
1	2.6	1.75 and 2.96	4	15.0	1.78 and 2.82
4	2.9	1.71 and 2.95	8	15.0	1.70 and 2.78
8	3.8	1.70 and 2.94	16	16.0	1.66 and 2.66
16	5.9	1.70 and 2.82	48	20.6	1.63 and 2.64
			72	43.3	1.60 and 2.56

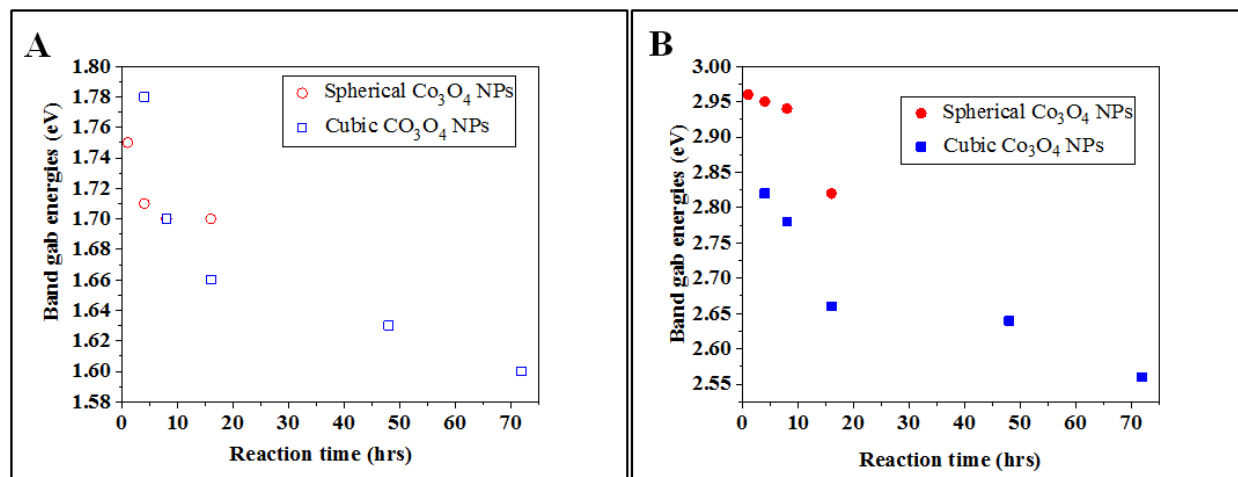


**Figure 4:22** Band gaps and electron transition energies of prepared  $\text{Co}_3\text{O}_4$  nanoparticles estimated from Tauc plots. (A)  $\text{O}^{2-} \rightarrow \text{Co}^{3+}$  and (B)  $\text{O}^{2-} \rightarrow \text{Co}^{2+}$  charge transfer process.

#### 4.1.4 Concluding remarks

Both XRD and TEM showed that cobalt oxide nanoparticles with different sizes and shapes were obtained in all cases. The XRD patterns showed a cubic  $\text{Co}_3\text{O}_4$  phase for all the prepared nanoparticles. The shape of the cobalt oxide nanoparticles changed from spherical to cubic when cobalt precursor was changed from cobalt nitrate to cobalt acetate. This was due to the presence of acetate ions that are acting as a capping molecules on the surface of the cobalt oxide nanoparticles. The FTIR spectroscopy and TGA analysis have indicated the presence of both the nitrate and acetate ions on the surface of cobalt oxide nanoparticles, and that their adsorption are not the same. A general trend was observed for all the prepared cobalt oxide nanoparticles. An increase in the amount of hydrogen peroxide decreased the size of the nanoparticles from 19.5 to

3.0 nm and 3.2 to 11.3 nm, for the nanoparticles prepared using cobalt nitrate and cobalt acetate. Similarly, the yield of the nanoparticles prepared from cobalt nitrate increased from 29 % to 98 % while those prepared from cobalt acetate increased from 23 % to 58 %. The UV-vis absorption studies of all the prepared cobalt oxide nanoparticles showed two absorption peaks which are due to showed to  $O^{2-} \rightarrow Co^{3+}$  and  $O^{2-} \rightarrow Co^{2+}$  charge transfer process.

Different reaction times were also used to study their effect on the size of the nanoparticles. An increase in the reaction time of oxidation by air from 1 to 16 hrs increased the spherical and cubic shaped nanoparticles size from 2.6 to 5.9 nm and 15.0 to 43.3 nm. Increase in the reaction time also increased the yield from 67 % to 98 % and 64 % to 89 % for spherical and cubic shaped cobalt oxide nanoparticles.

## 4.2 REFERENCES

- AMIRI, S. H., VAEZI, M. & KANDJANI, A. E. 2011. A comparison between hydrothermally prepared  $\text{Co}_3\text{O}_4$  via  $\text{H}_2\text{O}_2$  assisted and calcination methods. *Journal of Ceramic Processing Research*, 12, 327-331.
- CHAKRABARTY, S. & CHATTERJEE, K. 2012. A facile and general route to size-controlled synthesis of metal (Ni, Co and Mn) oxide nanoparticle and their optical behavior. *Nanoscience Methods*, 1, 213-222.
- FENG, J. & ZENG, H. C. 2003. Size-controlled growth of  $\text{Co}_3\text{O}_4$  nanocubes. *Chemistry of Materials*, 15, 2829-2835.
- HE, T., CHEN, D., JIAO, X., WANG, Y. & DUAN, Y. 2005. Solubility-controlled synthesis of high-quality  $\text{Co}_3\text{O}_4$  nanocrystals. *Chemistry of Materials*, 17, 4023-4030.
- JIANG, Y., WU, Y., XIE, B., XIE, Y. & QIAN, Y. 2002. Moderate temperature synthesis of nanocrystalline  $\text{Co}_3\text{O}_4$  via gel hydrothermal oxidation. *Materials Chemistry and Physics*, 74, 234-237.
- KISHORE, P. & JEEVANANDAM, P. 2013. Synthesis of cobalt oxide nanoparticles via homogeneous precipitation using different synthetic conditions. *Journal of Nanoscience and Nanotechnology*, 13, 2908-2916.
- SALAVATI-NIASARI, M., KHANSARI, A. & DAVAR, F. 2009. Synthesis and characterization of cobalt oxide nanoparticles by thermal treatment process. *Inorganica Chimica Acta*, 362, 4937-4942.
- SARFRAZ, A. & HASANAIN, S. 2014. Size Dependence of magnetic and optical properties of  $\text{Co}_3\text{O}_4$  Nanoparticles. *Acta Physica Polonica, A.*, 125, 75-78
- SONG, X. C., WANG, X., ZHENG, Y. F., MA, R. & YIN, H. Y. 2011. Synthesis and electrocatalytic activities of  $\text{Co}_3\text{O}_4$  nanocubes. *Journal of Nanoparticle Research*, 13, 1319-1324.
- SU, D., DOU, S. & WANG, G. 2014. Single crystalline  $\text{Co}_3\text{O}_4$  nanocrystals exposed with different crystal planes for Li- $\text{O}_2$  batteries. *Scientific Reports*, 4, 5767.
- THOTA, S., KUMAR, A. & KUMAR, J. 2009. Optical, electrical and magnetic properties of  $\text{Co}_3\text{O}_4$  nanocrystallites obtained by thermal decomposition of sol-gel derived oxalates. *Materials Science and Engineering: B*, 164, 30-37.
- WARANG, T., PATEL, N., SANTINI, A., BAZZANELLA, N., KALE, A. & MIOTELLO, A. 2012. Pulsed laser deposition of  $\text{Co}_3\text{O}_4$  nanoparticles assembled coating: role of substrate

temperature to tailor disordered to crystalline phase and related photocatalytic activity in degradation of methylene blue. *Applied Catalysis A: General*, 423, 21-27.

XIA, S., YU, M., HU, J., FENG, J., CHEN, J., SHI, M. & WENG, X. 2014. A model of interface-related enhancement based on the contrast between  $\text{Co}_3\text{O}_4$  sphere and cube for electrochemical detection of hydrogen peroxide. *Electrochemistry Communications*, 40, 67-70.

XIAO, J. & QI, L. 2011. Surfactant-assisted, shape-controlled synthesis of gold nanocrystals. *Nanoscale*, 3, 1383-1396.

XU, R. & ZENG, H. C. 2003. Mechanistic investigation on salt-mediated formation of free-standing  $\text{Co}_3\text{O}_4$  nanocubes at  $95^\circ\text{C}$ . *The Journal of Physical Chemistry B*, 107, 926-930.

YANG, Y.-P., LIU, R.-S., HUANG, K.-L., WANG, L.-P., LIU, S.-Q. & ZENG, W.-W. 2007. Preparation and electrochemical performance of nanosized  $\text{Co}_3\text{O}_4$  via hydrothermal method. *Transactions of Nonferrous Metals Society of China*, 17, 1334-1338.

ZHANG, Y., LIU, Y., FU, S., GUO, F. & QIAN, Y. 2007. Morphology-controlled synthesis of  $\text{Co}_3\text{O}_4$  crystals by soft chemical method. *Materials Chemistry and Physics*, 104, 166-171.

## CHAPTER 5

### 5.1 DEGRADATION STUDIES

To investigate the activity of the synthesized cobalt oxide nanoparticles, methylene blue was used as an organic pollutant. Methylene blue is one of the most commonly used dye for the textile industry. It is mostly known to possess many toxic effects to human beings and animals including irritation to the skin, heart rate and is resistant to degradation by conventional methods thus, human intervention is required to degrade this pollutant by chemical methods such as Fenton-like reaction. As discussed in Chapter 2, The Fenton process is widely used for the degradation of organic pollutants with hydroxyl radicals constituting the major oxidizing species. However, the Fenton process is found to suffer from drawbacks in the separation and regeneration of homogeneous catalysts (Hu et al., 2017, Wang et al., 2013). These drawbacks can be overcome by using heterogeneous catalytic oxidation in the Fenton-like systems, which can also provide the possibility of operating over a broader pH range.

As is well-known, the catalytic activities of heterogeneous catalysts are related to their shape and size. Heterogeneous catalysts are usually composed of assorted polycrystals with different exposed crystal planes, possessing several kinds of active sites, which exhibit different reactivities (Hu et al., 2008). The different reactivity and selectivity of these catalysts depend greatly upon the different arrangement manner of surface atoms and the number of dangling bonds on different crystal planes (Hu et al., 2008). In this work, the influence of size and shape of the prepared oxide nanoparticles was investigated on the degradation of methylene blue to establish a heterogeneous Fenton-like catalyst.

Table 5:1 shows five spherical and cubic shaped cobalt oxide nano-catalysts of different sizes selected, to study their influence of size on the degradation of methylene blue. The catalysts were given an hour to reach adsorption equilibrium (details of procedure in Chapter 3) and a negligible amount of decrease in the methylene blue concentration was observed. The beaker of the solution was covered with foil during the reaction to prevent photo-degradation.

**Table 5:1** Selected Co<sub>3</sub>O<sub>4</sub> nano-catalysts for each set (spherical and cubic) with different size range.

Spherical cobalt oxide nanoparticles		Cubic cobalt oxide nanoparticles	
Catalyst name	TEM size (nm)	Catalyst name	TEM size (nm)
N6	4.6	N13	6.6
N7	6.4	N14	6.8
N8	7.7	N15	10.8
N9	11.5	N23	16.0
N10	19.5	N25	43.3

### 5.1.1 Influence of size using spherical cobalt oxide nanoparticles on the degradation of methylene blue (MB)

#### 5.1.1.1 Comparison of discoloration of methylene blue in various degradation systems

Preliminary control experiments were carried out by degrading methylene blue (MB) in the absence of a catalyst. As shown in Figure 5:1(a), without the cobalt oxide nanoparticles, a negligible amount of degradation of methylene blue was observed and the intense absorption peak at around 660 nm was still observed even after 60 min reaction. This can be related to the low oxidation potential of H<sub>2</sub>O<sub>2</sub> compared with OH radicals (Wan et al., 2016). When the cobalt oxide nanoparticles were added to methylene blue solution, the absorption peak of methylene blue at 660 nm started decreasing and finally disappeared after 60 min Figure 5:1(b). This indicates that the spherical cobalt oxide nanoparticles catalyze the degradation of MB. The decrease in the intensity of the spectra in the presence of cobalt oxide nanoparticles and H<sub>2</sub>O<sub>2</sub> confirms that the combination of cobalt oxide nanoparticles and H<sub>2</sub>O<sub>2</sub> are necessary to achieve high percentages of methylene blue degradation.

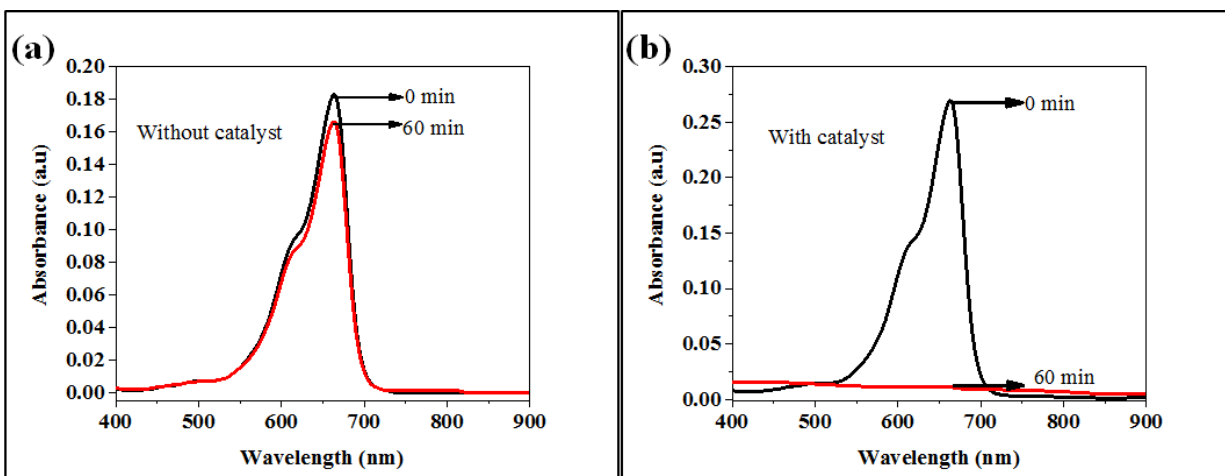


**Figure 5:1** Comparison of discoloration of methylene blue in various degradation systems namely (a) without and (b) with spherical  $\text{Co}_3\text{O}_4$  nanoparticles.

### 5.1.1.2 Spherical cobalt oxide nanoparticles size influenced on the degradation of methylene blue

Time dependent UV-vis absorption spectra of methylene blue (MB) catalyzed by the smallest and largest particle size (4.6 and 19.5 nm) at regular intervals is shown in Figure (5:2a and 5:2b). The rate at which the absorption peak of MB is decreasing is much faster when the particle size is 4.6 nm than 19.5 nm Figure (5:2a and 5:2b). This is attributed to the smallest average particle size distribution resulting from the 4.6 nm size.

The catalytic activity of methylene blues by spherical cobalt oxide nanoparticles of different sizes was then investigated. Figure (5:3a and 5:3b) shows the removal efficiency and percentage degradation of methylene blue. The percentage degradation of methylene blue (see Appendix A4.1 and A4.2 for calculations) for 4.6, 6.4, 7.7, 11.5 and 19.5 nm cobalt oxide nanoparticles were 98.7, 80.2, 60.8, 59.5 and 53.5 percent respectively, after 20 min. The activity data shows that the nanoparticle size of 4.6 nm exhibited higher catalytic activity as compared to the activity of all the other catalysts as shown in Figure (5:3a and 5:3b). The enhanced catalytic activity for the smallest nanoparticle may be explained in that the nanoparticles with smaller size have larger surface area which provide more active sites for adsorption of methylene blue on the surface of the catalyst which leads to efficient contact with the pollutant molecules (Dong et al., 2007, Espinosa et al., 2018, Wan et al., 2016, Warang et al., 2012). Another argument may be that the higher surface

area from the smallest size may produce  $\cdot\text{OH}$  radicals faster than the largest size on the surface of  $\text{Co}_3\text{O}_4$  nanoparticles. The higher surface area (coming from the smaller size) might increase the amount of pollutant adsorbing and the rate of hydroxyl radical formation (Wan et al., 2016).

Similar results have previously been reported that it is the adsorption property of heterogeneous catalyst that causes the improvement in the rate of pollutant degradation (Dhas et al., 2015, Wan et al., 2016, Wang et al., 2013).

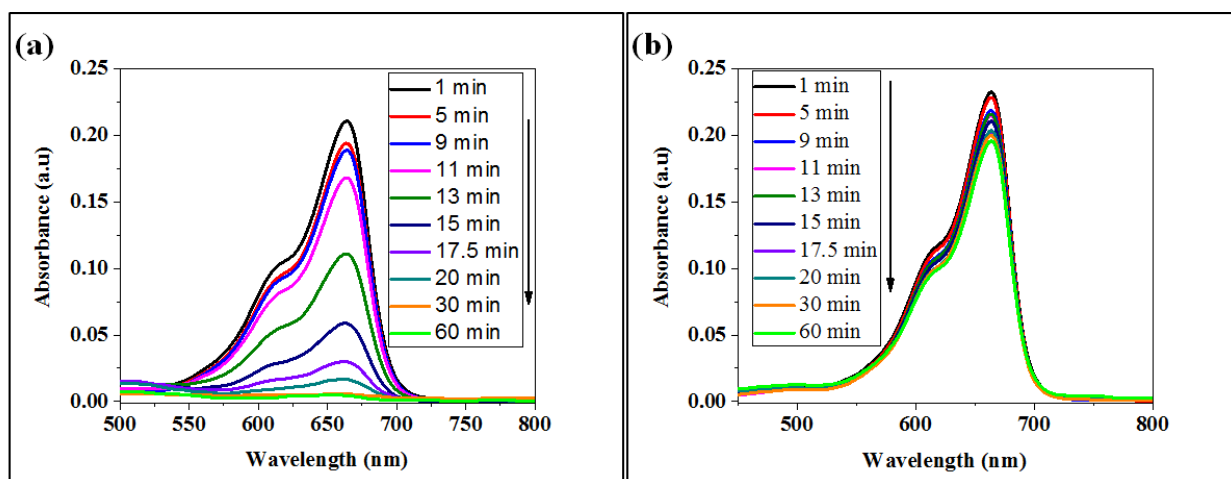


**Figure 5:2** Degradation of methylene blue using spherical  $\text{Co}_3\text{O}_4$  nanoparticles of (a) 4.6 nm (b) 19.5 nm.

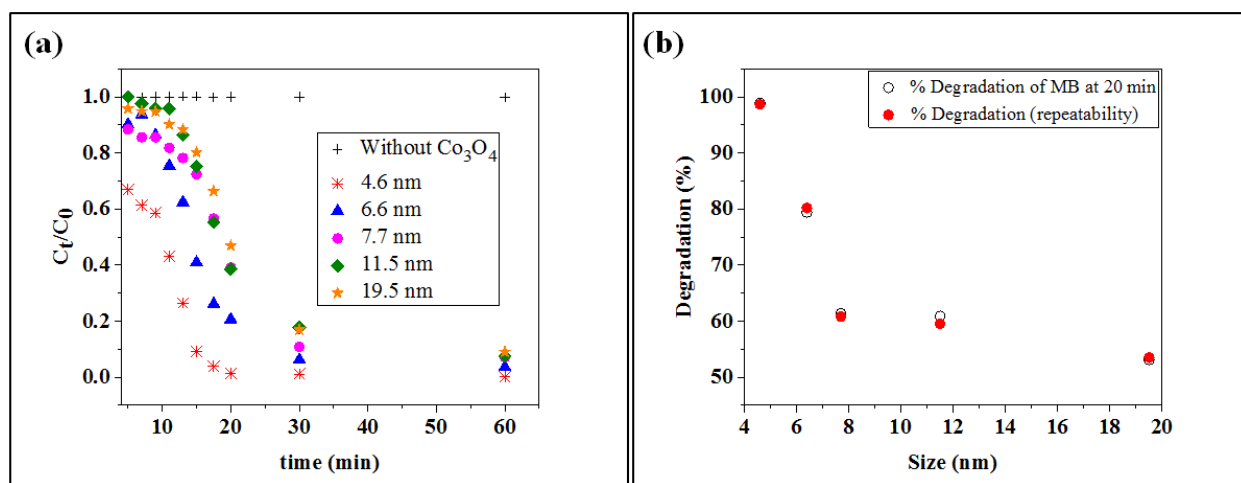


**Figure 5:3** (a) Removal efficiency of MB and (b) Percentage degradation of MB at 20 min with the repeated results for different sizes of spherical  $\text{Co}_3\text{O}_4$  nanoparticles.

### 5.1.1.3 Confirmation of the decolorization of the solution

Confirmation of the above observations on the degradation of methylene blue (MB) was further supported by FTIR spectroscopy. Leuco MB is the reduced form of MB, which is colourless in aqueous solution and can be re-oxidized when it is in contact with the atmospheric oxygen as reported by (Lee et al., 2017, Zidan et al., 2018, Ilunga and Meijboom, 2016). To confirm that the decolorization change of the solution was not due to the presence of leuco MB, FTIR spectroscopy was used. As seen in Figure 5:4(a), prior to degradation MB exhibited vibration bands centered at 3400 to 3500  $\text{cm}^{-1}$ , 2920  $\text{cm}^{-1}$  and 2850  $\text{cm}^{-1}$ , 1630  $\text{cm}^{-1}$ , 1380  $\text{cm}^{-1}$ , 1210  $\text{cm}^{-1}$  and 980  $\text{cm}^{-1}$  designated to the OH group, C-H asymmetric stretches, C=C or C=N double bonds, aromatic rings, C-H<sub>3</sub> bending vibrations, C-N stretch and C-H aromatic bending respectively. After treatment by the Fenton-like reaction, the majority of the characteristic bands mentioned above disappeared, indicating the degradation of MB molecule by breaking of central and side aromatic rings and demethylation (Figure 5:4b). Except the broad peaks at around 3500  $\text{cm}^{-1}$  to 3400  $\text{cm}^{-1}$  and 1637  $\text{cm}^{-1}$  which indicates the presence of hydroxyl ions due to the bending modes of water. Meanwhile, a new peak at around 1644  $\text{cm}^{-1}$  (see Figure 5:4b), appeared which might be due to the stretching vibration of COO<sup>-</sup> respectively, this may suggest that the carboxylic acids were the main products (Xu et al., 2011). Hue et al. (2017) has also observed complete degradation of methylene blue using a Fenton-like reaction and the reaction mechanism is explained in Chapter 3.

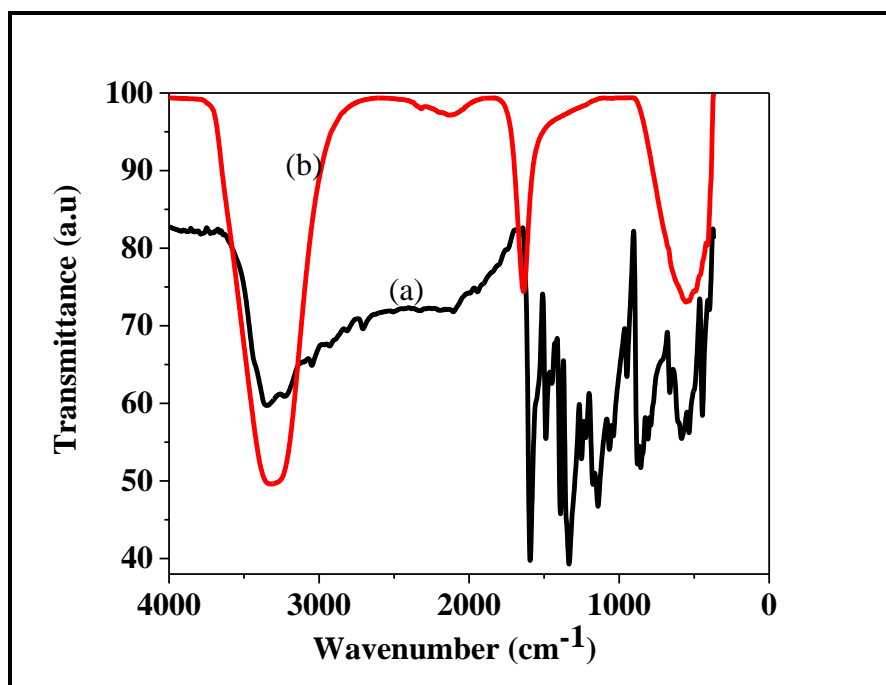


**Figure 5:4** FTIR spectra of (a) MB reaction mixture before degradation and (b) MB reaction mixture after degradation with  $\text{Co}_3\text{O}_4$  nanoparticles of 4.6 nm.

#### 5.1.1.4 Spherical cobalt oxide nanoparticles size influenced degradation kinetic studies

The rate of degradation kinetics was fitted to the pseudo-first-order and pseudo-second-order kinetics to determine which kinetic model gave the best fit. Results are shown in Figure 5:5 and Table 5:2. The data fitted the pseudo first order kinetics equation in terms of methylene blue well with a correlation coefficients values that are between 0.9402 and 0.9897  $\text{min}^{-1}$ . The rate constants were calculated for all five different sizes of spherical cobalt oxide nano-catalysts and were found to be between 0.0691 and 0.4118  $\text{min}^{-1}$  (see Table 5:2). Appendix A5.1 and A5.2 shows details of calculations. It was further observed that the reaction rates are influenced by the catalyst sizes. The kinetic results presented in Figure 5:5 were plotted after 10 min of the reaction and this was due to the induction periods that occurred during the first 10 min. Therefore one may argue that this reaction followed a two-stage degradation pseudo first order reaction which is composed of an induction period (first stage) and a rapid degradation stage (second stage). One of the most important current limitations in both homogeneous and heterogeneous catalysts is how to promote the Fenton reaction at neutral pH values without the need of excess  $\text{H}_2\text{O}_2$  (Espinosa et al., 2018). Typically, the Fenton process operates at acidic pH values. However, observation in the profiles

of an induction period indicates that the reaction becomes accelerated as it proceeds and the pH value decreases from the initial value. The induction period is defined as a period of time during which no measured reaction occurs or a time before a reaction suddenly increases in rate (Xu et al., 2011). Zhou et al. (2008) have observed a two-stage pseudo first order degradation kinetics for the oxidation of 3,4-chlorophenol in zero valent iron/H<sub>2</sub>O<sub>2</sub> system. Xu and Wang (2012) have also reported a two-stage pseudo first order degradation kinetics for the removal of 2,4-dichlorophenol using Fe<sub>3</sub>O<sub>4</sub>/H<sub>2</sub>O<sub>2</sub> and they concluded that this was caused by the induction periods.

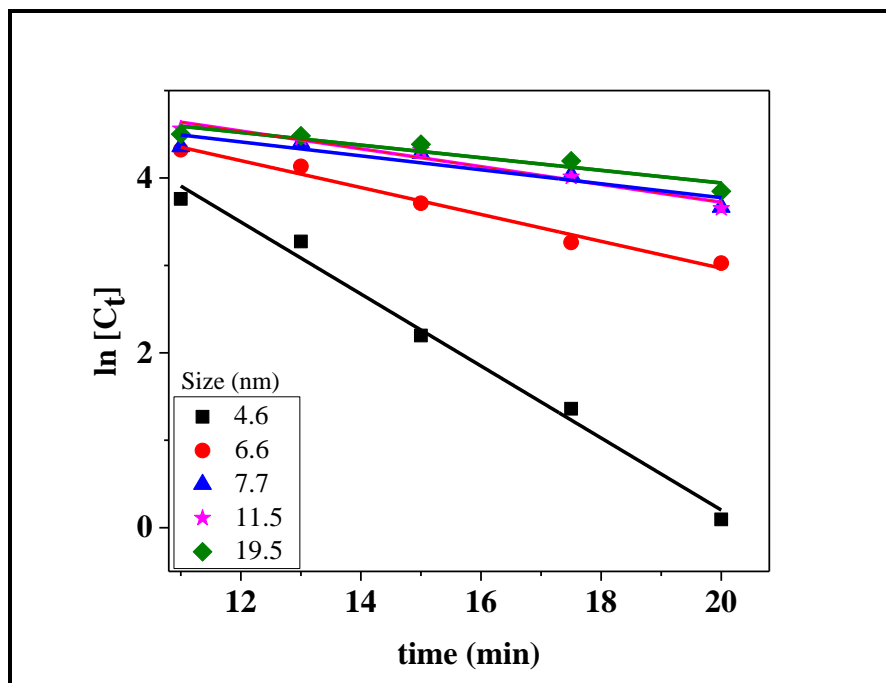


**Figure 5:5** Plot of  $\ln [C_t]$  against time for different sizes of spherical cobalt oxide nanoparticles on methylene blue degradation.

**Table 5:2** Size influenced degradation kinetics of MB using different sizes of selected spherical Co<sub>3</sub>O<sub>4</sub> nanoparticles.

TEM size (nm)	Degradation efficiency (%) at 20 (min)	Rate (k) (min <sup>-1</sup> )	Rate (k) (M.min) <sup>-1</sup>	R <sup>2</sup> first order	R <sup>2</sup> second order
4.6	98.9	0.412	0.082	0.989	0.974
4.6	98.7	0.392	0.061	0.964	0.909
6.6	79.4	0.154	0.005	0.983	0.909
6.6	80.2	0.155	0.004	0.966	0.977
7.7	64.4	0.102	0.005	0.963	0.907
7.7	60.8	0.087	0.002	0.911	0.926
11.5	60.9	0.093	0.002	0.961	0.849
11.5	59.5	0.079	0.003	0.997	0.948
19.5	53.1	0.069	0.001	0.940	0.826
19.5	53.5	0.068	0.001	0.900	0.800

#### 5.1.1.5 Turn Over Frequency of the results

The turn over frequency (TOF) is a surface specific activity and is defined as the moles of converted methylene blue molecules per min and exposed cobalt atoms on the catalyst surface. The TOF of the results were calculated using per surface cobalt atom from the sizes obtained by TEM and XRD sizes. Details concerning the calculation of TOF per surface cobalt atom of the cobalt oxide nanoparticles are provided in Appendix A6. The results of (Esswein et al., 2009, Wan et al., 2016) shows correlation between the calculated surface area using TEM sizes and the real surface area obtained from BET measurements (see Appendix A10 and A11). The constant number for surface cobalt atoms used was obtained from (Esswein et al., 2009). As can be seen in Figure 5:6, the TOF of the spherical cobalt oxide nanoparticles decreased with a decrease in the nanoparticles size. This may be due to the fact that, for TOF calculations, the smaller nanoparticles were not more agglomerated than the larger nanoparticles and that the cobalt site density remains constant in the tested size range. Dong et al. (2007), Wan et al. (2016) and Espinosa et al. (2018) have also reported a lower TOF in the smallest particles for the Fenton-like catalytic activity.

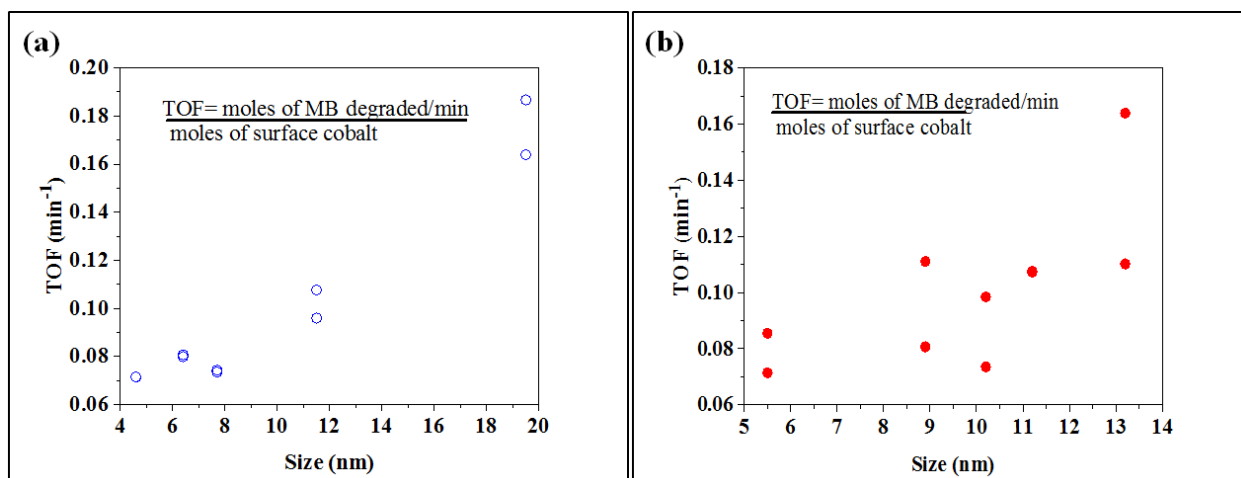


**Figure 5:6** TOF and repeated results of different sizes of spherical Co<sub>3</sub>O<sub>4</sub> nanoparticles calculated from (a) TEM and (b) XRD sizes.

#### 5.1.1.6 Leaching by oxalic acid

As already discussed in Chapter 2, the deactivation of the catalysts is of great importance, therefore, it is important to understand the factors that lead to the deactivation of the catalyst. Amongst the organic acids, oxalic acid has been reported as one of the intermediates of phenol oxidation and methylene blue degradation and it deserves a particular attention because of its ability to cause iron leaching from Fe-based catalysts (Di Luca et al., 2014, Rey et al., 2009, Xu et al., 2011). In this work, the influence of cobalt oxide (smaller and larger) particle size on the cobalt ions leached was investigated using oxalic acid. This experiment was done separately to monitor the cobalt ions leached at the same concentration of oxalic acid. For all the catalysts high cobalt leaching into the solution was observed and the smallest nanoparticle had the highest percentage of cobalt leached compared to the largest particle (see Table 5:3). This is due to larger surface area that are present on the smallest cobalt oxide nanoparticles. More cobalt ions are exposed to the surface therefore they become easily accessible to be leached by oxalic acid. Literature has also reported that high metal ions leaching could be due to the chelation of active metals by oxalic acid formed (Liotta et al., 2009).

**Table 5:3** Selected  $\text{Co}_3\text{O}_4$  catalysts for cobalt ions leached by oxalic acid.

TEM size (nm)	Cobalt ions leached (ppm)
4.6	98.0
19.5	78.4

### 5.1.2 Influence of size using cubic $\text{Co}_3\text{O}_4$ nanoparticles on the degradation of methylene blue (MB)

#### 5.1.2.1 Cubic cobalt oxide nanoparticles size influenced on the degradation of methylene blue

The catalytic degradation efficiencies of MB by different sizes of cubic cobalt oxide nanoparticles were obtained by plotting  $C_t/C_0$  time plots and is shown in Figure 5:7. Table 5:4 present the degradation efficiencies data, the rates constants and the correlation of coefficients obtained using different sizes of cubic  $\text{Co}_3\text{O}_4$  nanoparticles. As shown in Figure (5:7a and 5:7b), the catalytic activity increases with a decrease in the particle size and the cubic nanoparticle of 6.6 exhibited high catalytic activity compared to other cobalt oxide nanoparticle sizes. This results indicates that the higher surface area was beneficial in increasing the exposed active site number and adsorption of MB on the surface of the cobalt oxide nanoparticles, leading to a high degradation.

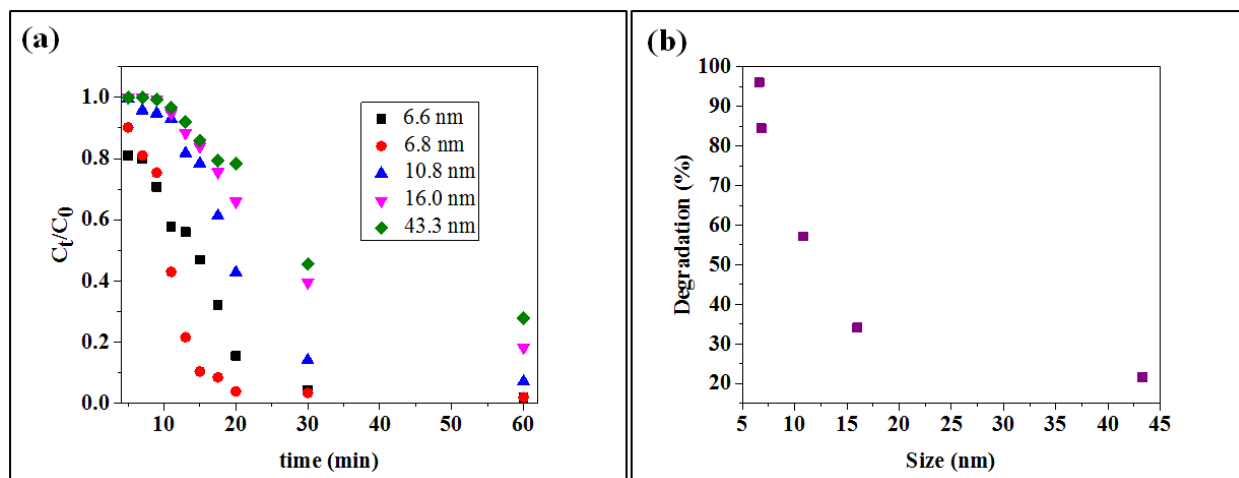


**Figure 5:7** (a) Removal efficiency of MB and (b) Percentage degradation of MB at 20 min of cubic  $\text{Co}_3\text{O}_4$  nanoparticles of different sizes

### 5.1.2.2 Cubic cobalt oxide nanoparticles size influenced degradation kinetic studies

The kinetics of the catalytic reaction of MB by different sizes of cubic  $\text{Co}_3\text{O}_4$  nanoparticles was evaluated and is shown in Figure 5:8. The results showed that the degradation kinetics fitted the pseudo first order kinetics equation well and good correlation coefficient values that are close to one ( $R^2 \sim 0.99$ ) were observed as seen in Table 5:4.

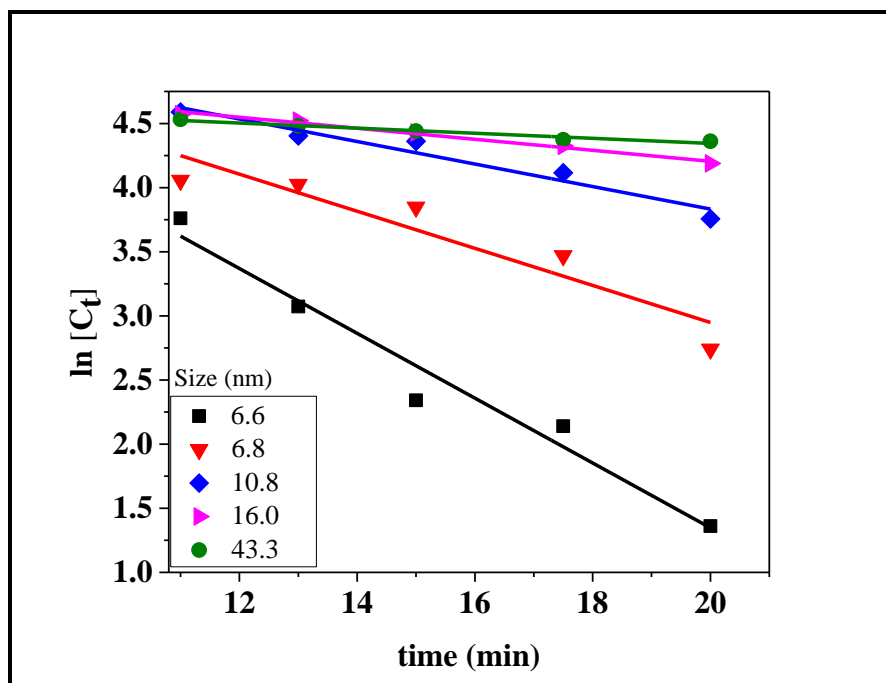


**Figure 5:8** Pseudo first order for different sizes of cubic  $\text{Co}_3\text{O}_4$  nanoparticles on the degradation of MB

**Table 5:4** Size influenced degradation of methylene blue using cubic  $\text{Co}_3\text{O}_4$  nanoparticles.

TEM size (nm)	Degradation efficiency (%) at 20 (min)	Rate (k) ( $\text{min}^{-1}$ )	Rate (k) ( $\text{M}\cdot\text{min}^{-1}$ )	$\text{R}^2$ first order	$\text{R}^2$ second order
6.6	96.1	0.253	0.015	0.987	0.966
6.8	84.5	0.146	0.012	0.972	0.962
10.8	57.2	0.088	0.0046	0.964	0.963
16.0	34.1	0.043	0.0009	0.960	0.906
43.3	21.6	0.019	0.0002	0.949	0.943

### 5.1.2.3 Turn Over Frequency of the results

Figure 5:9 shows the TOF of different sizes of cubic cobalt oxide nanoparticles. The results show an increase in TOF with increasing the particle size. This increase in TOF as the size increases can be explained by the ensemble theory, which assumes that a complex reaction like Fischer Tropsch (FT) synthesis cannot be catalysed by a single metal atom but requires a certain number of adjacent metal atoms in a specific geometric orientation to display catalytic activity as discussed in Chapter 2.

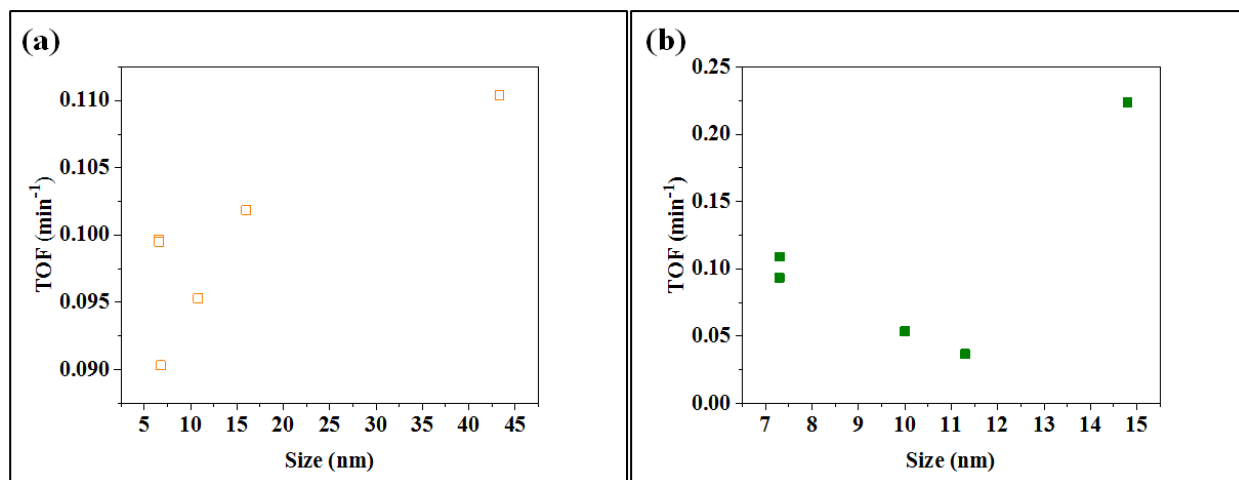


**Figure 5:9** TOF for the different sizes of cubic  $\text{Co}_3\text{O}_4$  nanoparticles calculated using (a) TEM and (b) XRD sizes

Furthermore, the influence of different sizes of cubic  $\text{Co}_3\text{O}_4$  nanoparticles was also examined on the cobalt ions leached using oxalic acid. Table 5.5 summarizes the results obtained. High amounts of cobalt ions leached were observed when the particle size was smaller compared to when the particle size is larger and this was due to larger surface area that are present on the surface of the smallest cobalt oxide nanoparticles (see Table 5:5).

**Table 5:5** Selected cubic  $\text{Co}_3\text{O}_4$  catalysts of different sizes for cobalt ions leached by oxalic acid.

TEM size (nm)	Cobalt ions leached (ppm)
6.6	82.4
43.3	67.8

### **5.1.3 Cobalt oxide nanoparticles shape influence on the catalytic activity of methylene blue (MB)**

The influence of shape of cobalt oxide nanoparticles was compared using two different shapes: spherical and cubic cobalt oxide nanoparticles. The TOF of each shape was combined in one graph as shown in Figure 5.10. The results did not show any shape dependence on the dye degradation. In contrast to this study, Bhatt et al. (2017) found that the shape of the nanoparticles influenced the rate of degradation of MB.

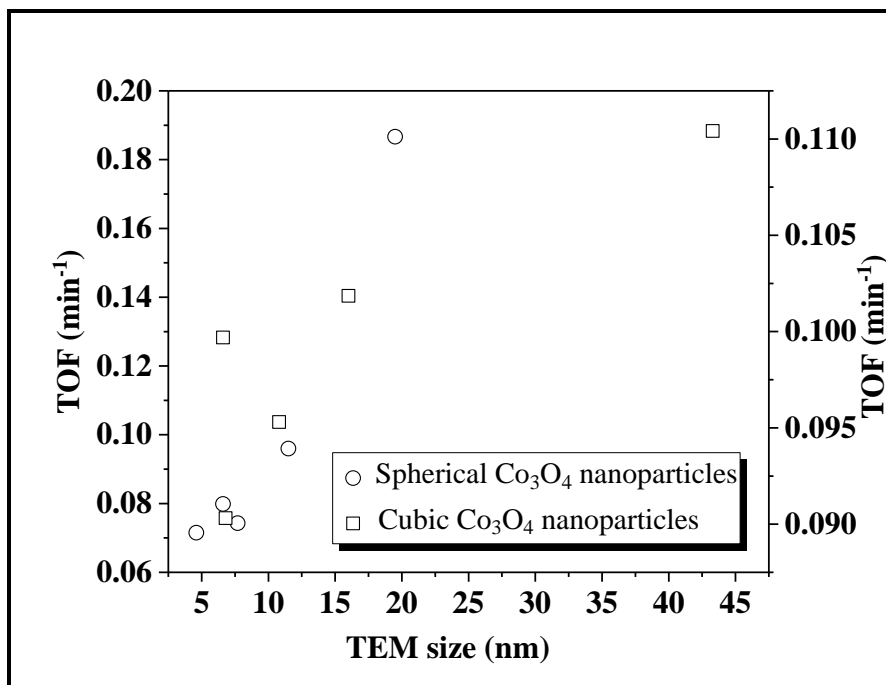


**Figure 5:10** Combined TOF for spherical and cubic Co<sub>3</sub>O<sub>4</sub> nanoparticles.

## 5.2 REFERENCES

- BHATT, C. S., NAGARAJ, B. & SURESH, A. K. 2017. Nanoparticles-shape influenced high-efficient degradation of dyes: Comparative evaluation of nano-cubes vs nano-rods vs nano-spheres. *Journal of Molecular Liquids*, 242, 958-965.
- DHAS, C. R., VENKATESH, R., JOTHIVENKATACHALAM, K., NITHYA, A., BENJAMIN, B. S., RAJ, A. M. E., JEYADHEEPAN, K. & SANJEEVIRAJA, C. 2015. Visible light driven photocatalytic degradation of Rhodamine B and Direct Red using cobalt oxide nanoparticles. *Ceramics International*, 41, 9301-9313.
- DI LUCA, C., MASSA, P., FENOGLIO, R. & CABELLO, F. M. 2014. Improved Fe<sub>2</sub>O<sub>3</sub>/Al<sub>2</sub>O<sub>3</sub> as heterogeneous Fenton catalysts for the oxidation of phenol solutions in a continuous reactor. *Journal of Chemical Technology and Biotechnology*, 89, 1121-1128.
- DONG, Y., HE, K., YIN, L. & ZHANG, A. 2007. A facile route to controlled synthesis of Co<sub>3</sub>O<sub>4</sub> nanoparticles and their environmental catalytic properties. *Nanotechnology*, 18, 435602.
- ESPINOSA, J. C., CATALÁ, C., NAVALÓN, S., FERRER, B., ÁLVARO, M. & GARCÍA, H. 2018. Iron oxide nanoparticles supported on diamond nanoparticles as efficient and stable catalyst for the visible light assisted Fenton reaction. *Applied Catalysis B: Environmental*, 226, 242-251.
- ESSWEIN, A. J., MCMURDO, M. J., ROSS, P. N., BELL, A. T. & TILLEY, T. D. 2009. Size-dependent activity of Co<sub>3</sub>O<sub>4</sub> nanoparticle anodes for alkaline water electrolysis. *The Journal of Physical Chemistry C*, 113, 15068-15072.
- HU, L., PENG, Q. & LI, Y. 2008. Selective synthesis of Co<sub>3</sub>O<sub>4</sub> nanocrystal with different shape and crystal plane effect on catalytic property for methane combustion. *Journal of the American Chemical Society*, 130, 16136-16137.
- HU, X., LI, R., ZHAO, S. & XING, Y. 2017. Microwave-assisted preparation of flower-like cobalt phosphate and its application as a new heterogeneous Fenton-like catalyst. *Applied Surface Science*, 396, 1393-1402.
- ILUNGA, A. K. & MEIJBOOM, R. 2016. Catalytic oxidation of methylene blue by dendrimer encapsulated silver and gold nanoparticles. *Journal of Molecular Catalysis A: Chemical*, 411, 48-60.
- LEE, S.-K., MILLS, A. & WELLS, N. 2017. Assessing photocatalytic activity using methylene blue without dye sensitisation. *Catalysis Today*, 331, 211-217.

- LIOTTA, L., GRUTTADAURIA, M., DI CARLO, G., PERRINI, G. & LIBRANDO, V. 2009. Heterogeneous catalytic degradation of phenolic substrates: catalysts activity. *Journal of Hazardous Materials*, 162, 588-606.
- REY, A., FARALDOS, M., CASAS, J., ZAZO, J., BAHAMONDE, A. & RODRÍGUEZ, J. 2009. Catalytic wet peroxide oxidation of phenol over Fe/AC catalysts: influence of iron precursor and activated carbon surface. *Applied Catalysis B: Environmental*, 86, 69-77.
- WAN, D., LI, W., WANG, G. & WEI, X. 2016. Size-controllable synthesis of Fe<sub>3</sub>O<sub>4</sub> nanoparticles through oxidation–precipitation method as heterogeneous Fenton catalyst. *Journal of Materials Research*, 31, 2608-2616.
- WANG, Q., TIAN, S. & NING, P. 2013. Degradation mechanism of methylene blue in a heterogeneous Fenton-like reaction catalyzed by ferrocene. *Industrial & Engineering Chemistry Research*, 53, 643-649.
- WARANG, T., PATEL, N., SANTINI, A., BAZZANELLA, N., KALE, A. & MIOTELLO, A. 2012. Pulsed laser deposition of Co<sub>3</sub>O<sub>4</sub> nanoparticles assembled coating: role of substrate temperature to tailor disordered to crystalline phase and related photocatalytic activity in degradation of methylene blue. *Applied Catalysis A: General*, 423, 21-27.
- XU, A., LI, X., YE, S., YIN, G. & ZENG, Q. 2011. Catalyzed oxidative degradation of methylene blue by in situ generated cobalt (II)-bicarbonate complexes with hydrogen peroxide. *Applied Catalysis B: Environmental*, 102, 37-43.
- XU, L. & WANG, J. 2012. Fenton-like degradation of 2, 4-dichlorophenol using Fe<sub>3</sub>O<sub>4</sub> magnetic nanoparticles. *Applied Catalysis B: Environmental*, 123, 117-126.
- ZHOU, T., LI, Y., JI, J., WONG, F.-S. & LU, X. 2008. Oxidation of 4-chlorophenol in a heterogeneous zero valent iron/H<sub>2</sub>O<sub>2</sub> Fenton-like system: Kinetic, pathway and effect factors. *Separation and Purification Technology*, 62, 551-558.
- ZIDAN, H., EL-GHAMAZ, N., ABDELGHANY, A. & LOTFY, A. 2018. Photodegradation of methylene blue with PVA/PVP blend under UV light irradiation. *Spectrochimica Acta Part A: Molecular and Biomolecular Spectroscopy*, 18, 1386-1425.

## CHAPTER 6

### 6.1 CONCLUSIONS AND RECOMMENDATIONS

#### 6.1.1 Conclusions

Polluted water has become a problem due to industrialization. In this study cobalt oxide nanoparticles were used as catalysts for the Fenton-like reaction to clean water. The main goal was to evaluate the impact of size and shape of cobalt oxide nanoparticles on the degradation of methylene blue.

The cobalt oxide nanoparticles were prepared using the precipitation oxidation method at atmospheric pressure and a temperature of 85 °C. The preparation parameters like the cobalt precursor, type of oxidant and time of reaction were varied to get different sizes and shapes. The XRD analyses indicated that pure cobalt oxide phase was obtained for all the prepared samples. XRD analyses interpreted with the Scherrer equation and TEM analyses indicated the formation of the nanoparticles in all cases.

The shape of the nanoparticles changed from spherical to cubic when the cobalt precursor changed from cobalt nitrate to cobalt acetate. The yield of the particles made of cobalt nitrate was 76 % which is much higher than the yield of 36 % for the particles made from cobalt acetate. The FTIR spectroscopy showed the presence of the precursor anions on the surface of the nanoparticles. The TGA results indicated that the acetate anions may be more strongly adsorbed than the nitrate anions on the cobalt oxide surface and this may have caused a slower particle growth rate explaining the lower yield. The stronger adsorbed acetate ions may have functioned as capping molecules, changing the shape of the nanoparticles.

Cobalt hydroxide is oxidized to cobalt oxide during the preparation. Oxygen and hydrogen peroxide were used as oxidizing agents. An increase in the amount of hydrogen peroxide from 0.14 mmol to 6.7 mmol caused a decrease in the spherical nanoparticles size from 19.5 to 3.0 nm and an increase in the yield from 29 % to 98 %. Similarly, an increase in the amount of hydrogen peroxide from 0.14 mmol to 6.7 mmol decreased the cubic shaped nanoparticles size from 11.3 to 3.2 nm and increased the yield from 23 % to 58 %. The decrease in size and increase in yield may be explained by an increase in the formation of cobalt oxide nuclei. The UV-vis spectroscopy

analyses indicated an increase in the band gap and electron transitions with an increase in the amount of hydrogen peroxide used. This showed that the band gap thus increased with a decrease in the particle size.

An increase in the time of oxidation by air from 1 to 16 hrs increased the spherical shape nanoparticles size from 2.6 to 5.9 nm and increased the yield from 67 % to 98 %. A similar trend was obtained for the cubic shaped nanoparticles where an increase in the reaction time from 4 to 16 hrs increased the size from 15.0 to 43.3 nm and increased the yield from 64 % to 89 %. The size ranges for the spherical and cubic particles were different due to different amounts of hydrogen peroxide used.

The catalysts were used in the Fenton-like reaction to degrade methylene blue. A high amount of degradation was only observed in the presence of a catalyst which shows that direct oxidation of methylene blue by hydrogen peroxide is negligible. FTIR analyses showed that degradation occurred and that the MB was not just decolorized to leuco methylene blue since the peaks from the methylene blue decreased after the degradation reaction.

The rate of reaction, the pseudo first order rate constant and amount of leaching increased with a decrease in the cobalt oxide particle size. This may be explained by an increase in the higher surface area with a decrease in the nanoparticle size. The increase in surface area may result in an increase in the amount of methylene blue adsorbed on the surface increasing the rate of reaction and it may also increase the rate of hydroxyl radical formation. The TOF, which is the mole of methylene blue converted per mol of surface cobalt atoms per minute, decreased with a decrease in the size for both the spherical and cubic nanoparticles. The TOF for the spherical and cubic nanoparticles were similar indicating that the catalytic activity may not be dependent on the shape.

Based on the data collected from this research, it can be said that the size of the heterogeneous Fenton-like catalyst should be as small as possible to obtain the most active catalyst and that it seems that shape is not a very important parameter that influences the activity of the catalyst.

### **6.1.2 Recommendations**

In this study, unsupported catalyst was used to study the effect of size and shape in the absence of mass transfer limitations and to make the size and shape measurements easier. The results indicated that one should aim for as small as possible particle sizes. In a supported catalyst, there is metal oxide-support interaction, which may yield a different activity and leaching trend. For example, more metal oxide-support interaction is expected to decrease leaching and more metal oxide-support interaction is expected for very small particles. Therefore, it is recommended that the effect of the metal oxide size in the presence of supports should be investigated. Different supports will also give different metal oxide-support interactions and it would thus be interesting to study the effect of support type on the activity of the catalyst while keeping the metal oxide nanoparticle size the same.

It can be suggested that the reusability studies of the catalyst should also be studied, this will give the knowledge about other types of deactivation such as sintering and poisoning. The degradation products should be identified using HPLC-MS or GC-MS as a function of time to determine the degradation pathway and to do more accurate leaching studies. Total organic carbon analyses should also be done to determine to what extent complete mineralization has taken place.

## APPENDIXES

### 7.1 A1 CALCULATIONS OF AVERAGE CRYSTALLITES SIZES FROM XRD USING SCHERRER EQUATION

The average crystallites sizes were calculated using the following equation:

$$D = K\lambda / \beta \cos\theta$$

Where K is the Scherrer constant of proportionality = 0.94

$\lambda$  is the X-ray wavelength of irradiation with 1.5406 Å ( $1.5406 \times 10^{-1}$  nm)

$\beta$  is the full width at half maxima in radians =  $1.06^\circ$  (0.0184 rad)

$2\theta, \theta$  is the scattering/ Bragg angle =  $30.68^\circ, 15.4^\circ$

D is the crystallites size of material in nm

Substitution of different values in the above equation gives different average crystallites sizes of  $\text{Co}_3\text{O}_4$  nanoparticles.

## 7.2 A2 CALCULATIONS OF COBALT OXIDE NANOPARTICLES YIELD

$$\begin{aligned}n \text{Co(NO}_3)_2 \cdot 6\text{H}_2\text{O} &= \frac{m}{M_r} \\ &= \frac{5.2081 \text{ g (weighed during the preparation)}}{291.03 \text{ g/mol}} \\ &= 0.0178954 \text{ mol}\end{aligned}$$

$$\frac{n_{\text{Co(NO}_3)_2 \cdot 6\text{H}_2\text{O}}}{n_{\text{Co}_3\text{O}_4}} = \frac{1}{3}$$

$$\text{Therefore number of moles (n) of Co}_3\text{O}_4 = \frac{0.0178954 \text{ mol}}{3} = 0.0059651 \text{ mol}$$

$$\begin{aligned}m_{\text{Co}_3\text{O}_4} &= n \cdot M_r \\ &= 0.0059651 \text{ mol} * 240.7972 \text{ g/mol} \\ &= 1.4364 \text{ g}\end{aligned}$$

$$\begin{aligned}\% \text{ yield of Co}_3\text{O}_4 &= \frac{\text{Actual mass of Co}_3\text{O}_4}{\text{Theoretical mass of Co}_3\text{O}_4} * 100 \\ &= \frac{1.4364 \text{ g}}{1.9164 \text{ g}} * 100 \\ &= 74.2\%\end{aligned}$$

The same calculations were carried out when  $\text{Co}(\text{CH}_3\text{COO})_2 \cdot 4\text{H}_2\text{O}$  was used as a cobalt source

### 7.3 A3 CALCULATIONS OF BAND GAB ENERGIES USING TAUC PLOTS

The band gap energies of the  $\text{Co}_3\text{O}_4$  nanoparticles were estimated from the absorption coefficient ( $\alpha$ ) and photon energy ( $h\nu$ ) using the following equation.

$$(\alpha h\nu) = A(h\nu - E_g)^n$$

Where:  $\alpha$  is the absorption coefficient,  $h\nu$  is the incident photon energy,  $A$  is constant and the value of  $n$  is 2 for the determination of optical band gaps of  $\text{Co}_3\text{O}_4$  nanoparticles. Then the value of band gaps of  $\text{Co}_3\text{O}_4$  nanoparticles was measured by extrapolating the intercept line on the photon energy ( $h\nu$ ) axis gives band gap in (eV).

#### **7.4 A4.1 CALCULATIONS OF METHYLENE BLUE CONVERSION RATES**

The conversion rates of methylene blue were calculated using the following equation.

$$\% \text{ removal} = C_0 - C_t / C_0 * 100$$

Where  $C_0$  is the initial concentration of methylene blue before the reaction and  $C_t$  is the final concentration of methylene blue after the reaction at a given time.

#### **7.5 A4.2 CALCULATIONS OF DEGRADATION EFFICIENCY OF METHYLENE BLUE**

Catalytic degradation efficiency of methylene blue by different sizes of  $\text{Co}_3\text{O}_4$  nanoparticles were obtained by plotting  $C_t/C_0$  plots, where  $C_0$  and  $C_t$  are the concentrations of methylene blue at the beginning and after a given time.

## **7.6 A5.1 CALCULATION OF THE PSEUDO-FIRST-ORDER RATE CONSTANTS**

The order of reaction of methylene blue in the  $\text{Co}_3\text{O}_4/\text{H}_2\text{O}_2$  system was calculated using the pseudo first order kinetics equation.

$\ln [C_t]$

Where  $[C_t]$  is the concentration of methylene blue at a given time intervals. The representative plots of  $\ln [C_t]$  versus time were presented and different correlations of coefficients ( $R^2 \sim 0.99$ ) were obtained.

## **7.7 A5.2 CALCULATIONS OF THE PSEUDO SECOND ORDER RATE CONSTANTS**

The order of reaction of methylene blue in the  $\text{Co}_3\text{O}_4/\text{H}_2\text{O}_2$  system was calculated using the pseudo first order kinetics equation.

$1/[C_t]$

Where  $[C_t]$  is the concentration of methylene blue at a given time intervals. The representative plots of  $1/[C_t]$  versus time were presented and different correlations of coefficients that were not close to one were obtained.

## 7.8 A6 CALCULATIONS OF TURN OVER FREQUENCY (TOF) PER SURFACE COBALT ATOMS

The number of surface cobalt atoms in the cobalt oxide spinel nanoparticles was calculated by assuming that the 100 crystal face is exposed in all cases (valid for the cubic and spherical nanoparticles synthesized in this study). On this face of the spinel unit cell two cobalt atoms are fully occupied, and 4 are half occupied, giving four total cobalt atoms. The unit cell edge lengths are 8.084 Å, and thus the density of surface cobalt atoms is  $6.1 \times 10^{18}$  surface cobalt atoms/m<sup>2</sup> (Esswein et al., 2009). Using 0.01 g of the 5.9 nm Co<sub>3</sub>O<sub>4</sub> nanoparticles gives 0.112 m<sup>2</sup> of total surface area, and thus  $6.8 \times 10^{17}$  surface Co atoms total in this sample.

Details concerning the calculation of turnover frequency per surface cobalt atom of the Co<sub>3</sub>O<sub>4</sub> nanoparticles are as below:

mass of catalyst used = 0.01 g

$p = m/v$

where  $p = 6.11 \text{ g/cm}^3$

$v = \frac{0.01 \text{ g}}{6.11 \text{ g/cm}^3}$

$6.11 \text{ g/cm}^3$

$= 0.00164 \text{ cm}^3$

$= \frac{1.64 \times 10^{18} \text{ nm}^3}{6.11 \text{ g/cm}^3}$  Total volume of catalyst used

5.9 nm sphere diameter is 2.95 nm radius

$A = 4\pi r^2 = 4 \times 3.14 \times (2.95)^2 \text{ nm}^2$

$= \frac{109 \text{ nm}^2}{6.11 \text{ g/cm}^3}$  Area of 1 particle

$V = \frac{4}{3}\pi r^3 = \frac{4}{3} \times 3.14 \times (2.95)^3 \text{ nm}^3$

$= \frac{859 \text{ nm}^3}{6.11 \text{ g/cm}^3}$  Volume of 1 particle

Number of particles used = Total volume / Volume of one particle

$= \frac{1.64 \times 10^{18} \text{ nm}^3}{859 \text{ nm}^3}$

$= 1.903 \times 10^{15}$  particles

Area of all particles used = Area of 1 particle \* number of particles

$= 109 \text{ nm}^2 \times 1.903 \times 10^{15}$  particles

$$= 2.08 \times 10^{17} \text{ nm}^2$$

$$= 0.208 \text{ m}^2$$

Number of cobalt atoms (surface)

$$6.1 \times 10^{18} \text{ surface of cobalt atoms / m}^2 * 0.208 \text{ m}^2$$

$$= 1.27 \times 10^{18} \text{ Co sites / Na } (6.023 \times 10^{23})$$

$$= 2.11 \times 10^{-6} \text{ moles of sites}$$

100 ppm is the initial concentration ( $C_o$ ) and ( $C_t$ ) is the final concentration at a given time.

$$\text{Average rate} = \frac{C_o - C_t}{\Delta t}$$

$$= \frac{(100 - 4.8) \text{ mg/L} * 0.1 \text{ L}}$$

$$20 \text{ min}$$

$$= 0.476 \text{ mg / min}$$

$$= 0.476 \times 10^{-3} \text{ g / min}$$

Mr of methylene blue = 319.85 g / mol

$$\text{Average rate} = \frac{0.476 \times 10^{-3} \text{ g/min}}{319.85 \text{ g/mol}}$$

$$= 1.488 \times 10^{-6} \text{ mol / min}$$

$$= 1.488 \times 10^{-6} \text{ mol / min}$$

Therefore

$$\text{TOF} = \frac{\text{Rate mol/min}}{\text{moles of sites}}$$

moles of sites

$$= \frac{1.488 \times 10^{-6} \text{ mol/min}}{2.11 \times 10^{-6} \text{ mol of sites}}$$

$$= 0.704 \text{ min}^{-1}$$

$$= 0.704 \text{ min}^{-1}$$

## 7.9 A7 CALCULATIONS OF TOF USING THE RESULTS OF Wan et al. (2016)

The data used to calculate the TOF was obtained from the article of Wan et al. (2016). Values of the TOF for other sizes were determined similarly.

mass of catalyst used = 0.01 g

$$\rho = m/v$$

where density of Fe<sub>3</sub>O<sub>4</sub> is 5.17 g/cm<sup>3</sup>

$$v = \frac{0.01 \text{ g}}{5.17 \text{ g/cm}^3}$$

$$= 0.001934 \text{ cm}^3$$

$$= 1.94 \times 10^{18} \text{ nm}^3$$

Total volume of catalyst used

30.0 nm sphere diameter is 15.0 nm radius

$$A = 4\pi r^2 = 4 \times 3.14 \times (15.0)^2 \text{ nm}^2$$

$$= 2826 \text{ nm}^2$$

Area of 1 particle

$$V = \frac{4}{3}\pi r^3 = \frac{4}{3} \times 3.14 \times (15.0)^3 \text{ nm}^3$$

$$= 14130 \text{ nm}^3$$

Volume of 1 particle

Number of particles used = Total volume / Volume of one particle

$$= \frac{1.93 \times 10^{18} \text{ nm}^3}{14130 \text{ nm}^3}$$

$$= 1.37 \times 10^{14} \text{ particles}$$

Area of all particles used = Area of 1 particle \* number of particles

$$= 2826 \text{ nm}^2 \times 1.16 \times 10^{14} \text{ particles}$$

$$= 3.87 \times 10^{17} \text{ nm}^2$$

$$= 0.386 \text{ m}^2$$

Number of cobalt atoms (surface) =  $\frac{\text{surface of cobalt atoms} \times \text{Area of all particles}}{\text{Na (6.023} \times 10^{23})}$

$$\text{Na (6.023} \times 10^{23})$$

$$= \frac{(6.1 \times 10^{18}) \text{ Co sites} \times 0.327 \text{ m}^2}{\text{Na (6.023} \times 10^{23})}$$

$$\text{Na (6.023} \times 10^{23})$$

$$= 3.92 \times 10^{-6} \text{ moles of sites}$$

100 ppm is the initial concentration ( $C_o$ ) and ( $C_t$ ) is the final concentration at a given time.

$$\text{Average rate} = \frac{C_o - C_t}{\Delta t}$$

$$= \frac{(100 - 3.7) \text{ mg/L} \times 0.1 \text{ L}}{20 \text{ min}}$$

$$= 0.4815 \text{ mg / min}$$

$$= 0.4815 \times 10^{-3} \text{ g / min}$$

Mr of Rhodamine B (RHB) = 47.02 g / mol

$$\text{Average rate} = \frac{0.4815 \times 10^{-3} \text{ g/min}}{47.02 \text{ g/mol}}$$

$$= 1.005 \times 10^{-6} \text{ mol / min}$$

Therefore

$$\text{TOF} = \frac{\text{Rate mol/min}}{\text{moles of sites}}$$

$$= \frac{1.005 \times 10^{-6} \text{ mol/min}}{3.32 \times 10^{-6} \text{ mol of sites}}$$

$$= 0.2566 \text{ min}^{-1}$$

**Table A6:** TOF results calculated using the results of Wan et al. (2016).

TEM size (nm)	TOF (min <sup>-1</sup> ) per surface cobalt
30	0.2566
70	0.5862
250	1.6362
600	2.6109

## 7.10 A8 CALCULATIONS OF TOF USING Espinosa et al. (2018) results

The data used to calculate the TOF was obtained from the article of Espinosa et al. (2018). Values of the TOF for other sizes were determined similarly.

mass of catalyst used = 0.01 g

$$\rho = m/v$$

where  $\rho = 5.17 \text{ g/cm}^3$

$$v = \frac{0.01 \text{ g}}{5.17 \text{ g/cm}^3}$$

$$= 0.00164 \text{ cm}^3$$

$$= \underline{1.93 \times 10^{18} \text{ nm}^3} \text{ Total volume of catalyst used}$$

2.2 nm sphere diameter is 1.1 nm radius

$$A = 4\pi r^2 = 4 \times 3.14 \times (1.1)^2 \text{ nm}^2$$

$$= \underline{15.19 \text{ nm}^2} \text{ Area of 1 particle}$$

$$V = \frac{4}{3}\pi r^3 = \frac{4}{3} \times 3.14 \times (1.1)^3 \text{ nm}^3$$

$$= \underline{5.57 \text{ nm}^3} \text{ Volume of 1 particle}$$

Number of particles used = Total volume / Volume of one particle

$$= \frac{1.93 \times 10^{18} \text{ nm}^3}{5.57 \text{ nm}^3}$$

$$= 3.47 \times 10^{17} \text{ particles}$$

Area of all particles used = Area of 1 particle \* number of particles

$$= 15.19 \text{ nm}^2 \times 3.47 \times 10^{17} \text{ particles}$$

$$= 5.28 \times 10^{18} \text{ nm}^2$$

$$= 5.2751 \text{ m}^2$$

Number of cobalt atoms (surface) = surface of cobalt atoms \* Area of all particles

$$\text{Na } (6.023 \times 10^{23})$$

$$= \underline{(6.1 \times 10^{18}) \text{ Co sites} \times 5.2751 \text{ m}^2}$$

$$\text{Na } (6.023 \times 10^{23})$$

$$= 5.34 \times 10^{-5} \text{ moles of sites}$$

100 ppm is the initial concentration ( $C_o$ ) and ( $C_t$ ) is the final concentration at a given time.

$$\text{Average rate} = \frac{C_o - C_t}{\Delta t}$$

$$\Delta t$$

$$= \frac{(100 - 0.1) \text{ mg/L} * 0.1 \text{ L}}{20 \text{ min}}$$

$$= 0.4995 \text{ mg / min}$$

$$= 0.4995 \text{ mg / min}$$

$$= 0.4995 * 10^{-3} \text{ g / min}$$

$$\text{Mr of Phenol} = 94.11 \text{ g / mol}$$

$$\text{Average rate} = \frac{0.4815 * 10^{-3} \text{ g/min}}{94.11 \text{ g/mol}}$$

$$= 5.3129 * 10^{-6} \text{ mol / min}$$

$$= 5.3129 * 10^{-6} \text{ mol / min}$$

Therefore

$$\text{TOF} = \frac{\text{Rate mol/min}}{\text{moles of sites}}$$

$$= \frac{5.3129 * 10^{-6} \text{ mol/min}}{5.34 * 10^{-5} \text{ mol of sites}}$$

$$= 0.01036 \text{ min}^{-1}$$

$$= 0.01036 \text{ min}^{-1}$$

$$= 0.01036 \text{ min}^{-1}$$

**Table A8:** TOF results calculated using the results of Espinosa et al. (2018).

TEM size (nm)	TOF (min <sup>-1</sup> ) Per surface cobalt	TOF (min <sup>-1</sup> ) Per total moles of cobalt
2.2	0.01036	0.004271
4.9	0.02123	0.003929
14.1	0.03054	0.001965
19.2	0.03164	0.001495

## 7.11 A9 CALCULATIONS OF TOF USING THE RESULTS OF Dong et al. (2007)

The data used to calculate the TOF was obtained from the article of Dong et al. (2007). Values of the TOF for other sizes were determined similarly.

mass of catalyst used = 0.01 g

$$p = m/v$$

where  $p = 6.11 \text{ g/cm}^3$

$$v = \frac{0.01 \text{ g}}{6.11 \text{ g/cm}^3}$$

$$= 0.00164 \text{ cm}^3$$

$$= 1.64 \times 10^{18} \text{ nm}^3$$

Total volume of catalyst used

3.5 nm sphere diameter is nm radius

$$A = 4\pi r^2 = 4 \times 3.14 \times (1.8)^2 \text{ nm}^2$$

$$= 38.465 \text{ nm}^2$$
 Area of 1 particle

$$V = \frac{4}{3}\pi r^3 = \frac{4}{3} \times 3.14 \times (1.8)^3 \text{ nm}^3$$

$$= 22.4379 \text{ nm}^3$$
 Volume of 1 particle

Number of particles used = Total volume / Volume of one particle

$$= \frac{1.64 \times 10^{18} \text{ nm}^3}{22.4379 \text{ nm}^3}$$

$$= 7.29 \times 10^{16} \text{ particles}$$

Area of all particles used = Area of 1 particle \* number of particles

$$= 38.465 \text{ nm}^2 \times 7.29 \times 10^{16} \text{ particles}$$

$$= 2.80 \times 10^{18} \text{ nm}^2$$

$$= 2.8057 \text{ m}^2$$

Number of cobalt atoms (surface) = surface of cobalt atoms\* Area of all particles

$$\text{Na } (6.023 \times 10^{23})$$

$$= \frac{(6.1 \times 10^{18}) \text{ Co sites} \times 2.8057 \text{ m}^2}{\text{Na } (6.023 \times 10^{23})}$$

$$\text{Na } (6.023 \times 10^{23})$$

$$= 2.84 \times 10^{-5} \text{ moles of sites}$$

100 ppm is the initial concentration ( $C_o$ ) and ( $C_t$ ) is the final concentration at a given time.

$$\text{Average rate} = \frac{C_o - C_t}{\Delta t}$$

$$\Delta t$$

$$= \frac{(100 - 59) \text{ mg/L} \times 0.1 \text{ L}}{20 \text{ min}}$$

$$= 0.205 \text{ mg / min}$$

$$= 0.205 \text{ mg / min}$$

$$= 0.205 \times 10^{-3} \text{ g / min}$$

$$\text{Mr of Phenol} = 94.11 \text{ g / mol}$$

$$\text{Average rate} = \frac{0.205 \times 10^{-3} \text{ g/min}}{94.11 \text{ g/mol}}$$

$$= 3.13 \times 10^{-6} \text{ mol / min}$$

$$= 3.13 \times 10^{-6} \text{ mol / min}$$

Therefore

$$\text{TOF} = \frac{\text{Rate mol/min}}{\text{moles of sites}}$$

$$\text{moles of sites}$$

$$= \frac{3.13 \times 10^{-6} \text{ mol/min}}{2.84 \times 10^{-5} \text{ mol of sites}}$$

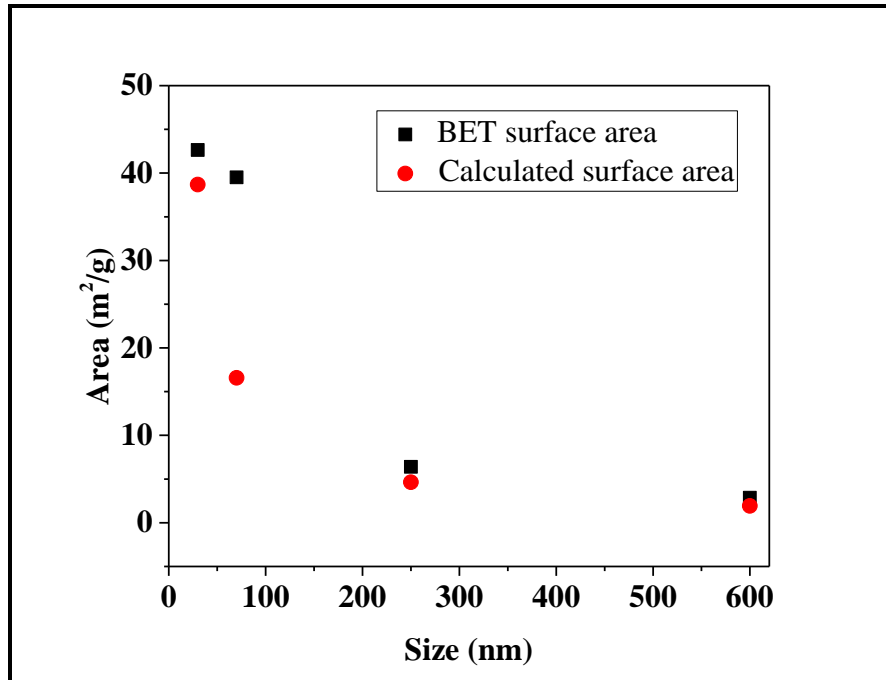
$$= 0.1103 \text{ min}^{-1}$$

$$= 0.1103 \text{ min}^{-1}$$

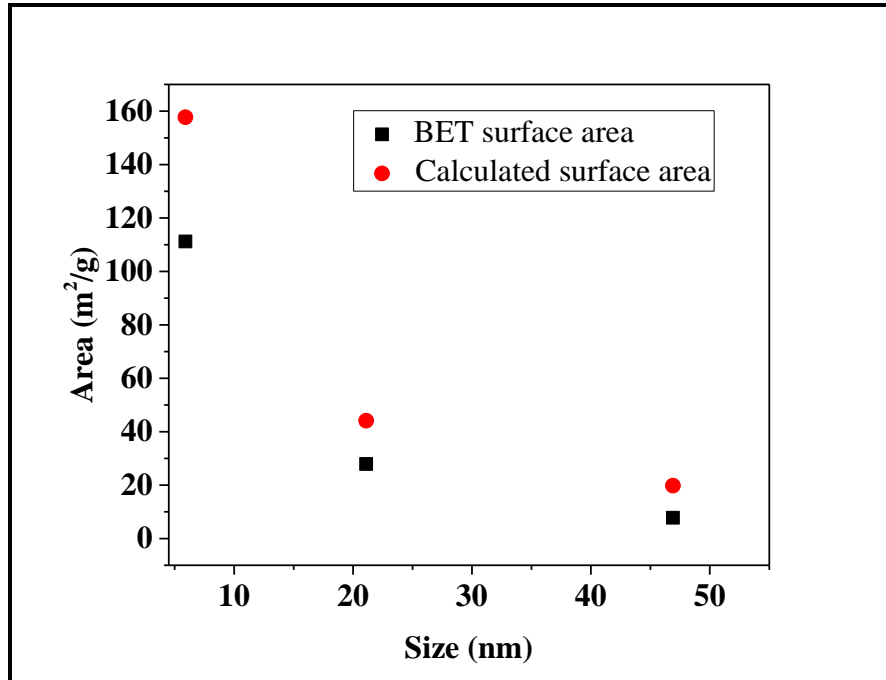
**Table A9:** TOF results calculated using the results of Dong et al. (2007).

TEM size (nm)	TOF (min <sup>-1</sup> )
3.5	0.3032
19.0	0.6292
70.0	2.8046

**7.12 A10 CORRELATION BETWEEN CALCULATED AREA AND BET SURFACE AREA FROM THE RESULTS OF Wan et al. (2016).**



**7.13 A 11 CORRELATION BETWEEN CALCULATED SURFACE AREA AND BET SURFACE ARE FROM THE RESULTS OF Esswein et al. (2009)**



ESSWEIN, A. J., MCMURDO, M. J., ROSS, P. N., BELL, A. T. & TILLEY, T. D. 2009. Size-dependent activity of  $\text{Co}_3\text{O}_4$  nanoparticle anodes for alkaline water electrolysis. *The Journal of Physical Chemistry C*, 113, 15068-15072.